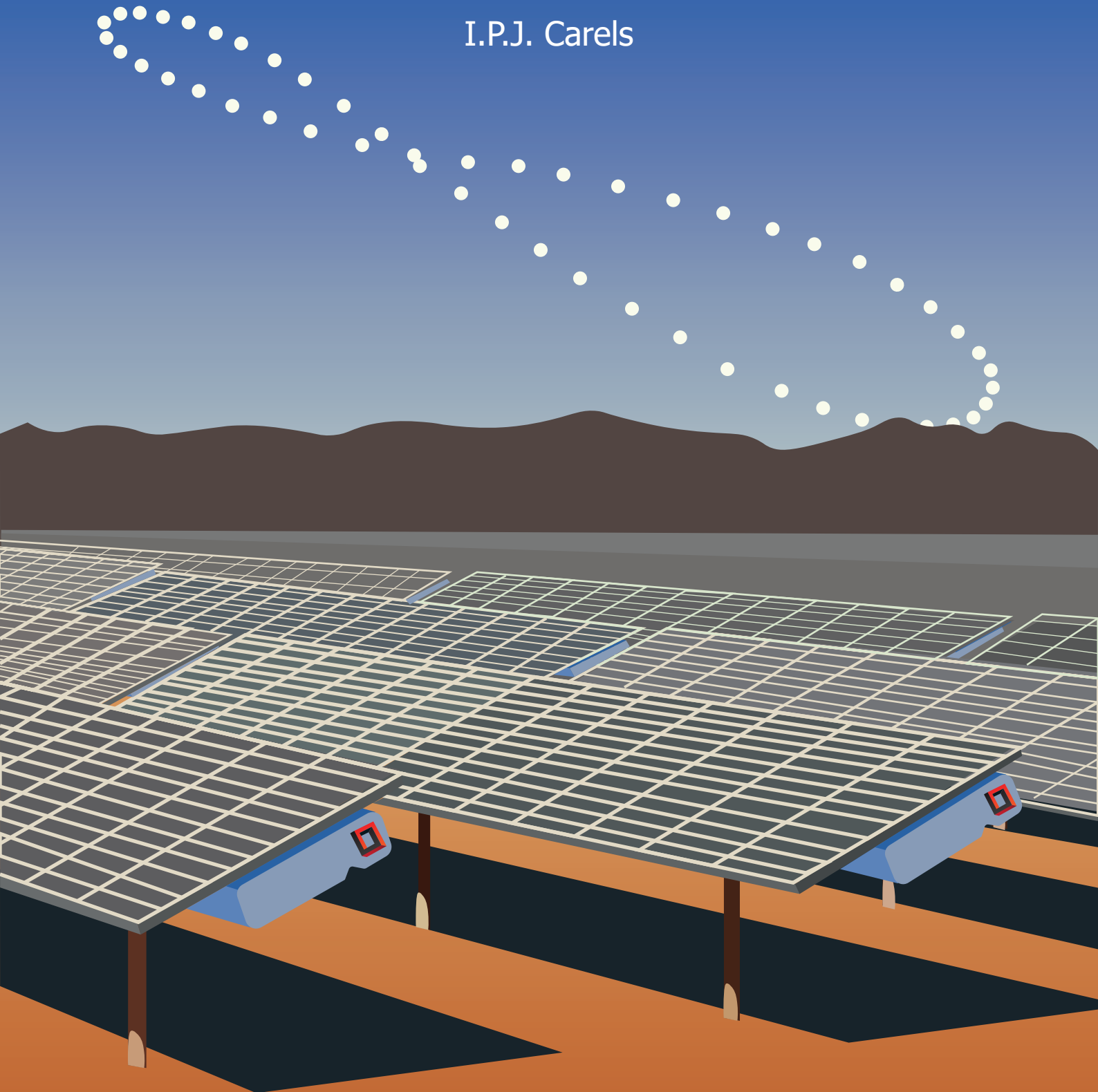


Dynamic model and preliminary design of a small-scale renewable methanol system

I.P.J. Carels



Dynamic model and preliminary design of a small-scale renewable methanol system

by

I.P.J. Carels

in partial fulfillment of the requirements for the degree of

Master of Science
in Mechanical Engineering

at the Delft University of Technology,
to be defended publicly on Wednesday October 24, 2018 at 15:00 PM.

Supervisor:	Prof. dr. ir. B. J. Boersma	TU Delft
Thesis committee:	Dr. ir. J. W. Haverkort,	TU Delft
	Dr. ir. R. Pecnik,	TU Delft
	Dr. ir. M. J. B. M. Pourquoi,	TU Delft
	Ir. J. van Kranendonk,	Zero Emission Fuels B.V.

This thesis is confidential and cannot be made public until October 24, 2022.

An electronic version of this thesis is available at <http://repository.tudelft.nl/>.

Abstract

Zero Emission Fuels B.V. develops a standalone System that produces renewable methanol from air and sunlight. In this thesis the steady-state model of this System is replaced with a Simulation Tool that can predict its behaviour for every minute of a year. The goal is to verify how technical design parameters influence methanol production and to determine if the business case target of 6.7 mole methanol per day is achievable. This thesis will contribute to the understanding of the System, speeds-up the design process and makes it possible to see the impact of fluctuating weather conditions throughout the year at different locations on earth.

The System as it was at January 1, 2018 is implemented in the Simulation Tool and its production determined for Tucson, Arizona in the year 2005. The result is an average daily production of 3.0 mole methanol with fluctuations from 1.0 mole during a cloudy winter day to 4.2 mole during a sunny summer day. The minute by minute production is found to be influenced by all System design parameters. They must thus be designed together to make sure the System performs optimally. The Alkaline Electrolysis uses the most energy of all subsystems.

Four options to improve the System are identified. These are 1) improving the power the Solar Panel produces, 2) improving the efficiency of each subsystem, 3) improving how the System is controlled and 4) integrating heat. A selection of these improvements shows that it is possible to produce 4.8 mole methanol per day.

The observed seasonal and daily fluctuating methanol production demonstrates the importance of the dynamic model developed in this thesis. Compared to the steady-state model it gives a more realistic view of methanol production and can be used to improve System design. However, to reach the business case target more technical improvements are needed. It should be realised that the design decisions will be based on technical, economical and political arguments.

Nomenclature

Table 1: This table contains a list of the words and abbreviations that are commonly used throughout this thesis

Word	Description
ZEF	Zero Emission Fuels B.V.
System	The device that converts sunlight and air to methanol
Plant	The device that converts air to methanol
SOL	Solar Panel subsystem
CO	Control subsystem
DAC	Direct Air Capture subsystem
FM	Fluid Machinery subsystem
AEC	Alkaline Electrolysis subsystem
MS	Methanol Synthesis subsystem
DS	Capillary Distillation subsystem
Simulation Tool	MatLab program in which the System Model is implemented
System Model	The mathematical models that describes the System
model	Set of functions to describe a subsystem
function	Set of equations to convert one entity into another
operation Mode	Physical action a subsystem executes
H ₂	Hydrogen
H ₂ O	Water
CO ₂	Carbon dioxide
MeOH	Methanol
PEI	Polyethylenimine (adsorbent)
KOH	Potassium hydroxide (electrolyte)

Table 2: This table contains a list of the symbols that are used throughout this thesis

Symbol	Description	Units
A	Area	[m ²]
A_{cell}	Electrode cell area	[m ²]
A_M	Solar panel azimuth angle	[°]
c_p	Specific heat at constant pressure	[kJ·kg ⁻¹ ·K ⁻¹]
DHI	Diffuse horizontal irradiance	[W·m ⁻²]
DNI	Direct normal irradiance	[W·m ⁻²]
E	Internal Energy	[J]
\dot{E}_{gnd}	Radiative heat exchange with the ground	[W·m ⁻²]
$\dot{E}_{\text{produced}}$	Internal Energy production	[W]
\dot{E}_{sky}	Radiative heat exchange with the sky	[W·m ⁻²]
GHI	Global horizontal irradiance	[W·m ⁻²]
\dot{G}_{dif}	Diffuse irradiance on the Solar Panel	[W·m ⁻²]
\dot{G}_{dir}	Direct irradiance on the Solar Panel	[W·m ⁻²]
\dot{G}_{gnd}	Ground reflected irradiance on the Solar Panel	[W·m ⁻²]
\dot{G}_M	Total irradiance on the Solar Panel	[W·m ⁻²]
\dot{G}_{ref}	Reflected irradiance	[W·m ⁻²]
ΔG_f	Gibbs energy of formation	[kJ·mole ⁻¹]
h	Specific enthalpy	[kJ·kg ⁻¹]
h_{conv}	Convective heat transfer coefficient	[W·m ⁻² ·K ⁻¹]
h_{rad}	Radiative heat transfer coefficient	[W·m ⁻² ·K ⁻¹]
ΔH_{evap}	Heat of evaporation	[kJ·kg ⁻¹]
I	Current	[A]
m	Mass	[kg]
\dot{m}	Mass flow rate	[kg·s ⁻¹]
\dot{n}	Molar production rate	[mole·s ⁻¹]
NOCT	Normal Operating Cell Temperature	[°C]
p	Pressure	[Pa]
\dot{Q}	Heat exchange with the environment	[W]
\dot{Q}_{conv}	Convective heat transfer	[W]
\dot{Q}_{peltier}	Heat extracted with a Peltier element	[W]
r_o	Outer radius	[m]
r_i	Inner radius	[m]
R_{cond}	Thermal resistance of conduction	[W·K ⁻¹]
R_{conv}	Thermal resistance of convection	[W·K ⁻¹]
R_{rad}	Thermal resistance of radiation	[W·K ⁻¹]
ΔS	Difference between the Seebeck coefficients	[W·A ⁻¹ ·K ⁻¹]
t	Time	[s]
Δt	Time step used in the numerical approximations	[s]
T_a	Ambient temperature	[K]
T_{sky}	Sky temperature	[K]
ΔT	Temperature difference	[K]
V	Volume	[m ³]
V_{act}	Voltage related to activation overpotential	[V]
V_{aec}	Operating voltage of the Alkaline Electrolysis	[V]
V_{ohm}	Voltage related to ohmic losses	[V]
V_{rev}	Reversible cell voltage	[V]
W	Work	[J]
\dot{W}	Power	[W]
η_{aec}	Energetic efficiency of the Alkaline Electrolysis	[-]
θ	Sun tilt angle	[°]
θ_M	Solar Panel tilt angle	[°]
κ	Thermal conductivity	[W·m ⁻¹ ·K ⁻¹]

Contents

Abstract	iii
Nomenclature	v
1 Introduction	1
1.1 Context	1
1.2 Company	1
1.3 Research Objectives	4
1.4 Methodology	4
2 Theory & Literature	5
2.1 Process Plant Design	5
2.2 Subsystems	6
2.2.1 General Modelling Approach	6
2.2.2 Solar Panel	8
2.2.3 Direct Air Capture	9
2.2.4 Alkaline Electrolysis	10
2.2.5 Methanol Synthesis	11
2.2.6 Capillary Distillation	12
2.3 Numerical Methods	13
2.3.1 Numerical Time Integration	13
2.3.2 Root-finding	14
2.3.3 Interpolation	15
2.4 Data Collection	16
3 Simulation Tool Design	17
3.1 Framework	17
3.2 Simulation Tool & System Overlap	19
4 System Implementation	21
4.1 Preprocessing	21
4.1.1 Import Data	22
4.1.2 Prepare Data	22
4.1.3 Allocate Memory	25
4.2 Processing	26
4.2.1 Solar Panel	27
4.2.2 Control	30
4.2.3 Direct Air Capture	32
4.2.4 Fluid Machinery	35
4.2.5 Alkaline Electrolysis	37
4.2.6 Methanol Synthesis	39
4.2.7 Capillary Distillation	41
4.3 Postprocessing	42
4.3.1 Visual Analysis	42
4.3.2 Key Performance Indicators	46
5 System Discussion	47
6 Improvements Identification	49
6.1 Increasing System Power	50
6.2 Improving Control	50
6.3 Increasing Subsystem Efficiency	51

6.4	Integrating Heat	51
6.5	Improved Models	52
6.5.1	Improved Control Model	52
7	Improvements Implementation	53
7.1	Increasing Subsystem Efficiency	53
7.2	Integrating Heat	54
7.2.1	Peltier Element Model	54
7.2.2	Case Studies	56
7.3	Improved Control Model	58
7.3.1	Decision function	58
7.3.2	Power function	58
7.3.3	Case Studies	59
8	Improvements Discussion	61
8.1	Increasing Subsystem Efficiency	62
8.2	Integrating Heat	62
8.3	Improved Control Model	63
9	Conclusions & Recommendations	65
9.1	Improved System	65
9.2	Conclusions	66
9.3	Recommendations	68
9.4	Final Remark	68
	Bibliography	69
A	Material Properties	71
B	Model Assumptions	73
C	Key Performance Indicators	77
D	Alkaline Electrolysis Experiments	79
D.1	Experimental Setup	79
E	Important System Parameters	81
F	Guidelines for System Design	83

1

Introduction

This chapter introduces the research that is presented in this report. The context for the research is sketched, the company, the System they develop and the model that describes it are also introduced. The research objectives are presented and the final section of this chapter focuses on the methodology.

1.1. Context

It has been widely accepted that CO₂ emissions are the main cause for global warming. Many scientists expect that this will pose a huge threat on both the environment and humanity. The main source for this problem is our energy consumption because it is accompanied with CO₂ emissions. As visually illustrated in Figure 1.1 in 2009 the energy consumption was still for 80 % provided for by burning fossil fuels [1] while only 20% came from renewable and nuclear sources. To solve the problems of global warming this percentage needs to drop. However, it is expected that hydrocarbons and especially liquid ones will always be used for example for the transportation sector, heating and the chemical industry. This is because of their high energy density and being easy to handle. It would thus be welcome if their advantages could be kept while the disadvantages related to CO₂ emissions are removed.

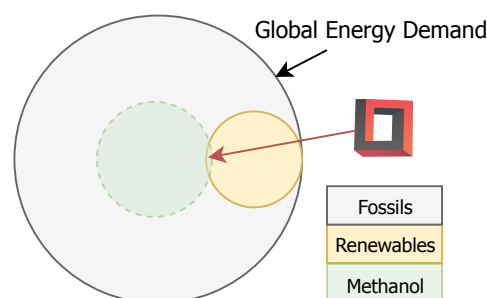


Figure 1.1: A schematic overview of the context of this research. The total global energy consumption in 2009 was provided for by renewables (12 %), fossil fuels (80 %) and nuclear sources (8 %) [1]. Zero Emission Fuels B.V. indicated with the red and black logo, tries to make methanol (MeOH), currently mainly made from fossil fuels, from renewables sources. Therefore, it operates at the overlapping area of MeOH and renewables.

1.2. Company

Zero Emission Fuels develops a System to produce methanol from CO₂ from the air with renewable energy from a Solar Panel. The company thus finds itself in the overlapping circles of methanol and renewable resources of Figure 1.1. The company vision and System they design to do this will be introduced next. The activities of the company and the models they use are also discussed because they demonstrate how this thesis is useful for the company.

Company Vision

The vision provides the guidelines for everything Zero Emission Fuels does. This vision is different from the vision of the traditional chemical industry. They believe in a number-up strategy which is related to small-scale product design and low costs. This can be compared to the more traditional scale-up strategy which is related to large-scale projects and high costs. In their opinion the number-up strategy leads to high learning and development rates and thus a quick drop in costs of their System due to mass production benefits. They expect that this allows them to compete with the traditional process industry within five years.

System

An overview of the System that is designed by Zero Emission Fuels is shown in Figure 1.2. The System consists of several subsystems which are indicated with capital letters throughout this thesis. The Solar Panel (SOL) creates electricity which is directed to the Plant by a Control (CO) unit. The only other input of the Plant is air. The technologies used in the Plant to produce methanol (MeOH) are fixed in this thesis. Carbon dioxide (CO_2) and water (H_2O) are captured from air using pressure and temperature swing adsorption in two Direct Air Capture chambers (DAC). The H_2O is then converted into hydrogen (H_2) using Alkaline Electrolysis (AEC). The CO_2 and H_2 are subsequently mixed and reacted into MeOH in the Methanol Synthesis (MS) reactor. In the final step the reactants MeOH and H_2O are separated using Capillary Distillation (DS).

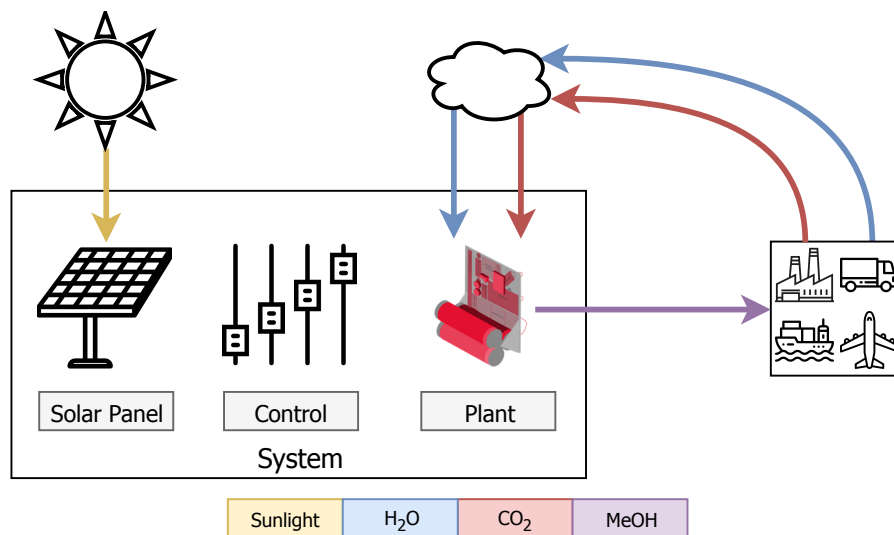


Figure 1.2: Schematic overview of the System within the environment. A Solar Panel converts sunlight into electric power. A Control unit subsequently distributes this power to the different subsystems of the Plant. The Plant uses the power to convert CO_2 and H_2O from the atmosphere into MeOH. The MeOH is used by some end user.

Company Activities

The company activities and how they interact provide insight into the relevance of this thesis. An overview of them is shown in Figure 1.3. Zero Emission Fuels verifies their System technically by building Subsystem Prototypes and performing experiments on them. Data from these experiments is combined with theory to make 3D transient Subsystem Models which support optimisation of subsystem design. The System is also investigated economically by modelling the costs and profits with the Business Case Model. The focus of this thesis is on the System Model, which forms the bridge between the technical and economical models. This model is needed to accurately predict System behaviour and to make sure that an optimally performing System is designed instead of a set of optimally performing subsystems.

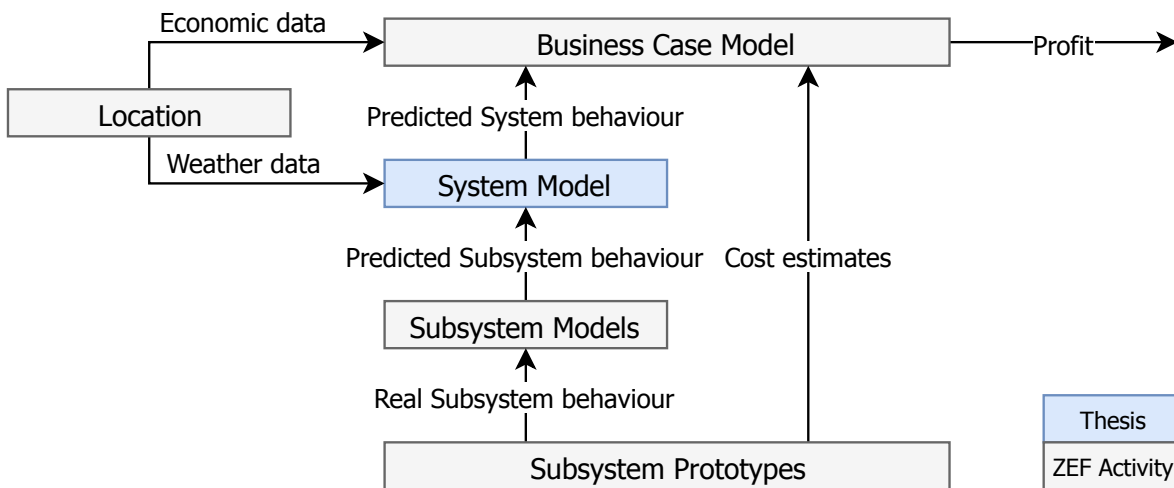


Figure 1.3: An overview of the interaction of different activities within Zero Emission Fuels. The Business Case Model predicts whether a profit is made based on economic data from the Location, predicted System behaviour and subsystem cost estimates. The System Model determines the System behaviour based on weather data from the Location and 1D quasi-steady-state Subsystem Models that are derived from predicted subsystem behaviour. This behaviour is predicted with 3D transient Subsystem Models which are verified with experimental data from the Subsystem Prototypes.

Steady-State System Model

The System Model is currently steady-state. Because of the continuously fluctuating environmental conditions this model is replaced in this thesis with a quasi-steady-state one. This increases the accuracy of the predicted System behaviour and allows for identification of the most important System parameters influencing the methanol production. The difference between these two models is shown in Figure 1.4. The steady-state System Model is the starting point of this thesis because it provides a feeling for the order of magnitude of the System parameters. Therefore, the results of this model are discussed next.

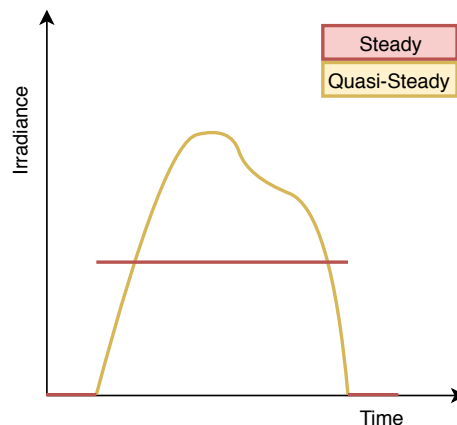


Figure 1.4: This figure shows a constant and fluctuating irradiance over time. It demonstrates the general difference between a steady-state model and a quasi-steady-state model. The variables have a constant value or fluctuate in time.

Solar Panel and Alkaline Electrolysis In the steady-state model $7.00 \text{ kWh}\cdot\text{day}^{-1}$ global horizontal irradiance is converted to $2.10 \text{ kWh}\cdot\text{day}^{-1}$ by a 300 Wp Solar Panel. The Solar Panel operates at a maximum current of around 10 A and a voltage of 30 V . The minimum efficiency for the Alkaline Electrolysis was chosen to be 60% , which corresponds to a maximum of $2.05 \text{ V}\cdot\text{cell}^{-1}$. Using experimental data, shown in Figure 4.22, it was determined that the maximum current density is $710 \text{ mA}\cdot\text{cm}^{-2}$ if the process takes place at $60 \text{ }^\circ\text{C}$. Coupling this data to the electrical characteristics of the Solar Panel it is determined that the minimum cell area is 14 cm^2 and that 16 cells in series are needed.

Direct Air Capture and Methanol Synthesis It is determined with the Business Case Model that 6.67 mole MeOH needs to be produced. The reaction ratio of CO₂ and H₂O to form MeOH is 1:3. This means that 6.67 mole CO₂ and 20.0 mole H₂O need to be adsorbed. It is assumed that there are 8.00 hours of operation for the Direct Air Capture chambers. Using two chambers and 1 hour cycles this means that in each cycle 0.42 mole of CO₂ and 1.25 mole H₂O needs to be adsorbed. The Direct Air Capture, using a polyethylenimine (PEI) adsorbent on an activated carbon monolith, adsorbs at ambient temperature and desorbs at 120 °C. Above that temperature the adsorbent deteriorates. Using the adsorbent loading isotherms from Sutanto [2], shown in Figure 4.17, it was determined that 0.22 kg PEI is needed per chamber on 0.73 kg monolith if the adsorbent loading is 30 wt%. The Methanol Synthesis reactor has to operate at 50 bars and 210 °C. At these conditions it was observed in experiments that the reactor reaches steady state in seconds [3]. No calculations have been performed on the design of the Capillary Distillation or Fluid Machinery.

1.3. Research Objectives

The main research objective 1) is to predict the production of Zero Emission Fuels' small-scale renewable MeOH System for every minute of a year at any location on earth. The results of this model 2) should be determined within 15 minutes. It is furthermore desired 3) to get insight into the variations in operation due to varying environmental conditions 4) to identify the most important System design parameters, 5) to give suggestions to improve the System design and 6) to verify the impact on methanol production of these improvements.

1.4. Methodology

The thesis starts with background information which can be found in chapter 2. The research objectives are tackled in the main body of the thesis. An overview of the main body is shown in Figure 1.5 and will be repeatedly used throughout this thesis as a guide for the reader.

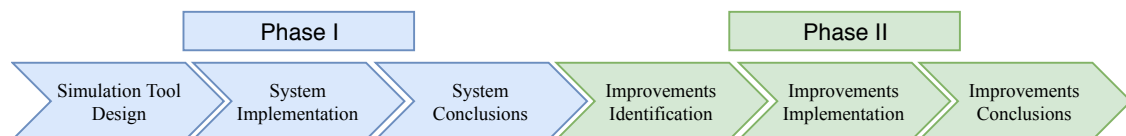


Figure 1.5: The six main chapters that make up the body of this thesis are separated into two phases. In the first phase a Simulation Tool is designed. Then the System design is implemented in this Tool. The first phase ends with a discussion of the results. In the second phase improvements for the System design are identified and subsequently implemented in the Simulation Tool. The second phase ends with a discussion of the results of the improvements.

The main body is subdivided into two phases with three chapters each. The first phase focuses on the first four research objectives: the behaviour and the most important System design parameters of the current System. In the first chapter of the first phase, chapter 3, a Simulation Tool is designed in which the System is implemented in chapter 4. Experimental data and design geometries are used when available, if not subsystem behaviour is approximated with first principles. The results of the first phase are discussed in chapter 5. The second phase focuses on the last two research objectives: the improvements. In chapter 6 five directions for improvements are identified. A selection of those improvements is implemented in the Simulation Tool in chapter 7 and their impact on MeOH production tested. The results of the improvements are discussed in chapter 8. The final chapter, chapter 9, concludes this thesis with an overview of the improved System design, conclusions for each research objective and recommendations for future research.

2

Theory & Literature

This chapter provides an overview of the theory and literature used in this thesis. In [section 2.1](#) general techniques used to design Process Plants are discussed. Background information about the technology used in each subsystem is discussed in [section 2.2](#). In [section 2.3](#) the numerical methods that are used for the modelling are discussed. The last section, [section 2.4](#) investigates some sources from which data can be extracted.

2.1. Process Plant Design

Smith describes an approach for process plant design which is referred to as an irreducible structure [\[4\]](#). The irreducible structure is similar to the hierarchical structure suggested by Douglas [\[5\]](#). This structure starts at the hearth of the process plant and then moves away from it by adding recycle streams and unit operations that form the balance of plant (BOP). In later phases heat integration is added and more detailed equipment included. This approach can be thought of as an onion in which different layers are added upon the previous ones as shown in [Figure 2.1](#). The Simulation Tool architecture is inspired by the irreducible structure because it makes sure that high level functionalities are maintained as more details are implemented. This makes it easy to swap subsystem models or insert a new location while maintaining the functionality of simulating a year minute by minute.

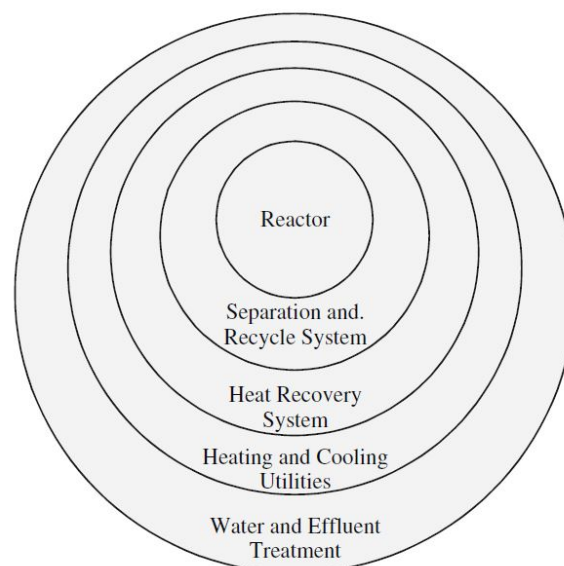


Figure 2.1: Schematic overview of the irreducible structure described by Smith [\[4\]](#). The Simulation Tool architecture was inspired by this approach because high level functionalities are kept as new layers are added.

2.2. Subsystems

In this section the literature about the subsystems is discussed. A detailed overview of them and how they are connected is given in Figure 2.2. First, the general approach to model each subsystem is given after which the Solar Panel, Direct Air Capture, Alkaline Electrolysis, Methanol Synthesis and Capillary Distillation are discussed.

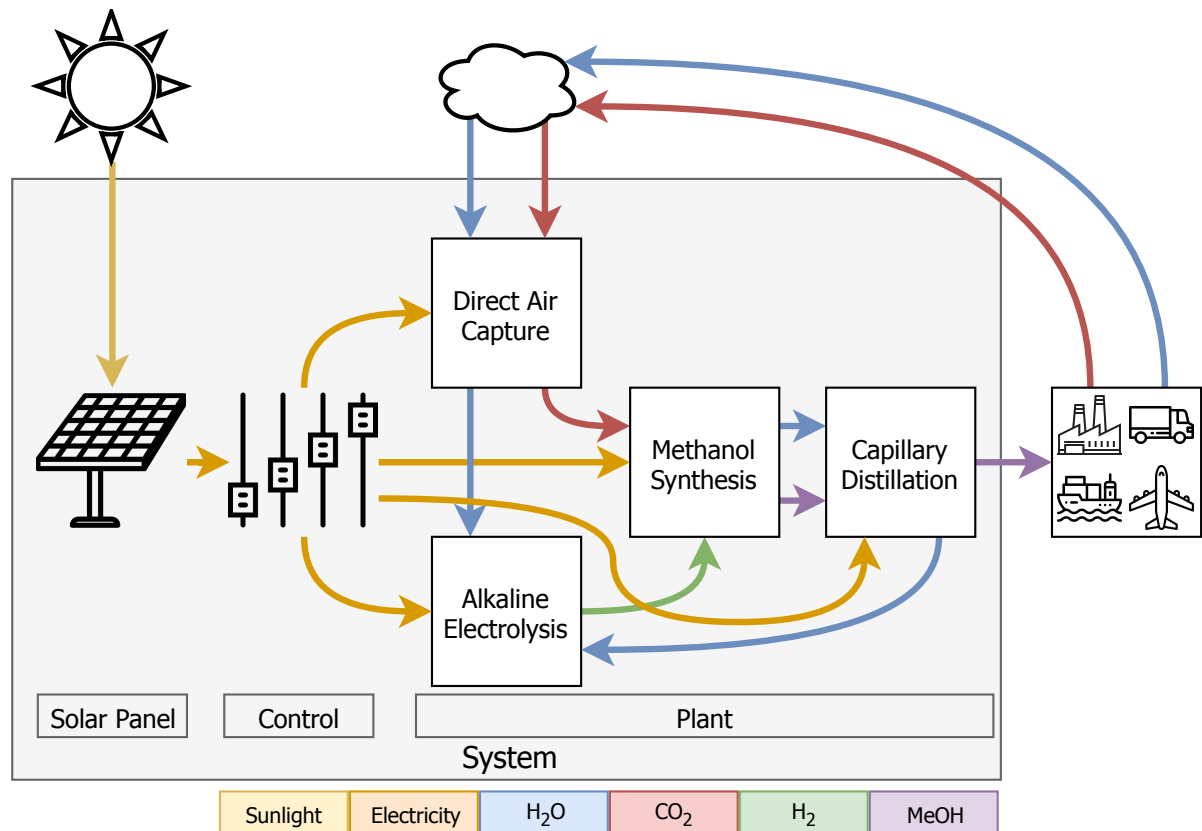


Figure 2.2: Overview of the System within the environment. The System forms a closed material cycle through the end user. The plant converts CO_2 and H_2O from the air into methanol using power from the Solar Panel. The power is distributed with the Control unit. The different subsystems of the Plant are Direct Air Capture, Alkaline Electrolysis, Methanol Synthesis and Capillary Distillation.

2.2.1. General Modelling Approach

All subsystems and buffers have the same basic characteristic, they convert some incoming variables into some outgoing variables influenced by the subsystem parameters, the power it receives and the state of the environment. This is shown in Figure 2.3. The most important variables that need to be calculated are the temperature and the mass that is converted. This is done through an energy and mass balance which are discussed in the next two subsections.

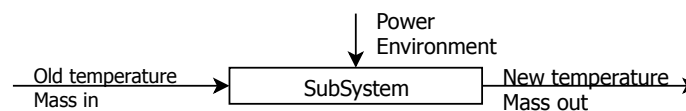


Figure 2.3: General working principle of any subsystem model. The model converts some incoming variables into outgoing variables under influence of the power provided to the subsystem as well as the state of the environment.

Energy Balance

The behaviour of all the subsystems is depending on the temperature. To find the temperature of each of the subsystems the energy balance has to be solved for each time step. The general form of this balance for an open system is shown in Equation 2.1. It is obtained from the thermal engineering textbooks of Bergman and Mills [6, 7].

$$\frac{dE}{dt} = \dot{Q} - \dot{W} + \sum_i \dot{m}_{in,i} h_{in,i} - \sum_j \dot{m}_{out,j} h_{out,j} + \dot{E}_{produced} \quad (2.1)$$

In this equation, E refers to the internal energy of the system, t to the time, \dot{Q} to the heat exchange with the environment, \dot{W} to the work produced by the subsystem, \dot{m} to the mass flow, h to the enthalpy of this mass flow and $\dot{E}_{produced}$ to the thermal energy created from chemical energy. The subscripts "in" and "out" refer respectively to the incoming and the outgoing streams. The sum indicates that there can be multiple incoming and outgoing streams. The internal energy, E , can be used to determine the temperature, T if it is assumed that the mass, m and heat capacity c_p don't change over time:

$$\frac{dE}{dt} = mc_p \frac{dT}{dt} \quad (2.2)$$

Heat Exchange, \dot{Q} The thermal resistance network approach of Bergman and Mills is used to find the heat exchange of the subsystem with the environment [6, 7]. The resistances are determined differently for different geometries and types of heat transfer. The resistances for conductive (R_{cond}), convective (R_{conv}) and radiative (R_{rad}) heat transfer for cylinders are used throughout this thesis because most subsystems are approximated by this geometry. These resistances are:

$$R_{cond} = \frac{\ln(r_o/r_i)}{2\pi Lk}, \quad R_{conv} = \frac{1}{2\pi r_o L h_{conv}}, \quad R_{rad} = \frac{1}{2\pi r_o L h_{rad}} \quad (2.3)$$

In these equations r_o and r_i refer to the outer and inner radius of the cylinder. L is the length of the cylinder, k the thermal conductivity of the material and h_{conv} and h_{rad} represent respectively the convective and radiative heat transfer coefficients. The total thermal resistance is determined by adding different thermal resistances from conduction, convection and radiation. To add these resistances the same rules of calculating the resistance of an electrical network apply. The heat exchange, \dot{Q} , can finally be determined by combining the temperature difference of the subsystem with the environment, ΔT , with the total thermal resistance, $R_{thermal}$:

$$\dot{Q} = \frac{\Delta T}{R_{thermal}} \quad (2.4)$$

Power, \dot{W} Power is created by the Solar Panel and distributed to each subsystem. In each subsystem it is partly used and partly converted into heat. How the power is used is different for all subsystems because different physical phenomena happen inside them. Therefore, how power is used exactly is discussed for each subsystem separately in the next subsections.

Mass Balance

The mass balance can be used to find how much of each chemical components is present throughout the System. The general form of this equation for an open system is:

$$\frac{dm}{dt} = \dot{m}_{in} - \dot{m}_{out} + \dot{m}_{produced} - \dot{m}_{consumed} \quad (2.5)$$

Not every subsystem has all these components. For a buffer the equation can be simplified since such a device only has an in and outflow. The other subsystem are more complex since they often consume or produce components depending on the power they receive. How this is related to production or consumption of mass will be discussed for each subsystem separately in the next subsections.

2.2.2. Solar Panel

The Solar Panel power is determined by the incoming irradiance and temperature of the photovoltaic cells. General information on all aspects of Solar Panels like their physical behaviour as well as the design of integrated and standalone systems is provided in the book by Smets [8]. In this thesis both the datasheet approach from Ortiz-Rivera [9] as well as the suggestions for direct coupling of a Solar Panel with an Electrolyser by Rahim [10] will be used. The temperature model will be based on a self constructed heat resistance network following the textbooks of Bergman and Mills [6, 7].

Electrical Model Much of the current literature focuses on a model that is based on the equivalent electrical circuit of the Solar Panel because it closely predicts the power that will be generated. Different levels of accuracy exist. Qi for example describes the electrical circuit in three different ways [11]. First with only the diode, then by adding a series resistance and finally by adding a shunt resistance. This electrical circuit, shown in Figure 2.4, is used to simulate a standalone Photovoltaic system. An advantage of the model of Qi is that it is able to track the maximum power point. A more comprehensive approach is suggested by Villalva [12]. In his paper an approach is given to estimate the series and shunt resistances and the diode constant, which are often unknown. Therefore, it becomes possible to estimate the electrical characteristics without the need for visually fitting the data on the datasheet figures. The approach of Villalva is based on a paper by Ortiz-Riviera [9].

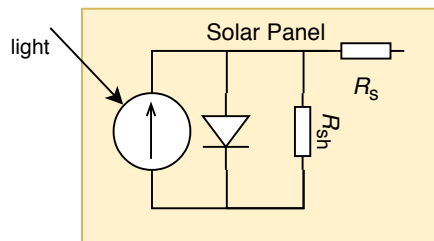


Figure 2.4: Equivalent electrical circuit to model the electrical behaviour of a Solar Panel as suggested by Qi [11]. The accuracy of the model is increased by adding a series resistance, R_s , and a shunt resistance, R_{sh} .

The power output of the Solar Panel is determined by the intersection point of the IV-curve of the Solar Panel and the IV-curve of the load. Rahim describes how the electrical operating point of a directly coupled Solar Panel and Electrolyser can be determined [10].

Temperature Model The temperature model of the Solar Panel functions as an input for the electrical model. Since temperature significantly influences the performance of the Solar Panel it is important to have a good approximation of its value. Mattei shows a straightforward formula in which the temperature is determined from the irradiance and the Normal Operating Cell Temperature, NOCT [13]:

$$T_{sol} = T_a + (\text{NOCT} - 20) \frac{I_{sol}}{800} \quad [^{\circ}\text{C}] \quad (2.6)$$

In this formula T_a represents the ambient temperature and I_{sol} the current the Solar Panel operates at. Mattei improves this model by replacing it with an energy balance in which convection is incorporated. Armstrong made an even more elaborate model by incorporating a thermal resistance network to model all physical layers and materials of the Solar Panel. He furthermore added environmental conditions and the mounting structure [14]. Armstrong states the importance of having a dynamic model: "During periods of rapidly changing conditions, a steady state model of the operating temperature cannot be justified because the response time of the PV panel temperature becomes significant due to its large thermal mass." The effect on Solar Panel temperature if mounted on a roof was investigated by Caluianu [15]. Another possibility to calculate the temperature is to construct a model based on first principles as described in the theoretical textbooks of Bergman or Mills [6, 7]. An advantage of such an approach is that it allows for incorporation of all known parameters while leaving out parameters that are unknown or unimportant for this thesis.

2.2.3. Direct Air Capture

The Direct Air Capture subsystem makes use of temperature and pressure swing adsorption to capture CO_2 and H_2O from the air. In this subsection first the adsorption technique is described in general after which the focus will be on the adsorption isotherms and kinetics.

Adsorption A general description of adsorption is given in the engineering textbook of Seader [16]. A summary of it is given here. In adsorption a solid called the adsorbent is used to remove low concentrations of a chemical from a stream. This can be done physically if the solute sticks when it comes in contact with the adsorbent or chemically by facilitating a reaction in which the solute is involved. The adsorption stage needs to be followed by a desorption stage if the adsorbent is fully loaded with chemicals. Because of this periodicity often two or more vessels are needed. Different techniques exist to regenerate the adsorbent. These are changing the temperature or pressure or using an inert gas or a fluid containing an even stronger adsorbent. In this thesis a combination of temperature and pressure change is used. The adsorbent is polyethylenimine (PEI).

Isotherms The adsorption equilibria are put into isotherms. These are used to determine the equilibrium amount of solute that can be adsorbed in the adsorbent at different temperatures and pressures. Seader states that "no acceptable theory has been developed to estimate adsorption equilibria. It is thus necessary to obtain data for a particular solute and adsorbent material of interest [16]." The data that is often obtained is the adsorbent solute loading as a function of solute concentration or partial pressure. The temperature is fixed which is why these are called adsorption isotherms. There are five different types of isotherms according to Brunauer which are all accompanied by a different type of equation to describe the physical phenomena occurring [17]. The five isotherms are shown in Figure 2.5. The most favourable behaviour is observed in Type I and II in which strong adsorption occurs if the pressure is increased.

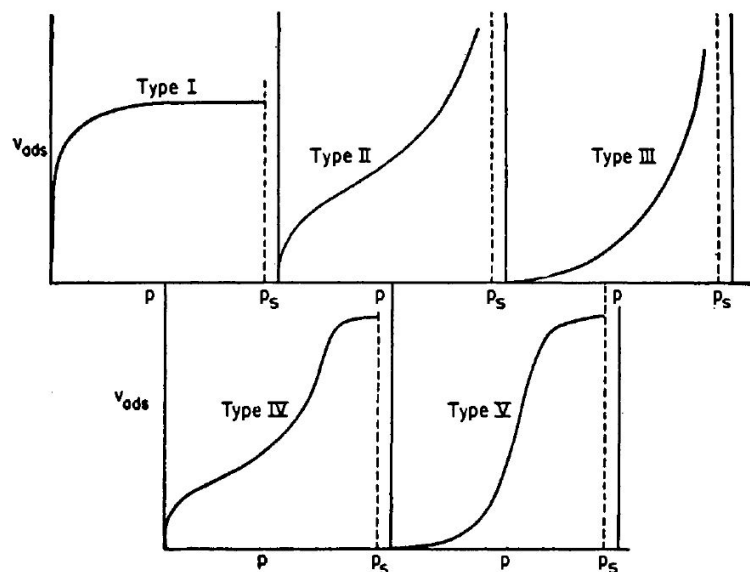


Figure 2.5: The five different types of isotherms as described by Brunauer [17]. Type I corresponds to unimolecular adsorption; Type II to multimolecular adsorption; Type III to multimolecular adsorption where the heat of adsorption of the first layer is less than that of succeeding layers; Types IV and V are the capillary condensation versions of Types II and III.

It is thus needed to have both an equation and experimental data of the specific adsorbent solute combination. In literature a study has been found that has determined the adsorption isotherms of CO_2 on a SiO_2/PEI adsorbent [2]. The experimental data demonstrates the favourable Type I adsorption and can be described with an Toth-equation. Since the adsorbent in the Direct Air Capture is also PEI but on activated carbon monolith instead of SiO_2 it is expected that a similar type of behaviour will occur. Due to absence of experimental data, the predicted isotherms of Sutanto are used in this thesis.

Kinetics The kinetics of the adsorption are important to understand because it determines the adsorption time. In literature it has been found that the most important limiting factor is the diffusion in the micro pores [17]. As long as the molecules can diffuse quick enough through the pores the kinetics can thus be neglected. Ebner has verified the adsorption time of a solid amine adsorbent (CARiACT G10) and uses 40 minutes half-cycle times [18]. In the results, Figure 2.6, it can be observed that at least 95 % of the final adsorbent loading is reached in around 15 minutes during both adsorption and desorption. Although another adsorbent is used, it is assumed in this thesis that as long as the half-cycles are in the order of 15 minutes the equilibrium loading can be reached. In other words, the adsorption is only limited by the amount of chemicals that pass the Direct Air Capture chamber if the adsorption is long enough.

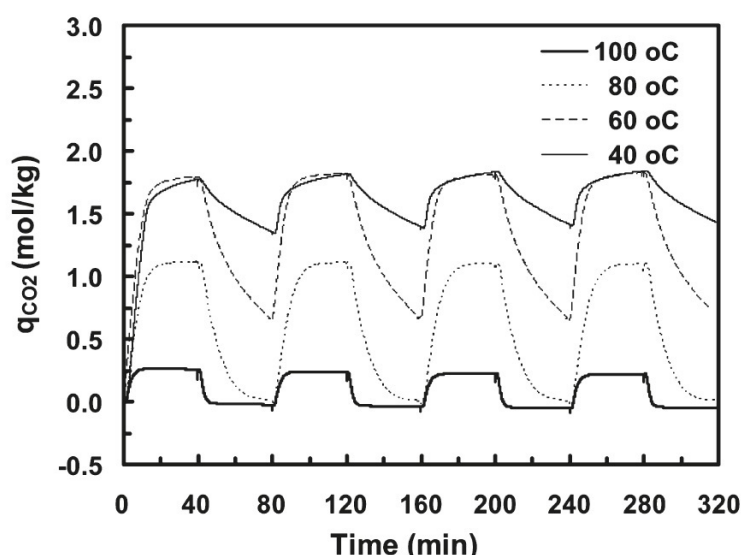


Figure 2.6: Experimental results from the paper of Ebner [18]: "CO₂ loading in a CARiACT G10 solid amine sorbent at 40, 60, 80, and 100 °C for adsorption of CO₂ at 1.2 % in N₂ and desorption cycles with a 40 min half-cycle time during four cycles. The gas flow rate was set at 60 cm³ · min⁻¹ and 1 atm." Although the half-cycle time is 40 minutes it can be observed that the adsorption (at 40 °C) is at around 95 % of the final loading after around 15 minutes and the desorption (at 100 °C) is completed after around 15 minutes.

2.2.4. Alkaline Electrolysis

The Alkaline Electrolysis model needs to convert H₂O into H₂. The first paragraph describes the electrolysis technique in general. The second one focuses on the characteristic equations that are used to describe this subsystem.

Electrolysis A general overview of hydrogen production is given in the engineering textbook of Godula-Jopek [19]. She describes the historical background, thermodynamic fundamentals of water splitting as well as specific techniques like Alkaline, PEM and high temperature electrolysis. For Zero Emission Fuels it is important that the electrolysis technique is well known, commercially available and cheap. Godula-Jopek endorses these facts by stating that the main advantage of Alkaline Electrolysis over other types of electrolysis is that it makes use of "abundant and inexpensive materials". She furthermore mentions various papers and examples of commercially available products. An overview of their performance is shown in Figure 2.7 which is based on a NASA technical memorandum [20]. It is assumed that the performance of this Alkaline Electrolysis is in the same order of magnitude. To improve efficiency of any electrolysis it is desired to minimise the operation voltage. The voltage is a function of the operating temperature as shown in Figure 4.22. It is thus beneficial to operate at an as high as physically possible temperature from an efficiency perspective.

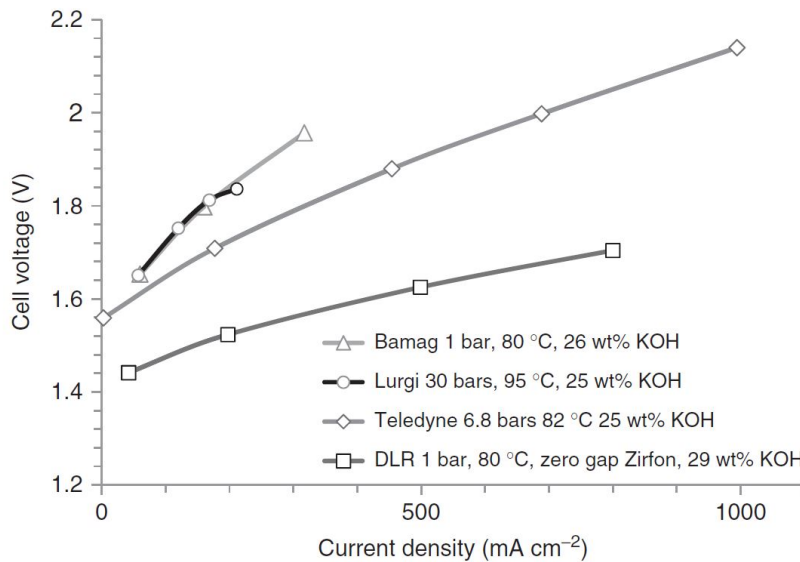


Figure 2.7: Polarisation curves of different alkaline electrolyzers from the engineering textbook of Godula-Jopek, originally published by NASA [19, 20].

Characteristic Equation The polarisation or IV curve is used to describe the Alkaline Electrolysis. The polarisation curves are described in general by Godula-Jopek [19]. Rahim describes a practical approach that is based on fitting of the characteristic equation on experimental data. This equation is:

$$V_{\text{aec}} = V_{\text{rev}} + V_{\text{act}} + V_{\text{ohm}} = V_{\text{rev}} + s \cdot \log \left(\frac{t_1 + t_2/T_{\text{aec}} + t_3/T_{\text{aec}}^2}{A_{\text{cell}}} I_{\text{aec}} + 1 \right) + \frac{r_1 + r_2 T_{\text{aec}}}{A_{\text{cell}}} I_{\text{aec}} \quad (2.7)$$

in which the coefficient, s , t_1 , t_2 , t_3 , r_1 and r_2 are implemented to fit the data and incorporate the temperature dependency. Furthermore, V_{rev} represents the reversible cell voltage, V_{act} the voltage related to the activation overpotential and V_{ohm} the voltage related to ohmic losses in the cell. The temperature of the Alkaline Electrolysis is indicated with T_{aec} and the current flowing through it with I_{aec} . The area of the cell is represented with A_{cell} . The linear dependency of the ohmic voltage on temperature is related to the fact that ohmic resistances increases linearly with temperature. The overpotential voltage is a more complex function of the temperature due to combined effects of reaction, concentration and bubble overpotential. This equation is used in this thesis because it can be fitted to experimental data.

2.2.5. Methanol Synthesis

The Methanol Synthesis reactor converts the reactants CO_2 and H_2 into the reaction products MeOH and H_2O . In the next two paragraphs the literature on the kinetics and reactor geometry is discussed.

Reaction Kinetics The model suggested by Bussche [21] is widely used for methanol synthesis processes. The basic idea of it is that the reaction constants for all equilibrium reactions are a function of temperature and pressure. Gutiérrez Neri and Basarkar determined in their Master thesis reports that a temperature of around 210 °C and a pressure of 50 bar is needed for the reactions to shift towards MeOH production and that the reaction reaches steady state in seconds [3, 22].

Reactor Geometry The reactor geometry and its operation are based on a novel concept suggested by Bos [23]. The reactor consists of a natural circulation loop with in-situ separation of the reaction products MeOH and H_2O such that conversion is achievable without the need for downstream processing. This reactor consists of a hot side at which the reaction takes place and a cold side in which the liquids can condensate and be separated from the gases. This concept is improved upon by adding heat integration such that the heat from the gases leaving the hot side is used to preheat the gases leaving the cold side. A schematic overview of this reactor is shown in Figure 2.8.

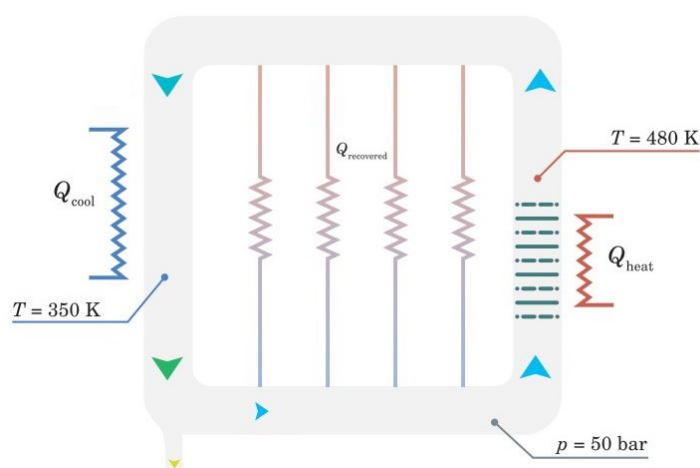


Figure 2.8: Schematic of the Methanol Synthesis reactor as illustrated in the thesis of Gutierrez Neri [22]. This design with in-situ separation is suggested by Bos [23] and improved upon by adding heat integration. The reaction takes place at the hot side where the catalyst sits. At the cold side the mixture partly condenses such that the liquid can be separated from the gases. To make sure the reaction kinetics show favourable behaviour the reactor operates at 50 bar.

2.2.6. Capillary Distillation

The Capillary Distillation makes sure that the feed from the Methanol Synthesis reactor is separated into MeOH and H₂O. In this type of distillation a countercurrent flow between the liquid and vapour phases is established utilising the principles of a heat pipe with a capillary wick. This allows for horizontal distillation. A schematic of the apparatus is shown in Figure 2.9.

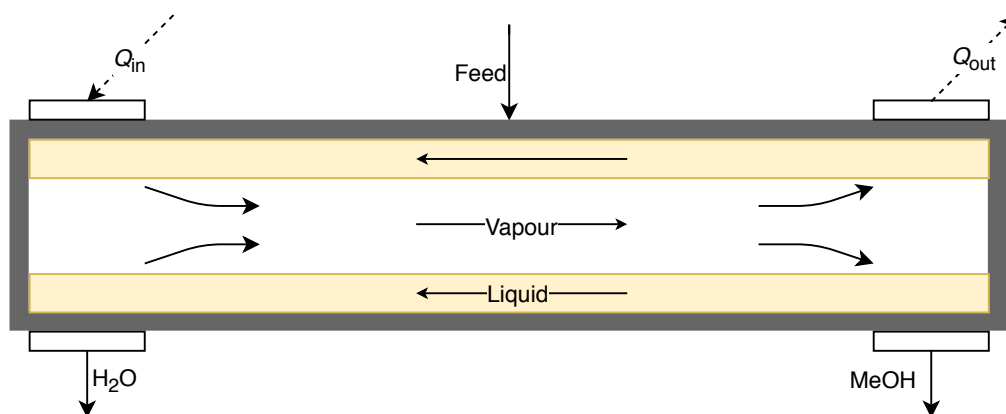


Figure 2.9: Schematic overview of the Capillary Distillation. The less volatile component will go to the hot side and the more volatile component to the cold side. The liquid moves through the capillary wick back to the hot side because the liquid is evaporated there. Due to the continuous contact between the vapour and liquid phase and the temperature gradient over the device a separation is achieved.

The working principle has been described and proven for MeOH water mixtures by Seok and Hwang [24]. The operating temperature is just below the boiling temperature of water at the hot side and just below the boiling temperature of MeOH at the cold side. A dynamic model to determine the temperature gradient and composition at various positions was constructed by Ramirez-Gonzales [25]. The main interest in this thesis is how much energy this subsystem needs to separate the feed. Therefore it is decided to not use the dynamic model but derive the energy needed for separation from first principles.

2.3. Numerical Methods

This section discusses numerical time difference, root-finding and interpolation methods used throughout this thesis. All of these numerical methods are obtained from the books of Vuik and Chapra [26, 27].

2.3.1. Numerical Time Integration

Numerical time integration methods are used to approximate the solution of a time differential for a initial-value problem as shown in Equation 2.8.

$$\begin{cases} y' = f(t, y), & t > t_0 \\ y(t_0) = y_0 \end{cases} \quad (2.8)$$

In this initial-value problem, y' refers to the time derivative which is some function, f of time, t and another variable, y . This problem is only valid for a time larger than the initial time, t_0 . y_0 is the initial-value which is needed to solve the initial-value problem.

Implicit versus Explicit An explicit method determines the value of the next time step based on values of the previous time step while an implicit method determines this value based on values of the next time step. The result of an explicit method can be determined directly while an implicit method requires that the equations are solved. The advantage of an implicit method over an explicit method is that it will not show numerical instabilities whatever the time step. This is useful for stiff systems in which large changes occur at the time scale of the time step. In this thesis the transients occurring on time scales lower than one minute have not been modelled. Therefore, it is likely that the System will show only behaviour in these time scales. To summarise, an explicit method requires less computation time and is easier to implement. Therefore an explicit method was chosen for this thesis.

Method Order The order of the method determines the accuracy of the approximation with respect to the real solution. A higher order method will be more accurate than a lower order one. It is decided to implement the Runge-Kutta4 method for the numerical time integration because this method is the most efficient in terms of the amount of function evaluations for the achieved accuracy. The general form of the approximation at the new time step with Runge-Kutta4, w_{n+1} is:

$$w_{n+1} = w_n + \frac{1}{6}(k_1 + 2k_2 + 2k_3 + k_4) \quad (2.9)$$

In which w_n represents the approximation at the old time step and k_1 to k_4 are the predictor values as described by Vuik [26].

Numerical Stability The stability is different for each numerical time integration method. The method can only be stable if the initial-value problem is stable which means that the eigenvalue, λ needs to be smaller than 0. The eigenvalue can be approximated in the neighbourhood of some point (t^*, y^*) with a Taylor expansion and comparison with the test equation ($f(t, y) = \lambda y + g(t)$):

$$y' = f(t^*, y^*) + (y - y^*) \frac{\partial f}{\partial y}(t^*, y^*) + (t - t^*) \frac{\partial f}{\partial t}(t^*, y^*) = \lambda y + g(t) \quad (2.10)$$

The eigenvalue of the test equation is known to be λ . Therefore, the eigenvalue of any initial-value problem can be approximated in the point (t^*, y^*) with:

$$\lambda = \frac{\partial f}{\partial y}(t^*, y^*) \quad (2.11)$$

The eigenvalue, λ can subsequently be used in the stability requirement for numerical time integration methods which states that the amplification factor, Q , should be smaller than one ($|Q(\lambda \Delta t)| \leq 1$) [26, 27]. The stability criteria is compromised at larger time steps for Runge-Kutta4 in comparison to other explicit methods which is another reason why it is used in this thesis.

2.3.2. Root-finding

Some root-finding methods will be used to find the zero of a nonlinear equations or an intersection points of multiple equations. An example of their applications is to find the intersection point of the Solar Panel and Alkaline Electrolysis as is shown in Figure 2.10. In this thesis the bisection, fixed-point iteration and Newton-Raphson methods are used.

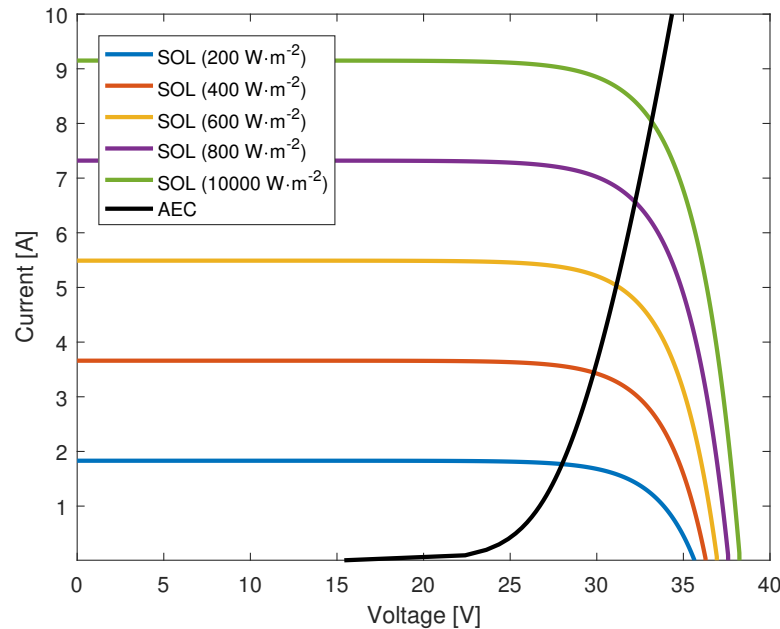


Figure 2.10: Example of how the root-finding methods can be used to find the intersection point or root of the Solar Panel (SOL) and Alkaline Electrolysis (AEC) IV-curves. The IV-curve for different levels of irradiance is shown.

Bisection This method finds the root of an equation by subdividing the interval in half each iteration. It chooses the interval to continue with based on whether the function returns a negative or positive result and continues until a manually set error has been reached. The advantage of this method is that it will always converge as long as the root falls within the interval that is searched. Because of the stability this method was implemented to find the electrical operating point of the System, in which the interval is known. The downside of this method is that it is not converging monotonously and that therefore it is slower than other methods.

Fixed-point Iteration This method finds the root of an equation or the intersection point of two equations by using the result of one equation as an input for the other. This method works very well to find the operating point of an electrical system with only the Solar Panel and Alkaline Electrolysis. This works because the Solar Panel current is a function of the voltage while the Alkaline Electrolysis voltage is a function of the current. After an initial guess of the voltage or current the result of one calculation can be used as input for the next. The fixed-point iteration is linear converging to its solution. A downside is that it does not always converge for every initial guess.

Newton-Raphson This method is the quickest method of the root-finding methods. It has quadratic convergence but only converges close to the solution. This method can thus only be used if in all situations throughout the year the method is expected to converge to a solution. This means that the initial guess has to be chosen carefully. The current of the Alkaline Electrolysis cannot be found directly from the equation quickly while this method might.

2.3.3. Interpolation

The different options for interpolation are discussed in this paragraph. They are obtained from the standard interpolation techniques that are implemented in MatLab's interpolation function. The options are Lagrange, Cubic Hermite and Cubic Spline interpolation. An overview of the results of these techniques applied to the solar irradiance is shown in [Figure 2.11](#).

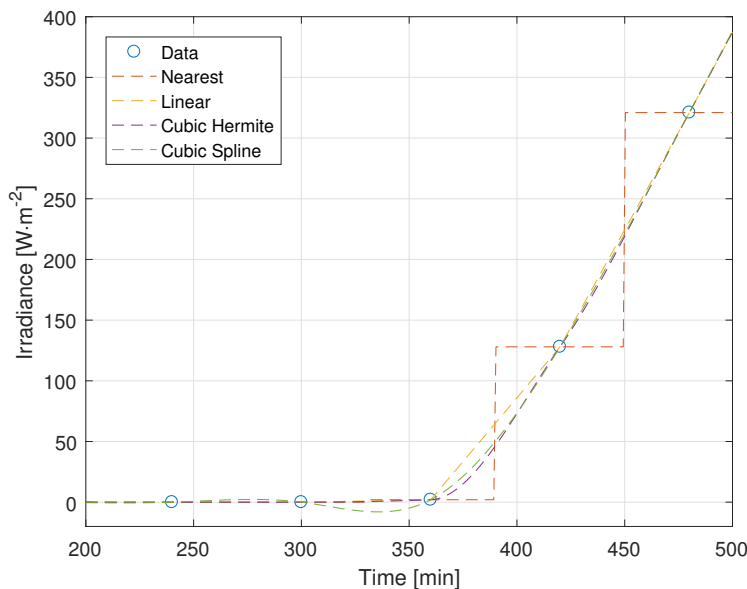


Figure 2.11: Overview of the differences of the interpolation techniques. Nearest point interpolation shows the largest errors. Linear interpolation is already closer to the expected solution but has larger errors if the direction of the curve changes. Cubic Hermite interpolation makes sure that the first derivatives are continuous but allows the second derivative to vary at the intersection point. The Cubic Spline interpolation forces the second derivative also to be continuous which results in an overshoot and wiggles around sudden change in the first derivative. The best choice to interpolate the irradiance is thus Cubic Hermite interpolation.

Lagrange Lagrange interpolation consists of constructing a polynomial of some order between two data points. In this paragraph zeroth order or constant, first order or linear and second order or quadratic interpolation are discussed. Constant interpolation takes the same value as the nearest, previous or next data point for the intermediate values. This is the easiest method to implement because the values only have to be copied for each moment in time. This method is the least accurate. A more accurate method is linear interpolation in which the intermediate values are approximated by a straight line between the data points. A higher degree of accuracy is obtained for quadratic interpolation. This type of interpolation estimates the intermediate value by drawing a second order polynomial through the data points. The downside of Lagrange interpolation is that the curves that are drawn through the data points are discontinuous in the first derivative in these data points.

Cubic Hermite Cubic Hermite interpolation is an option that makes the first derivative continuous. This function makes sure that the shape of the original function is preserved. Cubic Hermite interpolation is the most accurate of MatLab's interpolation functions to interpolate solar irradiance.

Cubic Spline Cubic Spline interpolation also makes the second derivative continuous. This technique is non shape-preserving but ideal to find intermediate values of continuously oscillating data. The fact that this function tries to make the second derivatives equal in the data points is also the downside of this method. By applying it on the solar irradiance it creates nonphysical wiggles with negative irradiances at sunrise and sunset. Therefore, this interpolation technique is not used in this thesis.

2.4. Data Collection

Data about the environmental conditions throughout the year are needed in this thesis. A few useful sources have been found. They all have different up and downsides which are discussed in this section. The three sources are SolarGIS, Meteonorm [28] and the Baseline Surface Radiation Network.

SolarGIS SolarGIS is useful for getting quick insight into average yearly irradiance through the iMaps application [29]. This software is accessible through the internet browser and is free to use. If data is desired for specific locations one has to pay. Using this software it could be determined that the desired average global horizontal irradiance of $7.00 \text{ kWh}\cdot\text{day}^{-1}$ is possible for some locations on earth. These locations are located in Chile, Namibia, the Red Sea area and Australia and are shown in Figure 2.12.

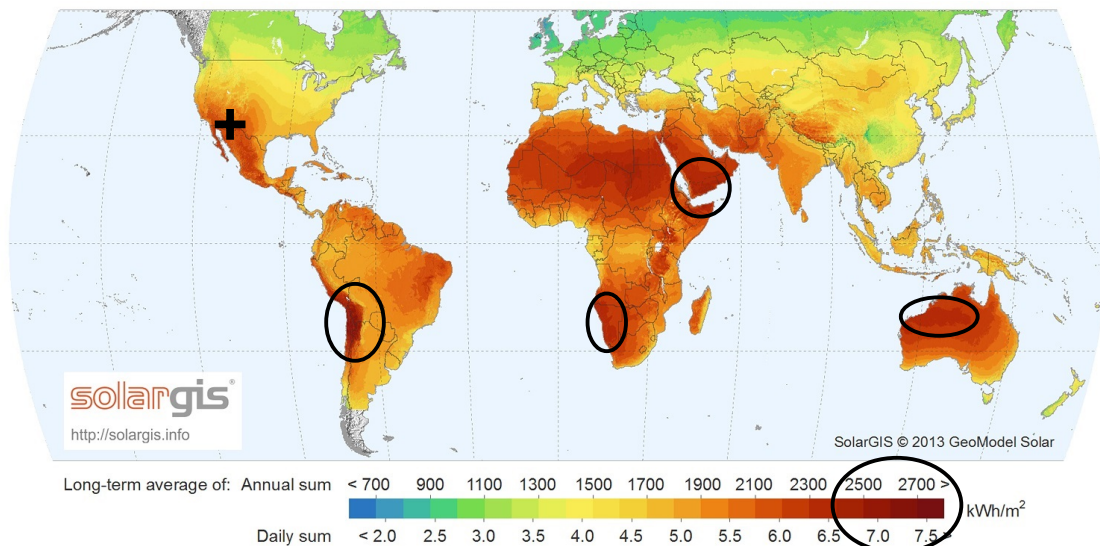


Figure 2.12: Overview of the global horizontal irradiance as provided by SolarGIS. The locations on earth having around $7.00 \text{ kWh}\cdot\text{day}^{-1}$ are indicated by the black circles [29]. The location used in this thesis, Tucson, Arizona is indicated with the black cross.

Meteonorm Meteonorm provides insight into average hourly irradiance for five predetermined locations on earth for free. This software does contain a lot of other weather stations and thus also other weather parameters like ambient, sky and ground temperatures and wind speed and direction. This software also provides data for other locations and even minute based data through payments. This software is used to obtain data for Tucson, Arizona. This location is indicated with the black cross in Figure 2.12.

Baseline Surface Radiation Network This is a research collaborative in which around 50 weather stations around the world are connected. These weather stations provide data for free to the people in the network in order to facilitate research or innovation. The data is even officially published. The weather stations measure different types of irradiances on a minute time scale. Some but not all locations also measure weather conditions like temperature and wind speed. Although the datasets from this collaboration are not investigated extensively no dataset of a full year was found which contained both irradiance as well as temperature and wind data. Another downside of this collaboration is that it only provides data for specified places on earth, which are not necessarily close to locations of interest for this thesis.

First Layer

The first layer is the System Model which makes sure that the inputs are converted into the desired outputs. The System Model interaction with the other activities of the company was introduced in [Figure 1.3](#). The nature of the inputs and the desired outputs gives information about what the System Model should do in subsequent layers.

Inputs The first input is location data for some location on earth. This data is extracted from Me-teonorm [28] for free. The data is in hours and contains information about irradiance, wind speed and temperature. The second input is given by the Subsystem Models and contains information about subsystem geometry and other parameters that are needed to describe subsystem operation.

Outputs The desired output of the System Model is the average daily methanol production and Solar Panel power. To improve design and understand the System the second desired output is the System behaviour for every minute of the year. Variables of interest are the temperature, power use or production, mass conversion and efficiencies.

Second Layer

The first layer can be separated into three steps: preprocessing, processing and postprocessing. The preprocessing step prepares the inputs such that the the model can perform the calculations in the processing step. The postprocessing step converts the results of the processing step into the desired outputs. By only doing the necessary calculations in the processing step for every minute of the year the Simulation Tool is kept as quick as possible.

Third Layer

The third layer is a more detailed version of the second layer. In the preprocessing step the data and geometries are imported and put in the right format. In this step memory is also allocated to improve the calculation speed of the processing step. The processing step forms the heart of the Simulation Tool. This is where the calculations are performed to determine the state of the System at every minute of the year. The Solar Panel power is determined, a Control model determines which subsystems are on and finally the new subsystem states are calculated. The postprocessing step makes sure that Key Performance Indicators are calculated and that plots for visual analysis are made.

Fourth Layer

The fourth layer contains the actual functions and classes that are called by the model. This layer is not shown in [Figure 3.2](#) but can be thought of as a more detailed version of the third layer.

Preprocessing In the preprocessing step the following functions are called. The data is imported from a text file, put in the right format and subsequently stored in a class that contains all the weather information of the chosen location. The data is prepared by using an interpolation function and a function which returns a subset of the data if it is desired to only model a certain day, week or month of the input data. The subsystem geometries and relevant parameters are imported and stored in classes for the subsystems with another function. Memory is then allocated to improve calculation speed and finally the initial conditions are assigned to the subsystem classes.

Processing In the processing step the time loop is called which calls four different functions each time step. The first function determines the electric power by using the incoming irradiance at that time step. The second function contains the control algorithm that determines whether the subsystems should be on or off. The third function contains the algorithm to solve the numerical difference schemes such that the new System state is calculated. The last function updates the masses in the buffers.

Postprocessing During the postprocessing one function focuses on converting the relevant subsystem states into useful outputs for the Business Case Model. Another calculates Key Performance Indicators to assess the System performance. The last function makes relevant plots of System variables for visual analysis.

3.2. Simulation Tool & System Overlap

The Simulation Tool as shown in Figure 3.2 is related to the System which is shown in Figure 2.2. Figure 3.3 shows how these two overlap. This figure provides insight into how and when different parts of the System are calculated. The preprocessing step makes sure that data is imported and prepared and that memory is allocated such that the processing step the state of the System can be calculated for every minute of the year. In the processing step the Solar Panel, Control and Plant are involved in the calculations. The postprocessing step has no physical representation with the System but makes sure that Key Performance Indicators are calculated and that Plots are made for visual analysis such that different Systems can be compared based on their performance. This figure is used in chapter 4 to guide the reader through the implementation of the System in the Simulation Tool.

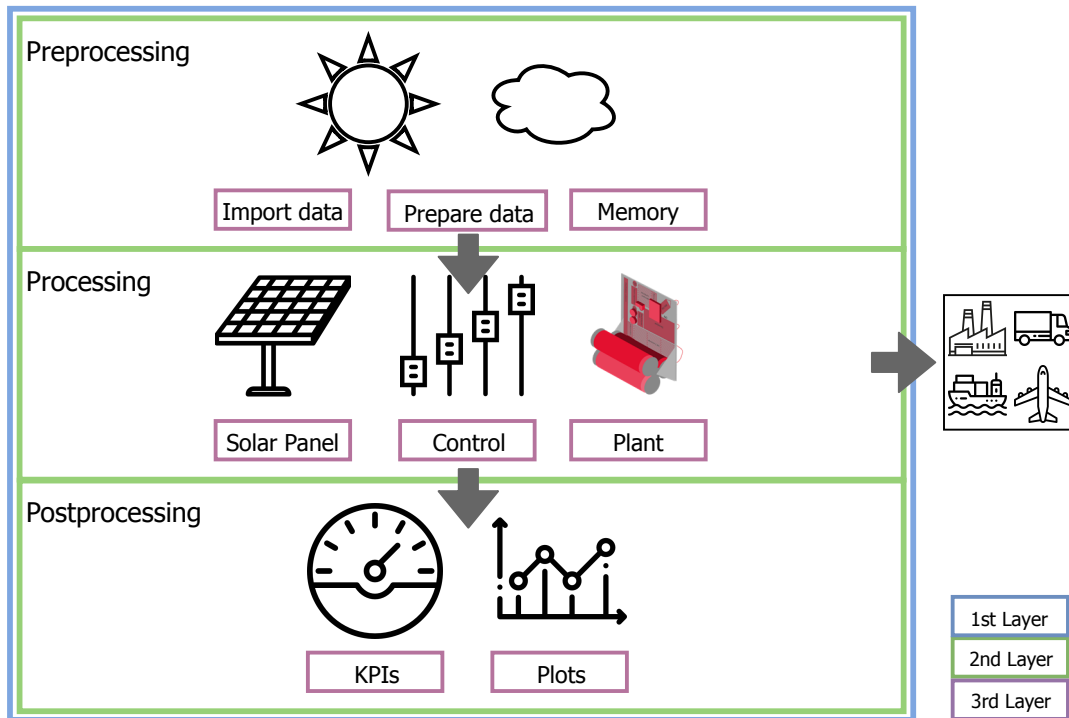


Figure 3.3: Schematic overview of the overlap of the Simulation Tool (Figure 3.2) and the System (Figure 2.2). The preprocessing step of the Simulation Tool is related to the external data and allocating memory. In the processing step the System behaviour is calculated for each minute of the year. The postprocessing step has no overlap with the physical System or the Environment but is used to analyse the results.

4

System Implementation

This chapter contains the second step in the main body of this thesis, as is shown in [Figure 4.1](#). It discusses the implementation of the System into the Simulation Tool. As can be seen in the figure showing the overlap of the System design and Simulation Tool, [Figure 3.3](#), this chapter will subsequently discuss the preprocessing, processing and postprocessing steps. In those sections all the relevant functions that are implemented will be discussed.

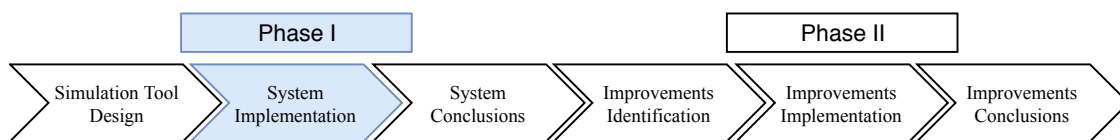


Figure 4.1: The second part of the main body of the thesis focuses on the implementation of the System into the Simulation Tool.

4.1. Preprocessing

The preprocessing step as shown in [Figure 4.2](#) is discussed first. The function of this step is to initialise the Simulation Tool such that the calculations in the processing steps can be executed continuously without interruption. These steps include importing and preparing data, allocating memory and storing them in classes such that calculated variables can easily be analysed. An overview of the parameters that are used in the models of the preprocessing is shown in [Appendix B](#).

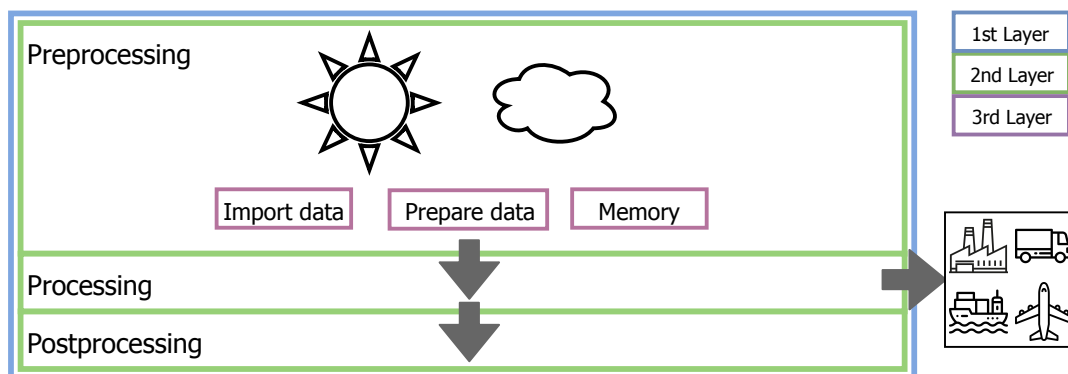


Figure 4.2: This section focuses on the preprocessing step of the Simulation Tool.

4.1.1. Import Data

Software called Meteonorm [28] was used to obtain the input data. Only for some locations on earth the data could be extracted for free. The location that is chosen to test the model is Tucson, Arizona because it has the highest irradiance. The data consists of global horizontal (GHI), direct normal (DNI) and diffuse horizontal (DHI) irradiances, pressure, ambient temperature, wind speed and the longitude and latitude of the exact location of the weather station.

Interpolation The data is given in hours but minute based data is needed for the model. Interpolation is applied to fix this. Cubic Hermite interpolation was chosen because it matched the irradiance pattern more accurate than constant, linear or cubic spline interpolation. The smoothness of the irradiance curve is related to the continuous change in relative position of the sun and earth.

Discussion It has to be noted that interpolation is not able to reconstruct the expected minute based changes like the passage of small clouds. To fix this more accurate data can be bought from Meteonorm or SolarGIS [28, 29]. Another possibility is to implement a stochastic modelling technique to predict minute data from hourly data. This is described in the papers of both Remund and Hoffmann [30, 31]. The main idea of their approach is to add a stochastic signal to the values predicted with interpolation. This signal gets different intensities based on the weather type of that day: sunny, cloudy or in between.

4.1.2. Prepare Data

The models that are used in the program need more input data than is available. The variables that are estimated in this subsection are the sun position, sky and ground temperatures, corrected solar irradiance, and the optimal Solar Panel angles.

Sun Position

The sun position is determined by using an approach suggested by Smets [8]. This approach calculates the position of the sun based on the current date and the trajectory of the sun which is determined with the Julian date. The accuracy is within arcminutes for 200 centuries around the year 2000 [8]. The result is shown in Figure 4.3.

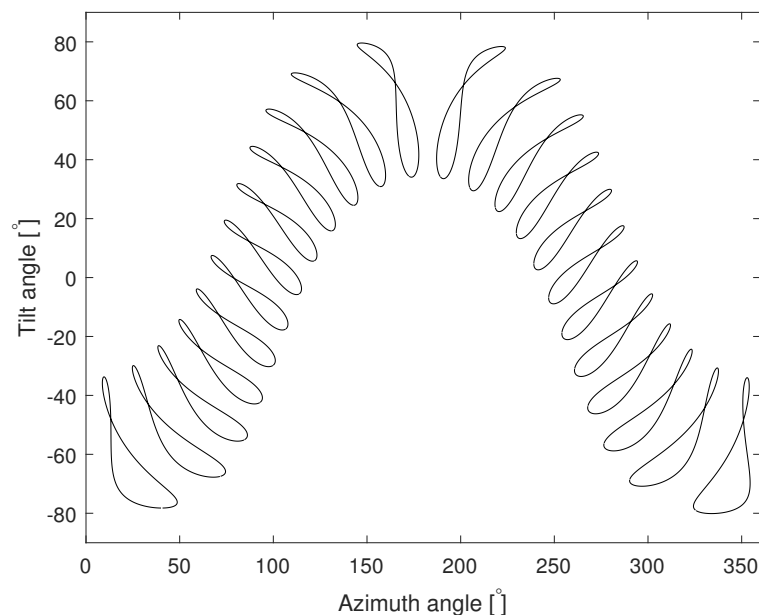


Figure 4.3: Sun analemmas for every hour of the day in Tucson Arizona, 2005. This figure shows 24 analemmas: one for every hour of the day. One analemma consists of 365 data points: one for every day. One data point represents the sun height and azimuth angle for a specific hour of the year.

Sky & Ground Temperatures

The second variables that are estimated are the sky and ground temperatures. The ground temperature is set equal to the ambient temperature. The sky temperature is determined with an approach suggested by Swinbank [32]:

$$T_{\text{sky}} = 0.0552T_a^{3/2} \quad [\text{K}] \quad (4.1)$$

Discussion In reality the ground temperature will differ from the ambient temperature because it is also influenced by the ground beneath the surface. As stated by Swinbank the relation for the sky temperature is only valid for clear skies [32]. Therefore, it is only applicable for moments of the day without cloud coverings. In the data a significant amount of cloudy days is observed. At those days the sky temperature should be closer to the ambient temperature than is predicted with this model.

Corrected Solar Irradiance

The global horizontal irradiance, GHI in Tucson, Arizona does not match the business case assumption of $7.00 \text{ kWh}\cdot\text{day}^{-1}$. In 2005 only $5.65 \text{ kWh}\cdot\text{day}^{-1}$ was available there. It is investigated whether a linear scaling can be implemented to correct this. There are three different types of irradiance, global horizontal irradiance, GHI, direct normal irradiance, DNI and diffuse horizontal irradiance, DHI. These three types of irradiance are shown in Figure 4.9 and related via this equation:

$$\text{GHI} = \cos(\theta)\text{DNI} + \text{DHI} \quad (4.2)$$

in which θ is the tilt angle of the sun in respect to a flat plane on the earth. From this equation it can be derived that the irradiances depend linear on each-other which means that all three types of irradiance data can be scaled using a scaling-factor, $S_{\text{irradiance}}$. This factor is determined by dividing the desired GHI with the actual GHI:

$$S_{\text{irradiance}} = \frac{\text{GHI}_{\text{desired}}}{\text{GHI}_{\text{actual}}} = \frac{7.00}{\text{GHI}_{\text{actual}}} \quad (4.3)$$

The resulting scaling factor for Tucson, Arizona is 1.24. The difference between the GHI data and the corrected GHI data for a random day of the year is shown in Figure 4.4.

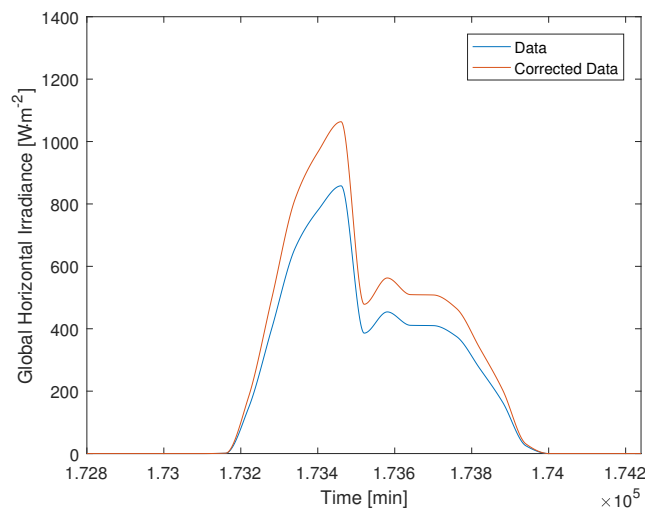


Figure 4.4: This figure shows how the irradiance data is corrected. In Tucson, Arizona the scaling factor is 1.24 to correct the average of $5.65 \text{ kWh}\cdot\text{day}^{-1}$ to $7.00 \text{ kWh}\cdot\text{day}^{-1}$.

Discussion The downside of this approach is that the irradiance data is increased by 24 % without taking into account variations in the amount of sun hours or sun position. For example, the hours that the sun is above the horizon and its height might be different from locations that actually have the desired GHI. The result is that a different amount of sun hours need to give 24 % higher irradiance. This means that the irradiance intensity increases to values that might not be physically realistic. Another shortcoming of this approach is related to differences in weather conditions. The higher amount of irradiance in other locations might not be due to variations in sun hours but due to other weather conditions. For example, other locations might have less cloudy days due to the presence of mountains like in Chile. The approach with the scaling factor is used because it will make sure that the energy input of the system more closely represents the business case assumption.

Solar Panel Angle Optimisation

During the preprocessing step the optimal Solar Panel angles need to be determined in order to maximise the MeOH production. An overview of these angles is found in the book of Smets and shown in Figure 4.5 [8]. These angles have to be optimised because they always positively influences the methanol production of the System because more sunlight will fall onto the Solar Panel. The angles only have to be determined once because the Solar Panel is assumed fixed in this thesis.

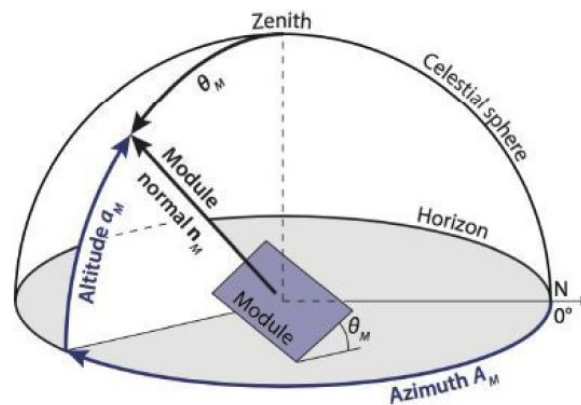


Figure 4.5: Illustration of the angles used to describe the orientation of a Solar Panel installed on a horizontal plane as found in the book of Smets [8]. The Solar Panel is indicated as "Module" in the figure. The azimuth, A_M and tilt, θ_M angles describe the Solar Panel orientation.

Algorithm The algorithm determines the optimal Solar Panel angles by calculating the amount of irradiance that falls on the Solar Panel. It does this for every minute of the year while varying the tilt angle from 0° to 90° and the azimuth angle from 0° to 360° . The average daily irradiance for all these angles is shown in Figure 4.6. The optimal tilt angle is 63° and the optimal azimuth angle is 165° .

Discussion The downside of this algorithm is that it needs to calculate the Solar Panel irradiance for all angles. Since the solution space forms a continuous solution with only one optimum the optimal angle can be determined quicker by using optimisation algorithms. A genetic algorithm was able to determine the optimal angle within a precision of $0.5 \cdot 10^{-6}$ within 40 seconds while the original algorithm took 240 seconds to find the optimal angle within a precision of 0.5° . Since the solution is a continuum with only one maximum optimisation algorithms that use the derivative are thought to be even faster than the genetic algorithm. The optimal Solar Panel angles need to be determined only once for every location on earth so using these optimisation algorithms is only fruitful if many different locations on earth are to be simulated after each-other.

It has to be noted that the optimal Solar Panel angle is determined by using the sun irradiance data for 2005. In different years the weather might be different which could influence the optimal angles slightly. Therefore, optimising the angle to a much higher accuracy based on this data set might not improve the output of different years significantly.

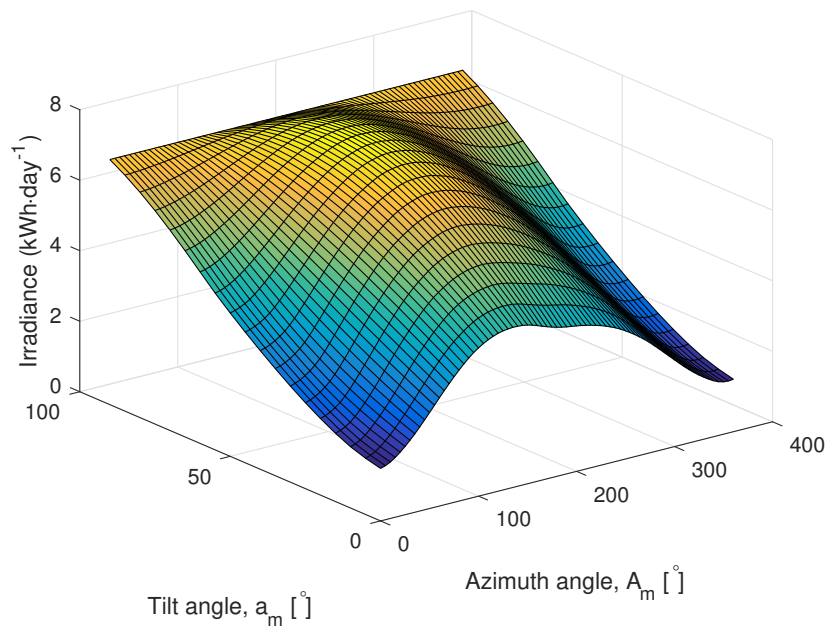


Figure 4.6: Solution space of the solar panel irradiance in Tucson, Arizona as function the tilt and orientation angles determined for a grid with 5° by 5° . The optimal tilt angle is 65° and the optimal orientation angle is 165° .

4.1.3. Allocate Memory

The final step of the preprocessing step is to allocate memory by creating vectors and filling them with zeros. This is done to improve calculation speed during the processing step. These vectors are grouped in so called classes to make it easier to interpret the results and analyse behaviour. Finally the first values of these vectors are filled by defining the initial conditions.

Classes There are four different classes used in the Simulation Tool. The first one contains all the information of the location like weather data and the location on earth. This class is called "InputData". The advantage of this is that it will be easy to add or create locations when new data sets get available. The second class contains all the variables of the subsystems. It is called "SubSystem". Since each subsystem has roughly the same variables one instance of this class is created for each subsystem. The third class is a subclass of the SubSystem class and contains all the relevant geometrical information. This class is called "Geometry". The fourth class is a separate class and contains all relevant properties of the materials used. This class is called "Material". Most of the material properties are assumed constant. If they were not constant they have been approximated by taking the average value over the typical range of operation of a certain subsystem.

Initial Conditions The initial conditions are needed because a numerical difference scheme is used to determine the new value of some of the calculated variables. The initial conditions of all subsystems are set equal to the values of the weather data for temperature and pressure.

4.2. Processing

The next step is to focus on the processing step of the Simulation Tool. This is shown in [Figure 4.7](#). In the processing step the System state is calculated for every minute of the year. First the input power is determined with the Solar Panel model. Then the Control model distributes this power to the subsystems. Finally, all new subsystem states are calculated based on the inputs they receive. This section discusses these three main steps of the processing step. The models that are used to update the subsystem states are also introduced in this section. All subsystems models that are discussed in this section follow the same outline. First the subsystem is introduced after which it is described how the subsystem operates. Then the functions that are implemented to calculate the subsystem state are discussed shortly. Every subsystem model ends with a paragraph in which the shortcomings or results of the model are discussed. An overview of the parameters that are used in the models is shown in [Appendix B](#).

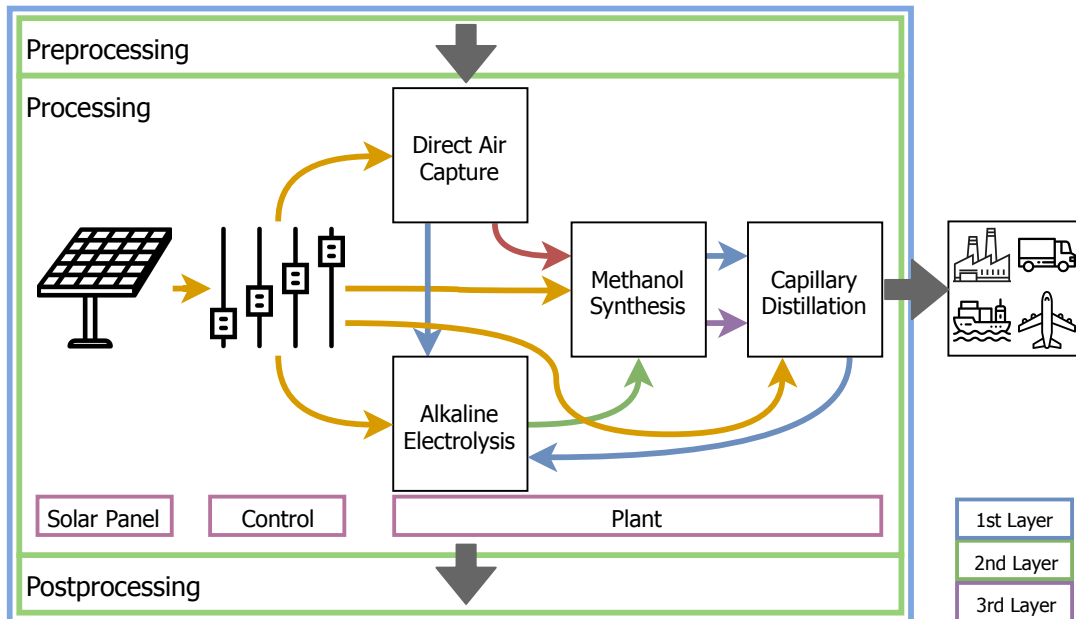


Figure 4.7: This section focuses on the processing step of the Simulation Tool. The amount of power is calculated, and a control algorithm determines which subsystem is on and which is off. Finally the subsystem states are updated.

4.2.1. Solar Panel

The main function of the Solar Panel model is to produce an IV-curve. This IV-curve is subsequently used in the Control model to find the electrical operating point of the System and thus the power output of the Solar Panel. To do this three functions are needed as shown in Figure 4.8. The Irradiance function converts the irradiance data into the irradiance that falls onto the Solar Panel. The Energy function determines the temperature of the Solar Panel by solving the energy balance. Finally, the IV-curve function translates the temperature and irradiance into the IV-curve.

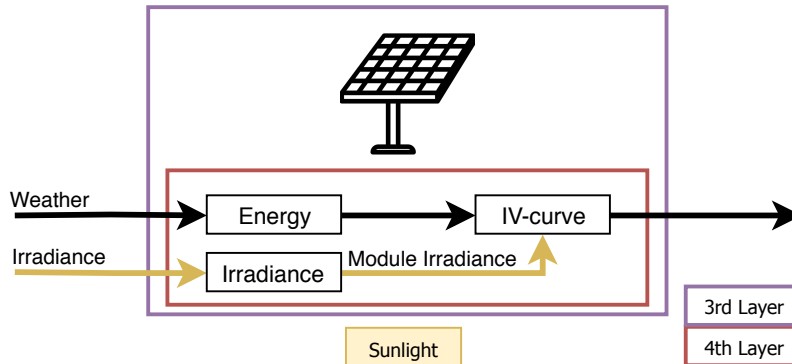


Figure 4.8: Schematic overview of the Solar Panel model and the functions it contains in the fourth layer of the Simulation Tool. The temperature and irradiance on the Solar Panel are determined such that the IV-curve can be calculated.

Operation Modes The Solar Panel automatically switches between on or off depending on whether sunlight falls onto it or not.

Irradiance Function The Irradiance function combines the irradiance data with the sun and Solar Panel tilt and azimuth angles to find the total irradiance on the Solar Panel as shown in Figure 4.9. The total Solar Panel irradiance is a combination of three types of irradiance: direct, diffuse and ground reflected. The projection of the vector pointing towards the sun on the vector representing the Solar Panel orientation determines the direct irradiance, \dot{G}_{dir} . To find the diffuse irradiance, \dot{G}_{dif} , the percentage of the Solar Panel oriented towards the sky, the Sky View Factor, is used. The ground reflected radiation, \dot{G}_{gnd} , is determined with the Sky View Factor and the albedo. The result of this function for two random days of the year is shown in Figure 4.10. As expected the three separate irradiances that fall onto the Solar Panel follow the same pattern as the three separate irradiances found in the data.

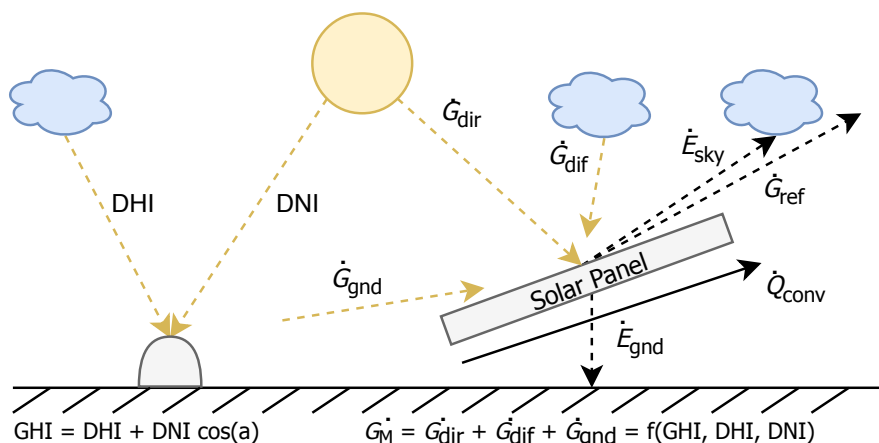


Figure 4.9: Solar Panel model to determine heat exchange of the Solar Panel with the environment. The Solar Panel irradiance, \dot{G}_M comes from the sun directly, \dot{G}_{dir} , via diffuse light, \dot{G}_{dif} and via reflection of the ground, \dot{G}_{gnd} . A part of this irradiance is reflected, \dot{G}_{ref} . At the same time the Solar Panel emits radiation to the sky, \dot{E}_{sky} and ground, \dot{E}_{gnd} . The Solar Panel is also subjected to convection, \dot{Q}_{conv} .

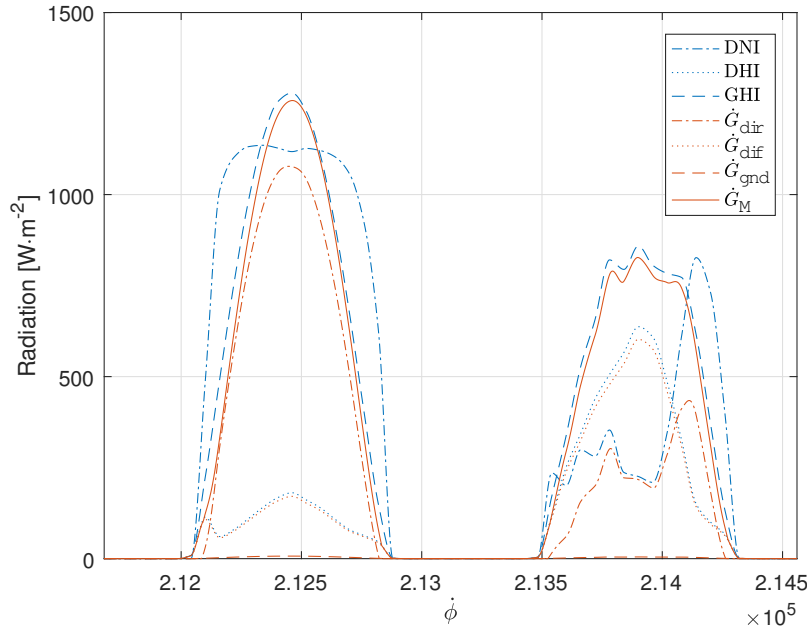


Figure 4.10: Corrected irradiance data (blue) is converted with the Irradiance function to Solar Panel irradiance (orange). The three different types of irradiance data relate to the three different components of the Solar Panel irradiance. The global horizontal irradiance and the ground reflected irradiance are similar just as the direct normal irradiance and the direct Solar Panel irradiance and the diffuse horizontal irradiance and the diffuse Solar Panel irradiance. In the second plotted day it can be observed that when the direct normal irradiance drops the diffuse horizontal irradiance increases since more light is reflected by the clouds.

Energy Function The temperature is determined by solving the energy balance of a self constructed simplified geometrical model. The model is shown in Figure 4.9. This was done since it allows for leaving out details or aspects that are unknown for now. As described in section 2.3 Runge-Kutta4 is used to solve the energy balance:

$$\frac{dT_{\text{sol}}}{dt} = \frac{1}{m_{\text{sol}}c_p}(\dot{Q}_{\text{sol}} - \dot{W}_{\text{sol}}) \quad (4.4)$$

T_{sol} represents the temperature of the Solar Panel, t the time, \dot{Q}_{sol} is the heat exchange with the environment. This term is determined by combining radiation and convection effects on a flat plate geometry. The conduction through the support structure is neglected since no information about this structure is available. \dot{W}_{sol} represents the power produced by the Solar Panel. This term is determined by the electrical operating point of the System. The mass of the panel, m_{sol} , as well as the heat capacity, c_p are estimated by assuming that the whole Solar Panel is made of glass. The values for these parameters can be found in Appendix B.

IV-curve Function The Solar Panel irradiance and temperature are then converted into an IV-curve using the approach of Villalva and Ortiz-Rivera [9, 12]. This approach is chosen because it is able to predict the electrical performance of the Solar Panel based on parameters found in the datasheet. This perfectly suits the purpose of this thesis because it predicts the performance by using known and realistic parameters. The approximated datasheet using this method is shown in Figure 4.11. The predicted IV-curves do not differ visually from the ones in the datasheet.

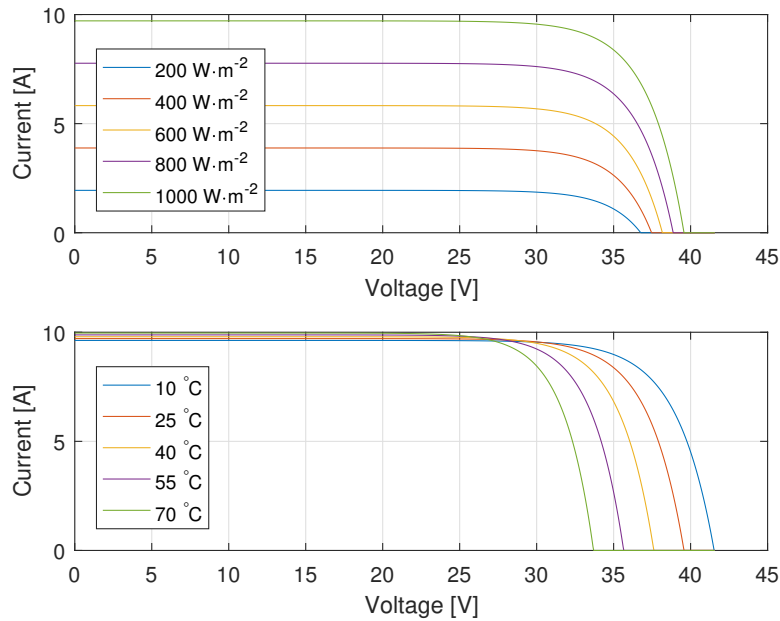


Figure 4.11: Solar Panel datasheet predicted using the approach suggested by Gradella Villalva and Ortiz-Rivera [9, 12]. The upper plot shows the IV-curves as function of different irradiances at Standard Test Conditions (STC). The lower plot shows the IV-curves as function of different temperatures at $1000 \text{ W}\cdot\text{m}^{-2}$.

Discussion The IV-curve function is able to estimate real behaviour with a high accuracy because it is designed to match the datasheet provided by the manufacturer. This approach makes it ideal to compare performance of different Solar Panel types from different manufacturers in future research. It has to be noted that the accuracy cannot be determined quantitatively because no data points are given in the datasheets. The insecurities in the IV-curve function are the sun position because it is determined with a model and the albedo because it differs for different types of soil and Solar Panel park configurations.

The accuracy of the IV-curve depends on the accuracy with which the Solar Panel temperature is determined by the Energy function. This function also contains some insecurities. The radiative heat exchange with the sky and the ground are based on estimated sky and ground temperatures not on data. A possibility to verify the approximated sky and ground temperatures is to compare them with paid datasets from Meeonorm. The convective heat transfer coefficient is based on an empirical equation provided by Engineering Toolbox [33]. This equation is only valid in the range from 2 to 20 $\text{m}\cdot\text{s}^{-1}$. Furthermore, this coefficient does not take into account any effects of geometry, angles or positioning near other objects. The Energy function approximates the Solar Panel by assuming it only consists of glass with a uniform temperature. Thermal conduction through the layers of the Solar Panel is not incorporated. The conduction through the mounting structure is also not taken into account. More details can be incorporated into the Energy function by following the approaches suggested by Mattei [13], Armstrong [14] or Caluianu [15].

The predicted temperature is not verified in this thesis. It is advised to check its accuracy with two checks first before spending time on a new model. The first one is to determine whether the maximum and minimum calculated temperatures are in the same order of magnitude as described in literature. The second is to see whether the predicted temperature change rates match literature. This can be investigated by comparing the step responses of experimental data and this Solar Panel model.

4.2.2. Control

The main function of the Control model is to determine the operation Modes of all the subsystems and to distribute the power that is provided by the Solar Panel to the subsystems. An overview of the Control model is shown in Figure 4.12. The Power function determines how much power is available by finding the intersection points of the IV-curve of the Solar Panel and Plant. The Decision function subsequently decides the operation Mode of each subsystem and distributes the power to them.

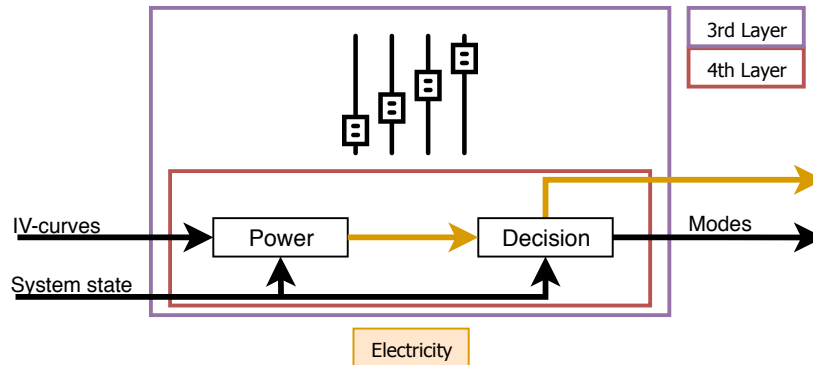


Figure 4.12: High level overview of the Control Model. The Power function determines the electrical operating point of the System. The Decision function subsequently distributes this power over the different subsystems and decides based on the previous System State what the new operation Mode of each subsystem will be.

Power Function The power function determines the power of the Solar Panel by finding the intersection point of the IV-curve of the Solar Panel and Alkaline Electrolysis. It is decided to only incorporate this subsystem because it is expected that it uses the most energy. Furthermore, the electrical characteristics of the other components have not been designed yet and are thus difficult to implement. The resulting electrical circuit is shown in Figure 4.13.

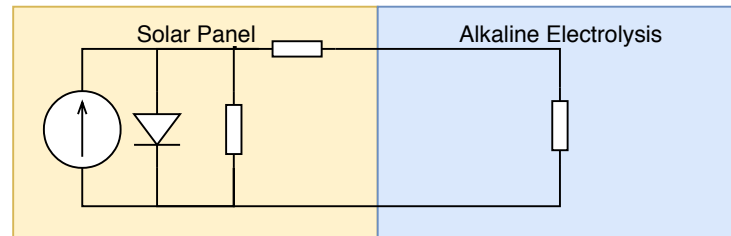


Figure 4.13: The equivalent electrical circuit used to determine the electrical operating point of the system. The Alkaline Electrolysis is coupled directly to the Solar Panel in order to prevent the need for a battery or a power distribution device.

The electrical operating point is determined with the approach suggested by Rahim [10]. This approach takes the characteristic equations of both the Solar Panel and Alkaline Electrolysis and finds the intersection point of them. This is shown in Figure 4.14. Since the characteristic equations are functions of each-other they are suitable for the fixed-point iteration root-finding method. The starting point for the fixed-point iteration is chosen to be the maximum power point because it is close to the root if the Alkaline Electrolysis is designed correctly. The electrical operating point of the system is as accurate as the root-finding method threshold that is implemented. If 0.1 % deviation in power is allowed this means that at maximum operation conditions of 400 W the error is allowed to be 0.4 W. The Solar Panel then runs at around 10 A which means that the error in voltage should be smaller than 0.04 V. The voltage error threshold is set to 0.01 V.

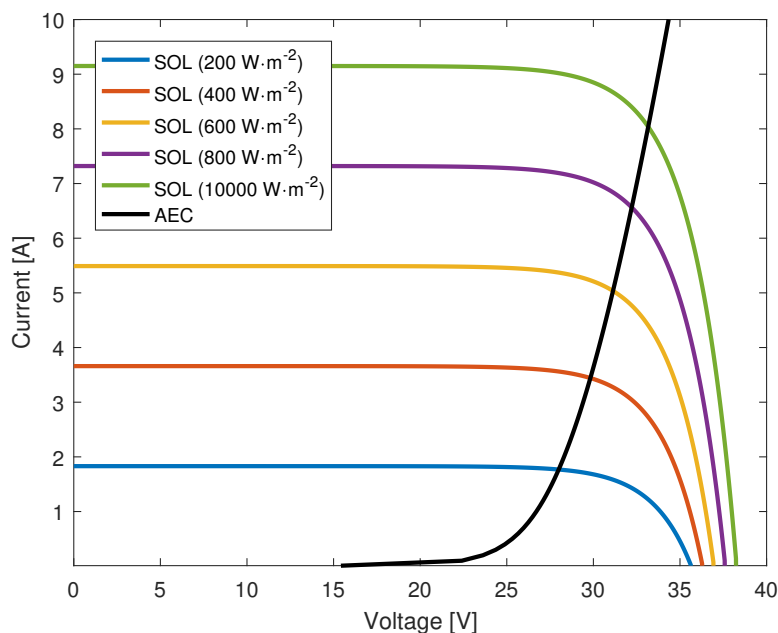


Figure 4.14: IV-curves of the Solar Panel (coloured) at different irradiances and the Alkaline Electrolysis (black). The intersection point of the IV-curves of the two subsystems is the electrical operating point that is determined with a fixed-point iteration algorithm.

Decision Function The Control model then chooses which subsystem is turned on or off. In order to be able to verify whether it behaves correctly it is decided to implement an easy to understand Decision function. The function takes the power of the Solar Panel and distributes it over the subsystems based on a manually assigned hierarchy. This means that the subsystem that is highest in the hierarchy first receives all the power it needs. If some is left it goes to the next one until all power is used. The hierarchy in descending order is: Control, the first chamber of the Direct Air Capture, heating up the Methanol Synthesis reactor, Capillary Distillation, the second chamber of the Direct Air Capture and finally the Alkaline Electrolysis. The Alkaline Electrolysis always receives the remaining power to make sure none is wasted. The Control model always gives priority to the first Direct Air Capture chamber because it has to make sure that the chambers can never adsorb, desorb or cool at the same time because there is only one fan, one heater and one cooling device available. To simulate the energy need of the devices used to control the System, like sensors, processors and actuators, it is assumed that 5 Watt is needed. An additional advantage of this hierarchical Decision function is that it allows for implementation of new subsystems one after the other without changing the behaviour of previous ones.

Discussion A downside of the Power function is that the electrical characteristics of only one subsystem are incorporated. This might result in non-physical results in which certain subsystems could receive a different amount of energy compared to the amount it would have gotten if it would participate in the electrical circuit. It is expected that the Power function still provides a good insight in the significance of any losses that might arise from the mismatch between the IV-curves of the Plant and the Solar Panel.

Considering the root-finding method the convergence speed is important to keep the simulation time within the predetermined maximum of 15 minutes. Fixed-point iteration does not converge as quickly as Newton-Raphson. Another downside of this method is that it does not converge for every initial-guess. To prevent this the Alkaline Electrolysis IV-curve is restricted to certain bounds.

The downside of the decision function is that it does not make the model flexible or reactive to specific situations. Using this approach it can be imagined that the Direct Air Capture is switched on while the CO₂ buffer is full.

4.2.3. Direct Air Capture

The Direct Air Capture model must predict how much CO₂ and H₂O are adsorbed and desorbed. This model is shown in Figure 4.15 and uses two functions. The Energy function determines the temperature in each chamber. This temperature is subsequently sent to the Mass function in which the amount of adsorbed or desorbed components is determined. An overview of the parameters used in these functions can be found in Appendix B.

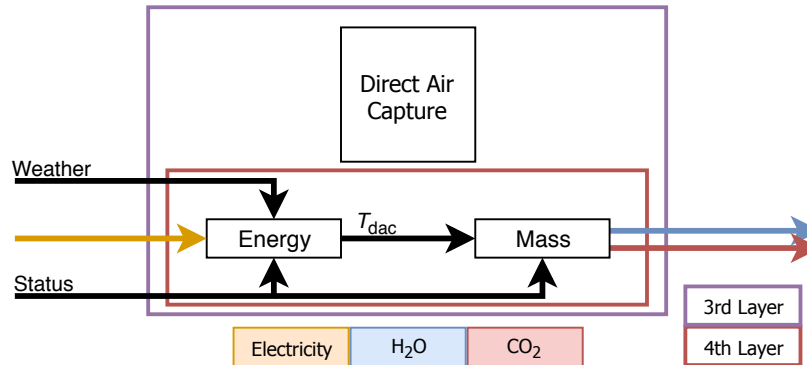


Figure 4.15: High level overview of the Direct Air Capture model. First the temperature is determined with the Energy function which is then used to determine the adsorbed or desorbed mass with the Mass function.

Operation Modes The Direct Air Capture chambers know 4 different Modes. If no power is available the Direct Air Capture is off. If power is available the chambers are adsorbing, desorbing or cooling. This paragraph describes how the Direct Air Captures alternates between these Modes.

Adsorption The loading of the sorbent is calculated for every minute of the year. It can therefore be determine whether the sorbent is saturated. Adsorption starts as soon as power becomes available and the sorbent is not saturated. The power is sent to a fan that blows air through the monolith. The temperature is equal to the ambient temperature and the pressure to the ambient pressure.

Desorption Desorption starts when the adsorbent is saturated. During desorption the chamber is sucked vacuum and the heater is turned on in order to increase the temperature. It is assumed that the pump creates a vacuum of 0.1 bar instantly. It is assumed that any gases that are desorbed are immediately removed from the chamber. Desorption stops as soon as the predetermined temperature of 120 °C is reached. This temperature is chosen because at that temperature almost all components are desorbed and above it the adsorbent will deteriorate.

Cooling The last operation Mode is cooling. No adsorption or desorption occurs because the doors are closed until the chamber is again colder than 40 °C. This is needed to prevent undesired reactions of the adsorbent with oxygen. The pressure is assumed to stay at 0.1 bar.

Energy Function The Energy function calculates the temperature of the Direct Air Capture chambers. This is done by discretization and subsequent solving of the Energy balance using Runge-Kutta4. The geometry of the Direct Air Capture chamber is simplified into a multi-layered cylinder, which is shown in Figure 4.16. The monolith is surrounded by the heater and a final layer of insulation. The heat loss is only determined in radial direction. The sides are assumed well insulated. The heat exchange with the environment is determined by solving a heat resistance network with a total thermal resistance of 10 K·W⁻¹.

Mass Conversion Function The Mass conversion function calculates how much CO₂ and H₂O is present in the Direct Air Capture chambers at any moment in time. To do this the adsorption Isotherms need to be determined since they determine the saturation loading of the adsorbent. In the adsorption stage the Fan determines the airflow through the monolith and thus the adsorption. The isotherms and fan are discussed next.

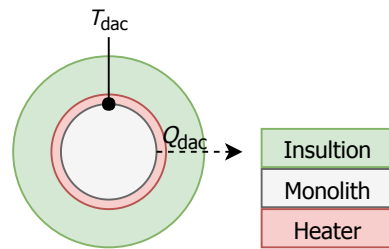


Figure 4.16: Overview of the different layers of the simplified Direct Air Capture subsystem. The heat loss, \dot{Q}_{dac} , is determined each time step with a thermal resistance network with an overall thermal resistance of $10 \text{ K}\cdot\text{W}^{-1}$.

Isotherms The amount of components the adsorbent can adsorb is depending on the temperature and pressure. Until experiments have been conducted on the activated carbon monolith with PEI the Toth-equation for the SiO_2/PEI adsorbent as described by Sutanto will be used to model the sorbent loading [2]. The resulting CO_2 isotherms are shown in Figure 4.17. It is assumed that by influencing the weight percentage PEI the adsorbent is able to adsorb CO_2 and H_2O in the desired ratio of 1:3.

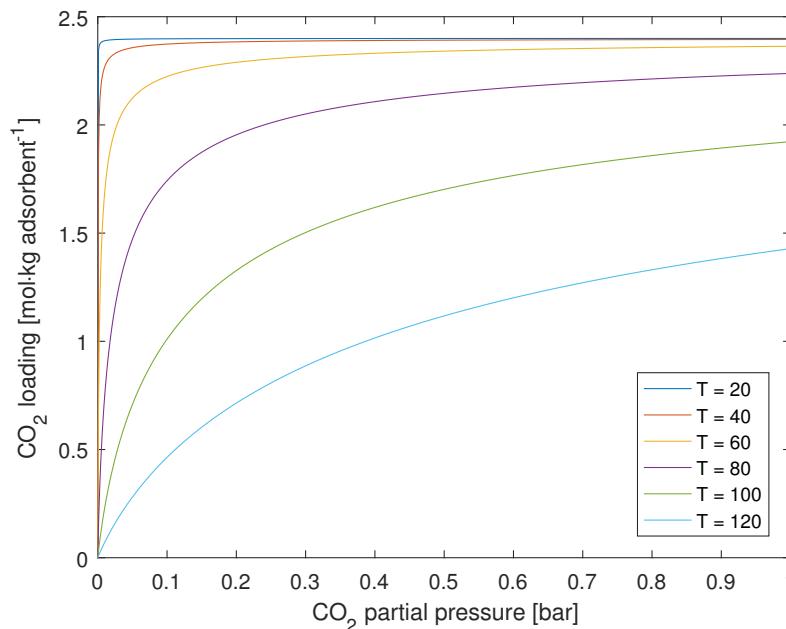


Figure 4.17: Isotherms of CO_2 adsorption on a SiO_2/PEI adsorbent obtained from the approach described by Sutanto [2].

Fan In the adsorption stage a fan blows air through the monolith. The amount of air going through the monolith is important because it is assumed that the adsorption is limited by the amount of gases passing through as long as the adsorption process takes around 15 minutes. This is described in more detail in subsection 2.2.3. To estimate the air passing through an experiment is performed to measure the pressure drop. This pressure drop is subsequently used to determine the volumetric air flow with the datasheet of a 15 W fan (Sunon model PMD1212PMB2-A). Specifically the air flow-static pressure characteristics are used. It was found to be $0.7 \cdot 10^{-2} \text{ m}^3 \cdot \text{s}^{-1}$. To allow for any inefficiencies of the fan or air passing through without getting close to the monolith a performance factor was added of 0.1. This means that it is assumed that 10 % of the CO_2 passing through the monolith is actually adsorbed.

Verification The Direct Air Capture model is verified by doing a test run on one day. The results are shown in Figure 4.18. The upper plot shows the maximum and actual sorbent loading of CO₂ in both chambers. The lower plot shows the operating Modes of both chambers. The intended working of the model is achieved since the chambers are never in the same operation Mode and there is alternation between Modes if the thresholds are exceeded. The model switches from off to adsorbing if power is available, from adsorbing to desorbing if the sorbent is full, from desorbing to cooling if the maximum temperature for desorption is reached and from cooling to adsorbing if the minimum temperature for adsorption is reached. Furthermore, due to the priority of the first chamber the second chamber goes through less cycles. The adsorption takes 25 minutes and each cycle around 0.25 mole CO₂ and around 0.75 mole H₂O is adsorbed. The desorption takes 10 minutes and the cooling 15 minutes. This means that less is absorbed per cycle than determined with the steady-state model: 0.42 mole CO₂ and 1.25 mole H₂O. This is partially balanced with more cycles: 20 instead of 16.

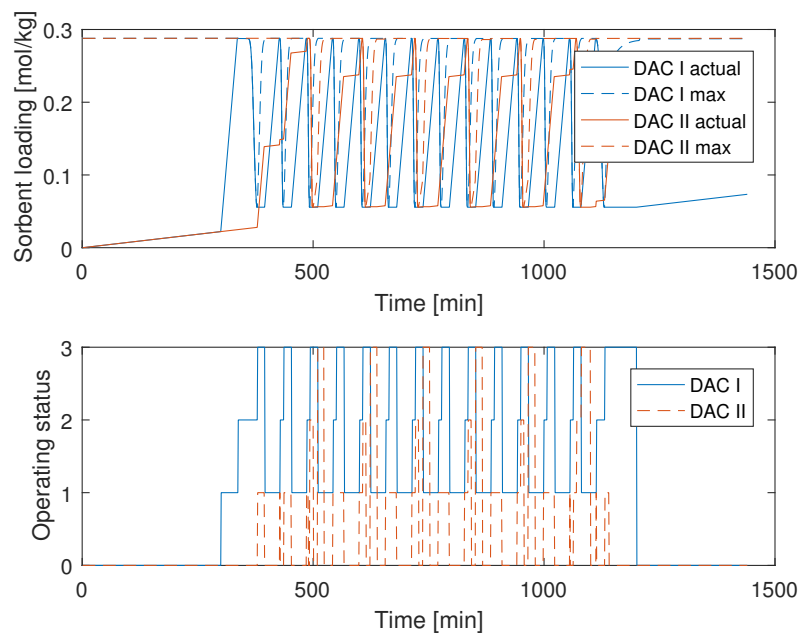


Figure 4.18: Results of the Direct Air Capture model during one day. The upper plot shows the maximum and actual sorbent loading of CO₂ in both chambers. The lower plot shows the operating status of both chambers: 0 = off; 1 = adsorbing, 2 = desorbing and 3 = cooling. The intended working of the model is achieved since the chambers are never in the same operating condition and there is an alternation between statuses if the programmed thresholds are exceeded. The model switches from off to adsorbing if power is available, from adsorbing to desorbing if the sorbent is full, from desorbing to cooling if the maximum temperature for desorption is reached and from cooling to adsorbing if the minimum temperature for adsorption is reached.

Discussion The Direct Air Capture properly shifts from one Operation Mode to the next based on the predetermined thresholds. In reality these values need to be measured by sensors. Measuring temperature is widely known but a sensor that measures the saturation of the adsorbent is not. This needs to be derived from indirect measurements. The incoming CO₂ concentration can for example be compared to the outgoing one which is a measure for whether adsorption is still occurring. Another possibility is to set a timer on the adsorption.

Energy Function The Energy function assumes that all heat produced by the heater is distributed to the monolith. The monolith is made from carbon which has a reasonable heat conduction. Therefore, it was assumed that a homogeneous temperature distribution would be the result. However, conduction can only occur in the monolith through the thin walls. It was observed that this causes an undesired temperature gradient to develop over the monolith. For the model to be valid as well as for the real performance the design of the monolith and heater should be such that the heat is distributed quicker. This makes sure that the whole monolith is desorbed at the same time and prevents local hotspots at locations where the monolith is in contact with the heater.

Isotherms The Direct Air Capture model represent the SiO₂/PEI adsorbent not PEI on activated carbon. As already been pointed out, the isotherms need to be determined experimentally for every combination of adsorbent, support structure and solute. The method to measure the isotherms is described in subsection 2.2.3. If the results of the experiments come in the parameters of an isotherm equation should be fitted onto the data. The type of adsorption that is observed determines which equations suits best. It is expected that the isotherms are similar to the SiO₂/PEI ones. However, they might adsorb more per kg because of the higher pore size and thus area of activated carbon in comparison with SiO₂. It also needs to be pointed out that Sutanto explicitly stated that they fitted the data for the temperature range of 60 - 120 °C. Below it they saw different behaviour.

The model assumes that all desorbed gases are removed from the chambers directly by the Fluid Machinery during desorption. No gases will thus accumulate and the pressure will remain constant at the vacuum pressure of 0.1 bar. This assumption needs to be verified or a model should be implemented that incorporates these dynamics. It is assumed that the ratio in which H₂O and CO₂ are adsorbed is 3:1. It needs to be determined if this ratio can be influenced by choosing the wt% of the adsorbent or by varying operating conditions.

Fan The assumption that the fan blows through a certain volume of air has to be verified together with the assumption that the adsorption process is limited by the amount of gases going through, not the adsorption kinetics themselves. Experiments could for example measure the air flow through the monolith, the fan power and the input and output air compositions.

4.2.4. Fluid Machinery

The Fluid Machinery model must make sure that the desorbed chemicals are compressed to 50 bar. To do this it is desired to know how much energy is needed to compress the desorbed components. The Compression function that does this is discussed in this subsection. It has to be noted that the Fluid Machinery is not introduced before in this thesis because it is seen as a part of the Direct Air Capture.

Operation Modes The Fluid Machinery switches on if the Direct Air Capture is desorbing.

Compression Function The device that will be used for the compression is a reciprocating pump with three compression stages. The exact design of it and its performance are unknown. The mechanical behaviour e.g. movements of the reciprocating pump, are not of interest in this thesis. However, it is important to determine the amount of energy needed for compression to see whether it is significant. Therefore, this device is simplified by only looking at the thermodynamic work needed to compress the gases and multiply this with a factor that incorporates energetic losses of the pump. The work is determined by integrating the pressure over the change in volume as described by Moran [34]:

$$W = \int_{V_1}^{V_2} p dV \quad (4.5)$$

In this equation, W represents the work needed for compression of a component, p is the pressure and dV the change in volume at the initial time step, V_1 and the volume at the final time step, V_2 .

Results The work was calculated by using the thermodynamic properties of CO₂ and H₂O with the RefProp plugin for MatLab. In Figure 4.19 the isotherms from 20 - 120 °C as well as three compression stage for both adiabatic and isothermal compression are shown. The pressure is integrated over the specific volume, dv instead of the volume, dV to determine the work per kg. The molar mass is subsequently used to convert it to work per mole. 2.06 MJ·mole⁻¹ is needed for adiabatic and 0.524 MJ·mole⁻¹ for isothermal compression of H₂O. Considering CO₂ an adiabatic compression of 0.747 MJ·mole⁻¹ and isothermal compression of 0.477 MJ·mole⁻¹ is found. The real compression work will be somewhere in between but it is expected to be closer to the isothermal case because the small amounts of gases will be cooled by the walls of the compressors and tubing before the next compression stage. The energy input for the Fluid Machinery is determined by dividing the isothermal work by an estimated efficiency of 20 %. This means that only 20 % of the energy the Fluid Machinery receives will be converted into compression of the desorbed gases.

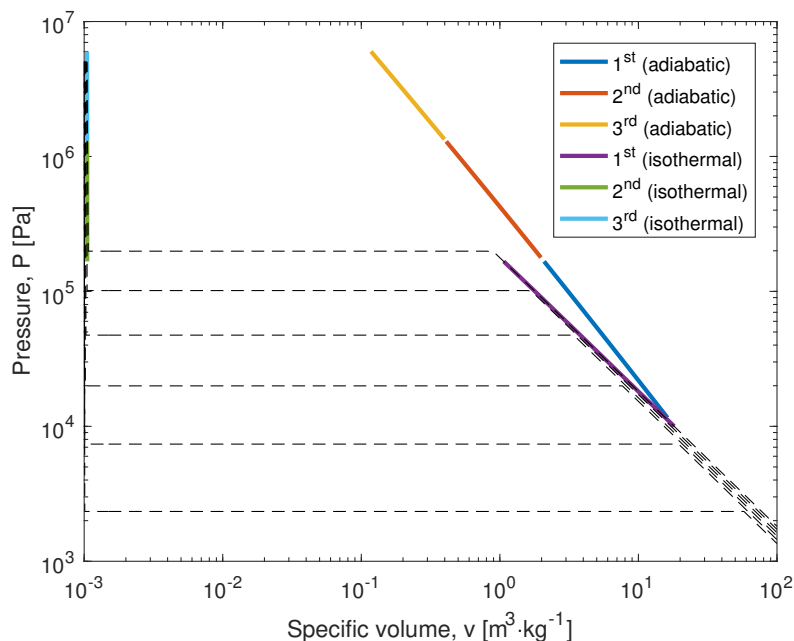


Figure 4.19: pV-diagram of water with isotherms of 20 - 120 °C (bottom to top) and three stages of both adiabatic and isothermal compression. After the first stage of the isothermal compression the gases are cooled to 100 °C in order to prevent compression through the two phase region. Adiabatic compression of one mole H₂O needs 2.06 MJ, isothermal compression needs 0.524 MJ.

Discussion Experiments are needed to verify the assumption that the Fluid Machinery compresses the desorbed components with 20 % energetic efficiency. The model does not take into account the rate at which the gases are compressed. It is assumed that they are immediately removed from the Direct Air Capture chambers. In reality the compression rate will fluctuate because the received power from the Solar Panel fluctuates. This means that the pressure inside the Direct Air Capture chambers might fluctuate which influences the desorption rate. To investigate this behaviour the Direct Air Capture and Fluid Machinery models need to be connected.

To predict how the mechanical parameters influence the Fluid Machinery efficiency the approach suggested by Farzaneh-Gord can be used [35]. In this paper the movement of the piston as well as the angular velocity of the electrical motor are incorporated. To improve the understanding of this subsystem it is furthermore advised to also incorporate the intermediate flash tanks. This will support optimisation of the compression ratios for each stage as well as the amount of stages.

4.2.5. Alkaline Electrolysis

The Alkaline Electrolysis model has to determine how much H_2O is converted in H_2 . In Figure 4.20 an overview of the model is given. First, the Energy function determines the temperature which is used as an input for the Mass Conversion function. An overview of the parameters used in the Alkaline Electrolysis model is shown in Appendix B.

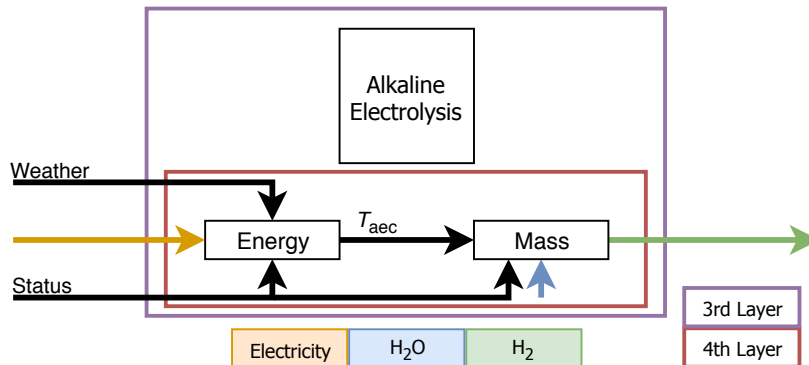


Figure 4.20: High level overview of the Alkaline Electrolysis model.

Operation Modes The Alkaline Electrolysis knows three different operation Modes. It can be off, on or on & cooling. The cooling makes sure that the electrolyte temperature does not become higher than the design temperature because it becomes increasingly aggressive at higher temperatures. A maximum operation temperature of 90 °C is found in literature [19]. It is decided by Zero Emission Fuels to operate at 60 °C. The Alkaline Electrolysis thus switches from on to on & cooling at 60 °C.

Energy Function In the Energy function Runge-Kutta4 is used to determine the temperature. The geometry of the Alkaline Electrolysis is shown in Figure 4.21. To determine the steady-state heat exchange with the environment, \dot{Q}_{aec} , this subsystem was simplified to a concentric cylinder with a layer of thermal insulation, a layer of steel to withstand the pressure and a layer of PVC to withstand the electrolyte. The total thermal resistance was taken to be 5 K·W⁻¹. The internal heat production is determined by multiplying the power with 1 minus the energetic efficiency: $1 - \eta_{aec}$.

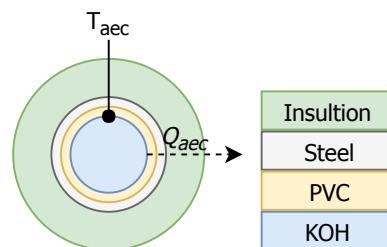


Figure 4.21: Overview of the different layers of the simplified Alkaline Electrolysis. The heat loss, \dot{Q}_{aec} , is determined each time step with a thermal resistance network.

Mass Conversion Function The Mass Conversion function uses the IV-curve to determine the operating voltage, V_{aec} as function of the current going through it. The operating voltage determines the energetic efficiency, η_{aec} , by dividing the open circuit voltage, V_{ocv} by it. The energetic efficiency is then used together with the power given to the Alkaline Electrolysis, \dot{W}_{aec} , and Gibbs energy of formation of H_2 from liquid H_2O , $\Delta G_{f,H_2}$, to find the H_2 production rate, \dot{n}_{H_2} :

$$\eta_{aec} = \frac{V_{ocv}}{V_{aec}}, \quad \dot{n}_{H_2} = \frac{\dot{W}_{aec} \eta_{aec}}{\Delta G_{f,H_2}} \quad (4.6)$$

IV-curve The IV-curve was characterised by fitting the experimental data to the equation as suggested by Rahim [10] and described in more detail in subsection 2.2.4. How the experiments are conducted is stated in Appendix D. The result is shown in Figure 4.22. In this figure it can be observed that the voltage decreases for lower current densities. This means that the energetic efficiency increases. The current density can be decreased by increasing the electrode cell area. This is the reason why the cell area of the Alkaline Electrolysis has been increased to 30 cm² from the original 14 cm² of the steady-state model that was described in chapter 1.

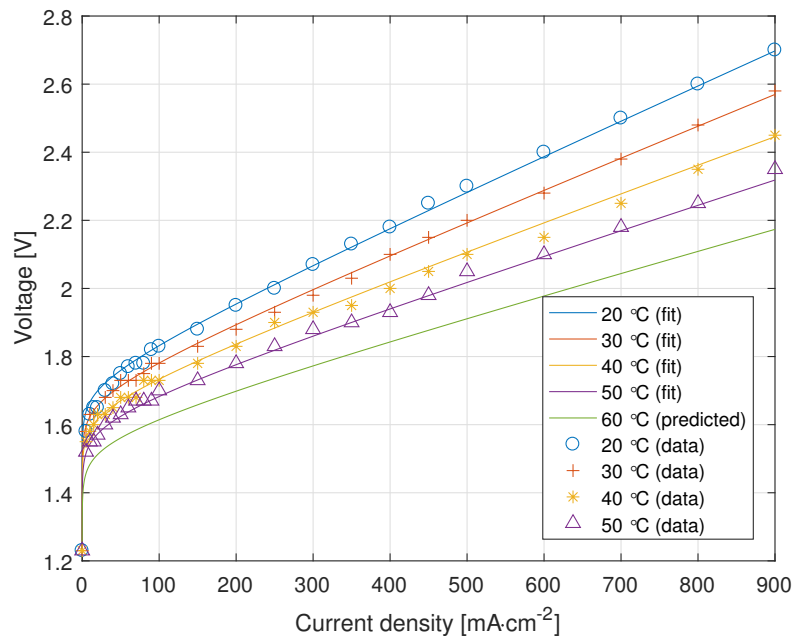


Figure 4.22: Results of the Alkaline Electrolysis voltage measurements and the curves fitted with MatLab's non-linear least-squares solver. To operate at an efficiency of 60% ($2.05 \text{ V}\cdot\text{cell}^{-1}$) at 60 °C the maximum current density is $710 \text{ mA}\cdot\text{cm}^{-2}$.

Verification The Alkaline Electrolysis model is tested on a random day of the year 2005 in Tucson, Arizona are shown in Figure 4.23. The upper plot shows how much power this subsystem receives and how much is converted into heat and H₂. The bottom plot shows the amount of H₂ produced every minute. It can be observed that more H₂ is produced as the power input increases. At the same time the efficiency drops as the power input increases due to an increase in current density. The heat generated by this subsystem makes sure that the temperature increases from ambient to the maximum operating temperature, 60 °C, in about 60 minutes. This means that this subsystem needs to be cooled throughout the rest of the day in order to guarantee safe operation.

Discussion The Mass function is expected to be reasonably accurate because it is based on experimental data. It has to be noted that the effect of pressure is not incorporated in the IV-curve although this effect is clearly observed and described by Godula-Jopek [19]. In reality the efficiency will decrease slightly at higher pressures.

The measurements of the IV-curve were conducted at 20 - 50 °C and are subsequently extrapolated to 60 °C. It has to be noted that the conductivity of the 30 wt% KOH solution drops above this temperature. Therefore, the predicted performance increase might not be realistic. To prevent this problem the KOH wt% can be increased since it is observed that higher wt% KOH have an optimum for electrical conduction at higher temperatures. On the other hand, the measured data falls well within the range that is described by Godula-Jopek [19]. A better performance can even be expected if compared to the DLR Alkaline Electrolyser operating at 80 °C which was shown in Figure 2.7.

The cell area was increased in this model to improve the efficiency. In reality this is an economical trade-off between the increase in cost associated with the larger electrodes and larger casing versus the increase in H₂ production.

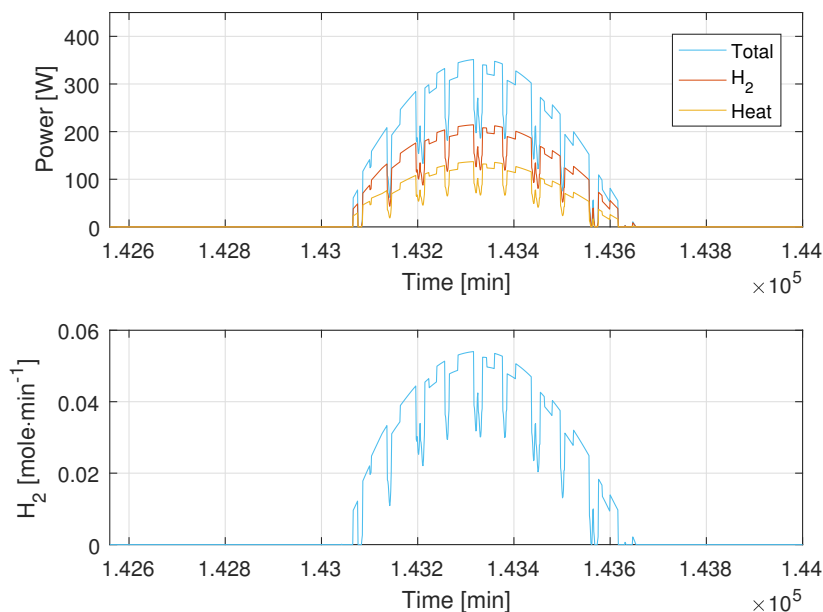


Figure 4.23: Results of the Alkaline Electrolysis models during one day. The upper plot shows the total power sent to this subsystem as well as the amount that is converted into H₂ and heat. The lower plot shows the amount of H₂ that is produced each minute. As the amount of power received by the Alkaline Electrolysis increases the H₂ production increases as expected. From these plots it can furthermore be derived that the efficiency decreases as the power input increases.

4.2.6. Methanol Synthesis

The Methanol Synthesis model converts CO₂ and H₂ into MeOH and H₂O. In Figure 4.24 an overview of the model is given. The Energy function determines the temperature of the reactor. The Mass Conversion function converts the feed into the reaction products. An overview of the parameters that are used to model the Methanol Synthesis are shown in Appendix B.

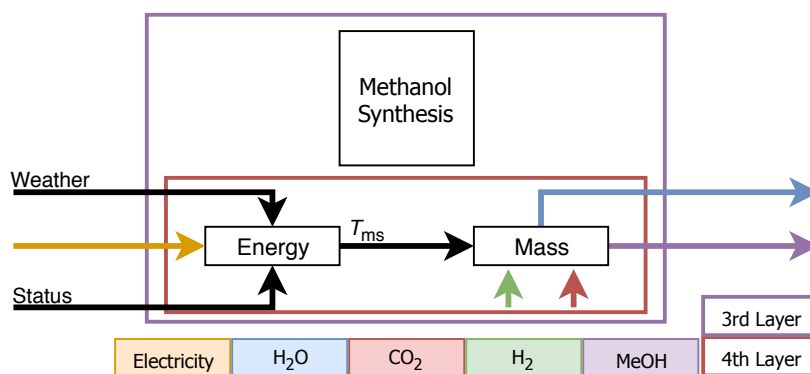


Figure 4.24: High level overview of the Methanol Synthesis model.

Operation Modes The Methanol Synthesis knows three different operation Modes. It can be off, heating or producing MeOH. This subsystem starts heating until the desired operating temperature is reached. If it is hot the temperature is kept constant and MeOH and H₂O is produced. The reactor has a hot and a cool side. The hot side is continuously 210 °C the cool side 70 °C. Since the steady-state heat exchange depends linearly on the temperature difference with the environment only the average temperature of the reactor was determined. The threshold value for switching from heating to producing is thus set to 140 °C instead of 210 °C.

Energy Function At the basis for the Energy function is again the energy balance which is discretised using Runge-Kutta4. The geometry of the Methanol Synthesis reactor is a circular tube that is connected with itself to form an infinite loop which allows for recirculation. This was shown in subsection 2.2.5. This geometry is simplified to a cylinder of finite length which only exchanges heat through the outer wall. The radiation to itself is neglected. The simplified geometry is shown in Figure 4.25. The steady-state heat exchange with the environment was determined using a total thermal resistance of $10 \text{ K}\cdot\text{W}^{-1}$. The mass of the reactor is assumed to be 2 kg.

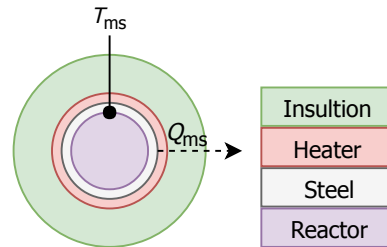


Figure 4.25: Overview of the different layers of the simplified Methanol Synthesis Reactor. The heat loss, Q_{ms} , is determined each time step with a thermal resistance network with a total thermal resistance of $10 \text{ K}\cdot\text{W}^{-1}$.

Mass Conversion Function In the experiments conducted by Basarkar it was observed that the reactor reached a steady-state after a couple of seconds [3]. This was also observed in the 3D transient dynamic model constructed by Gutierrez Neri [22]. Since this model is on a minute scale it was assumed that the reactor was able to produce as soon as it becomes the desired temperature of $210 \text{ }^\circ\text{C}$. No model was implemented to determine the conversion rate or reaction kinetics. It was simply assumed that as long as the reactor is at the elevated temperature for a couple hours per days all CO_2 and H_2 can be converted.

Discussion The Methanol Synthesis model is one of the less accurate ones of all subsystem models. The reaction kinetics are not incorporated and the temperature difference inside the geometry is neglected. Furthermore, the Mass Conversion function does not contain any conversion rates based on reaction kinetics. The energy that is needed to heat the feed or to keep it recirculating is also not incorporated although the energy for this might be provided for by the exothermic reaction. It does also not incorporate the heat recovery of the heat pipes. The results of this model should therefore be interpreted carefully.

Since the Methanol Synthesis reactor is hot for quite some hours per day this means that there is also room for improvement considering the energy use of this subsystem. A new model in which the mass conversion is more accurate can determine more accurately how many hours of operation are needed. If less hours are needed this subsystem can be started at a later time of the day and more energy can be given to other subsystems. To improve this a 1D quasi-steady state model needs to be derived from the 3D experiments and 3D transient model investigated by Basarkar and Guitierrez Neri [3, 22].

4.2.7. Capillary Distillation

The Capillary Distillation model needs to separate the MeOH, H₂O mixture from the Methanol Synthesis into two separate streams. An overview of the model is shown in Figure 4.26. This model is only used in the second part of the thesis after chapter 6. In the first part the Capillary Distillation is simplified to a heater of 25 W switching on as long as the Methanol Synthesis reactor is hot.

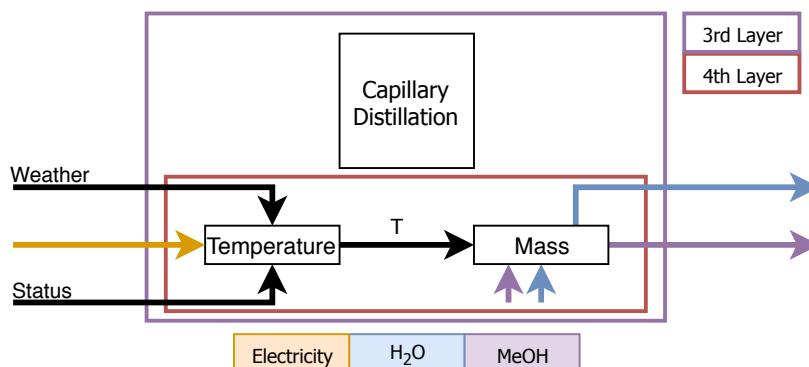


Figure 4.26: High level overview of the Capillary Distillation model.

Operation Modes The Capillary Distillation knows three operation Modes. It can be off, heating or separating. Separation starts if a certain temperature is reached because above it the components will start to evaporate. It is assumed that when evaporation starts the separation process also takes place.

Energy Function To determine how much feed is evaporated and thus separated the temperature of the Capillary Distillation needs to be calculated by solving the energy balance. The energy balance is again discretised using Runge-Kutta4. The steady-state heat exchange is determined by solving a heat resistance network with a total thermal resistance of 10 K·W⁻¹.

Mass Conversion Function The Experimental results from Seok show that a good separation is achievable [24]. To be useful for this thesis these findings have to be reformulated such that an estimate can be made of how much mixture can be separated as function of the energy this subsystem receives every minute. It is assumed that a continuous temperature gradient exists in the tube where one end is at the boiling point temperature of pure water, 100 °C, and the other at the boiling point temperature of pure methanol, 64 °C. It is assumed that the liquids and gases are in equilibrium throughout the tube. Since the temperature of the whole tube is higher than the boiling point temperature of pure methanol and the vapour-liquid equilibrium of the mixture is monotonously increasing it has been derived that at least all methanol must evaporate. To have a safe estimate for the energy need of the distillation it is also assumed that all water evaporates. Using these assumptions the energy needed for separation of 1 mole feed, $E_{DS, \text{evap}}$, is:

$$E_{DS, \text{evap}} = \Delta T \frac{(c_{p, \text{H}_2\text{O}} + c_{p, \text{MeOH}})}{2} + \frac{\Delta H_{\text{evap}, \text{H}_2\text{O}} + \Delta H_{\text{evap}, \text{MeOH}}}{2} = 47.5 \text{ kJ} \cdot \text{mole}^{-1} \quad (4.7)$$

In this equation the specific heat of the feed components are indicated with $c_{p, \text{H}_2\text{O}}$ and $c_{p, \text{MeOH}}$, and the heat of evaporation with $\Delta H_{\text{evap}, \text{H}_2\text{O}}$ and $\Delta H_{\text{evap}, \text{MeOH}}$. It is assumed that the feed enters at 60 °C and is heated to 100 °C, the temperature increase, ΔT is thus equal to 40 °C. All the energy this subsystem receives that is not put into heating is used for separation.

Discussion The Capillary Distillation model assumes that all MeOH and H₂O is evaporated at least once. Since this costs a lot of energy it may be worthwhile to investigate this assumption with experiments or a more accurate model. A more accurate model of this subsystem might decrease the predicted energy consumption because the amount of mixture that is evaporated before separation is thought to be overestimated. It also has to be noted that this model was only incorporated in the second phase of the thesis. In the first part the Capillary Distillation energy use was modelled by assuming it uses 25 W as long as the Methanol Synthesis is at its operating temperature of 210 °C.

4.3. Postprocessing

This section discusses the postprocessing step. This is the last step of the Simulation Tool as can be seen in Figure 4.27. First the results are visually analysed in subsection 4.3.1 to verify subsystem behaviour and discuss the predicted System behaviour at different types of days of the year. In subsection 4.3.2 the Key Performance Indicators are discussed since they provide insight into the average daily operation of each subsystem and the System as a whole.

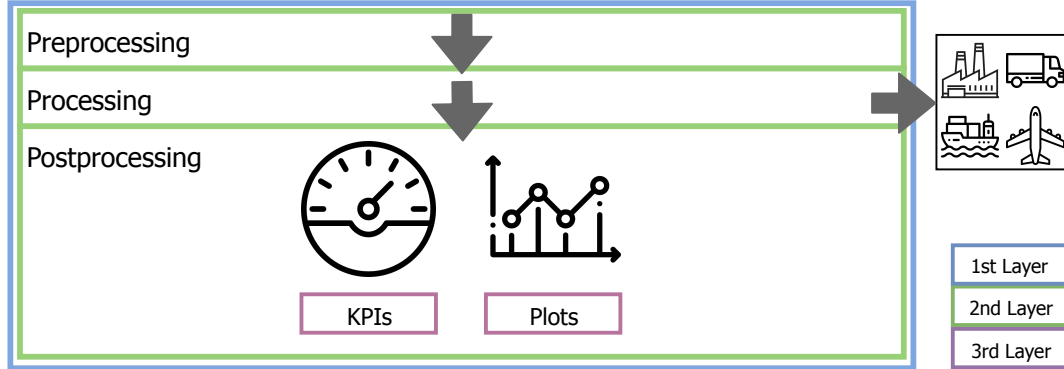


Figure 4.27: This section focuses on the postprocessing step of the Simulation Tool. The Key Performance Indicators are calculated and some plots made for visual analysis of the results.

4.3.1. Visual Analysis

In this section the results are visually analysed in order to say something about the behaviour of the System during different days of the year. Some typical days that give good insight in varying behaviour as function of varying weather conditions have been chosen. These are two summer and two winter days. One sunny, the other cloudy. The days are chosen at random and thus not represent extreme values. The main purpose was to show the order of magnitude of the variations that can occur over the year. An overview of the observations that are discussed throughout this subsection is shown in Table 4.1.

	unit	Sunny Summer	Cloudy Summer	Sunny Winter	Cloudy Winter
T_{ambient}	[K]	301.6	300.0	288.6	286.3
GHI	[kWh]	11	5.2	4.3	2.0
$t_{\text{sol,on}}$	[hh:mm]	13:30	13:30	09:20	09:20
E_{sol}	[kWh]	2.9	1.3	1.9	0.67
$T_{\text{sol,max}}$	[K]	317.2	307.0	304.7	295.7
$n_{\text{dac,cycles}}$	[-]	17	14	13	6
$t_{\text{ms,on}}$	[hh:mm]	11:00	09:22	07:47	03:11
$t_{\text{ms,hot}}$	[hh:mm]	00:42	01:34	00:41	00:41
$t_{\text{aec,on}}$	[hh:mm]	08:25	04:25	06:33	01:48
$t_{\text{aec,hot}}$	[hh:mm]	01:00	05:23	01:31	02:12

Table 4.1: Overview of the observations at the 4 different days that are analysed in this subsection. It shows the possible variation between different days of the year and the importance of the quasi-steady state model compared to the steady-state model in which all these parameters were assumed constant. T_{ambient} is the average ambient temperature, GHI the total irradiance, $t_{\text{sol,on}}$ the time the Solar Panel produces energy, E_{sol} the total energy it produces, $T_{\text{sol,max}}$ the maximum temperature of the Solar Panel, $n_{\text{dac,cycles}}$ the amount of adsorption cycles the Direct Air Capture goes through, $t_{\text{ms,on}}$ the time the Methanol Synthesis is at its operating temperature, $t_{\text{ms,hot}}$ the time it takes between the first minute the Methanol Synthesis receives power and it to reach the operating temperature, $t_{\text{aec,on}}$ the time the Alkaline Electrolysis is at its operating temperature and $t_{\text{aec,hot}}$ the time it takes between the first minute the Alkaline Electrolysis receives power and it to reach the operating temperature.

Summer Days

The temperature and power development during the two typical summer days that are analysed in this subsection are shown in [Figure 4.28](#).

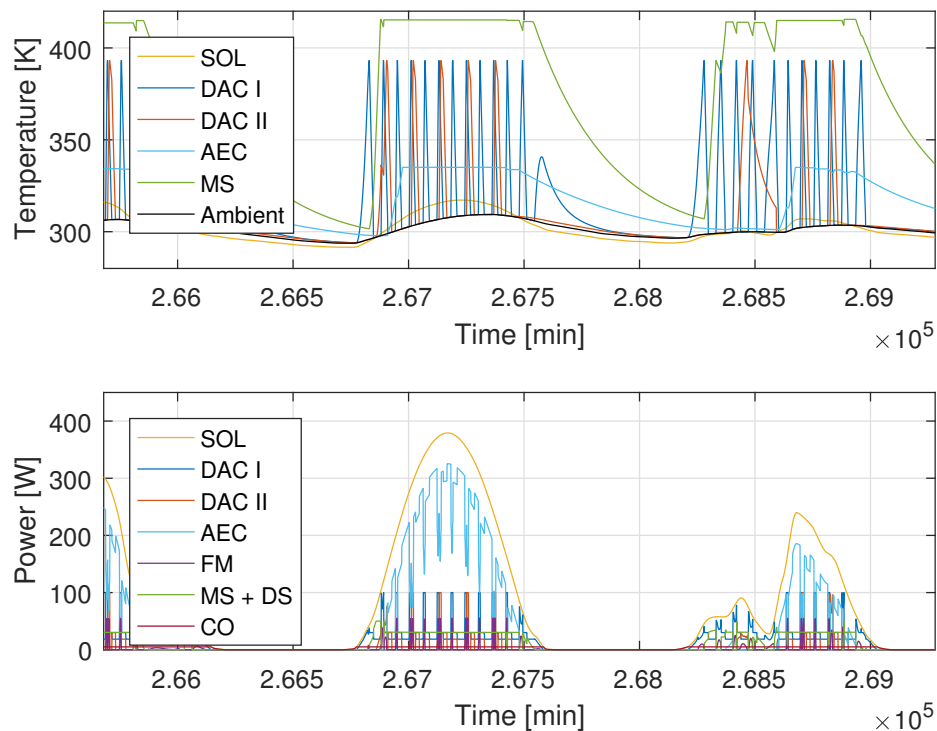


Figure 4.28: Temperature and Power development during a sunny and cloudy summer day in Tucson, Arizona. The data shown corresponds to July 5, midday until July 7, midnight.

Weather and Solar Panel The average ambient temperature of these days is 301.6 K and 300 K respectively. The total global horizontal irradiance is 11 kWh and 5.2 kWh. The Solar Panel provides more than 5.0 W during 13 hours and 30 minutes during both the sunny day and cloudy day. The total daily Solar Panel energy produced is 2.9 kWh and 1.3 kWh. The maximum Solar Panel temperature is 317.2 K on the sunny day and 307.0 K on the cloudy day.

Subsystems The effect of these varying conditions on the subsystems is significant. The Direct Air Capture does 17 cycles during the sunny day and only 14 cycles during the cloudy day. The Methanol Synthesis reactor is producing for 11 hours and reaches the operation temperature in 42 minutes during the sunny day. The reactor temperature drops twice during the sunny day and four times during the cloudy day. During the cloudy day the reactor produces for 9 hours and 22 minutes and reaches the operation temperature in 94 minutes. The Alkaline Electrolysis operates above 330 K for 8 hours and 25 minutes and reaches this temperature in 1 hour after it is first switched on. During the cloudy day the operation time above 330 K is 4 hours and 50 minutes and this temperature is reached in 5 hours and 23 minutes after it is first switched on.

Winter Days

The temperature and power development during the two typical winter days that are analysed in this subsection are shown in Figure 4.29.

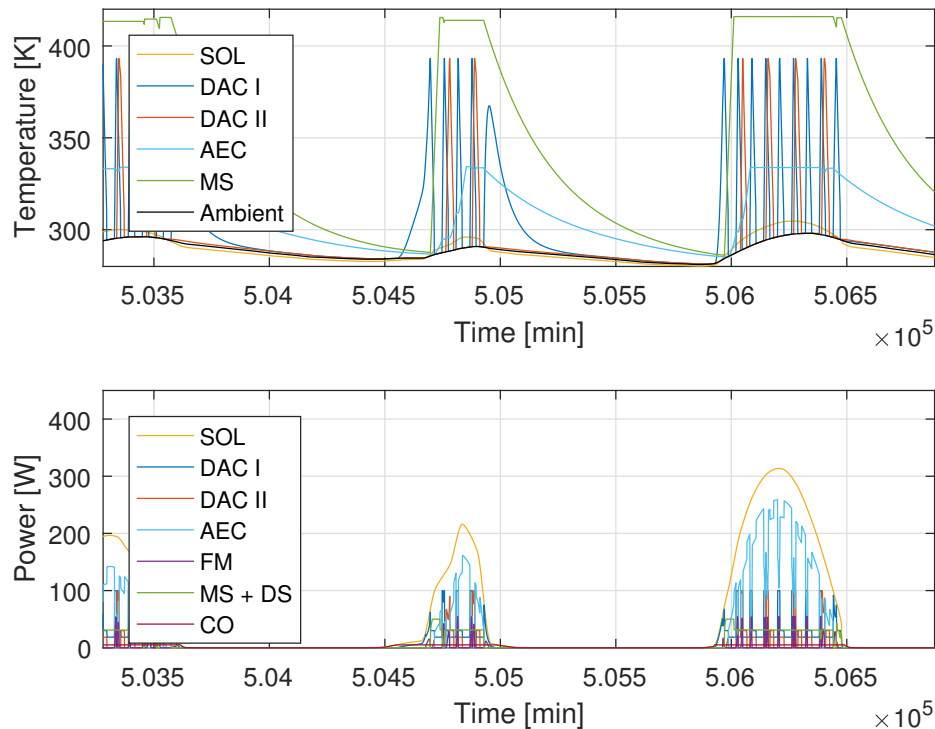


Figure 4.29: Temperature and power development during a cloudy and summer winter day in Tucson, Arizona. The data shown corresponds to December 16th midday until December 18th midnight.

Weather and Solar Panel The average ambient temperatures of the cloudy and sunny days are 286.3 K and 288.6 K respectively. The daily global horizontal irradiance is 2.0 kWh and 4.3 kWh. The Solar Panel provides more than 5 W during 9 hours and 20 minutes during both the sunny day and cloudy day. The total daily Solar Panel energy produced is 0.67 and 1.9 kWh. This difference directly influences the maximum Solar Panel temperature of 295.7 K on the cloudy day and 304.7 K on the sunny day.

Subsystems The effect on the different subsystems is directly observed. The Direct Air Capture does 13 cycles during the sunny day and only 6 cycles during the cloudy day. The Methanol Synthesis reactor is producing for 7 hours and 47 minutes and reaches the operation temperature in 41 minutes during the sunny day. The reactor temperature drops once due to lack of power during both the sunny and cloudy day. During the cloudy day the reactor produces for 3 hours and 11 minutes and reaches the operation temperature in 41 minutes. During the sunny day the Alkaline Electrolysis operates above 330 K for 6 hours and 33 minutes and reaches this temperature in 1 hour and 31 minutes after it is first switched on. During the cloudy day the operation time above 330 K is 1 hours and 48 minutes and this temperature is reached in 2 hours and 12 minutes after it is first switched on.

Other Observations

Apart from the factual observations some other relevant observations are discussed in this subsection.

Solar Panel The Solar Panel warms up during the day and cools below the ambient temperature at night. The warming up of the device is caused by the irradiance during the day and the fact that not all of it is converted into power. The Solar Panel cools down at night below ambient temperature due to the radiation exchange with the sky.

Direct Air Capture The Direct Air Capture chambers alternate between heating up and cooling down due to the cyclic behaviour of the pressure-temperature swing adsorption. Cooling the chambers down is quicker than heating it up. This is related to the fact that the sorbent contains much less H₂O and CO₂ after desorption and the fact that the heat exchange with the environment supports cooling down. The differences between the sunny and cloudy days are also clear for this subsystem. The amount of cycles both chambers go through are different and the cycle times differ. This is caused by the fact that less power is available for heating during the cloudy day. Another thing that draws the attention is the fact that some desorption stages at the end of the day are not finished. Since the cycle is not finished the power supplied to the Direct Air Capture chambers during their last cycle can be seen as a loss because both chambers cool down to ambient temperature over night and thus need reheating the next day.

Alkaline Electrolysis The Alkaline Electrolysis starts to heat up as soon as it receives power. During the sunny summer day it can be observed that after approximately one hour a temperature above 330 K is reached. This means that the rest of the day this subsystem needs to be actively cooled in order to guarantee safe behaviour. It was already discussed that the performance of the Alkaline Electrolysis decreases for lower temperatures. In these results it can be observed that the subsystem temperature gets close to the ambient temperature every night. This means that the efficiency at the beginning of each day is lower than desired. Since this subsystem uses the most power it is desirable to investigate the possibilities to investigate its efficiency.

Methanol Synthesis The Methanol Synthesis reactor heats up in about 40 minutes during a sunny day. After the reactor is hot the power supplied to it can be decreased such that it will keep it hot. Some fluctuations of the temperature can be observed around the design temperature of 413 K. The small decreases in temperature are caused by the fact that other subsystems get priority over the available power. Especially during a low irradiance day as the cloudy ones this results in some moments during the day in which the reactor switches off.

Capillary Distillation It can be observed that the Capillary Distillation is absent in the temperature plots of [Figure 4.28](#) and [Figure 4.29](#). This is because the Energy and Mass functions were not used in this part of the thesis. The Capillary Distillation is present in the power plots because this subsystem is switched on as soon as the Methanol Synthesis becomes hot. It will use 25 W continuously.

4.3.2. Key Performance Indicators

In this subsection Key Performance Indicators are used to indicate how each subsystems behaves on an average day. A list of the key performance indicators can be found in ???. An overview of the average energy use and production per day of each subsystem is shown in Figure 4.30. These values are referred to throughout this subsection.

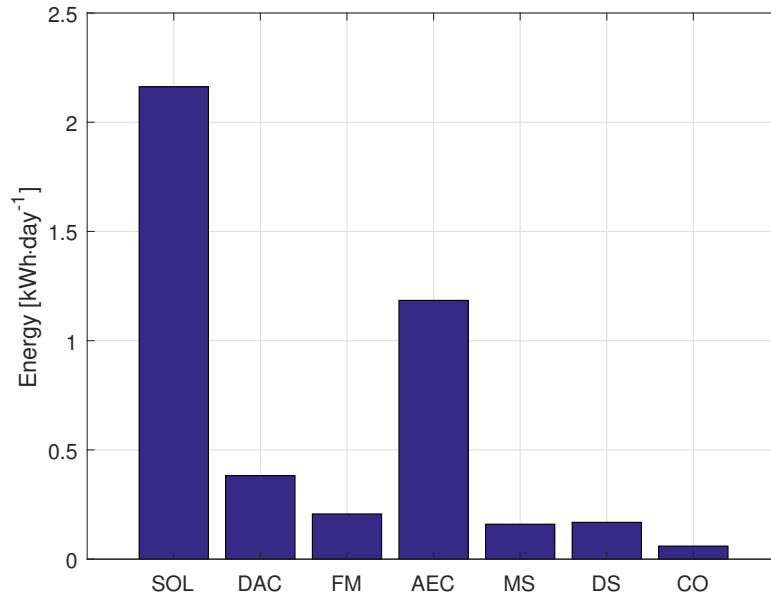


Figure 4.30: Overview of the average daily energy use of the different subsystems. The subsystems displayed are the Solar Panel (SOL), the Direct Air Capture (DAC), the Fluid Machinery (FM) the Alkaline Electrolysis (AEC), the Methanol Synthesis (MS), the Capillary Distillation (DS) and the Control (CO).

Solar Panel If the Solar Panel were to operate at its maximum power point an efficiency (total GHI to energy) of 31.2% was found, thereby producing 2.18 kWh from 7.00 kWh GHI. The actual energy produced by the Solar Panel is lower because the electrical characteristics of the Plant do not perfectly match the Solar Panel. The load was simplified by only looking at the Alkaline Electrolysis. The actual output was observed to be 2.16 kWh·day⁻¹.

Control The Control was on as long as the Solar Panel produced energy. It uses an average of 0.06 kWh·day⁻¹ (2.8 %) if it is assumed that 5 W is needed continuously.

Plant The heat for desorption is provided by an electric heater of 50 W. Heat is removed during cooling with 30 W to have cycle times of around 1 hour. The Direct Air Capture uses 0.38 kWh·day⁻¹ to adsorb 3.0 mole CO₂ and 9.1 mole H₂O. 0.09 kWh·day⁻¹ is used for cooling, 0.29 kWh·day⁻¹ is used for the adsorption and desorption. The power provided to the Fluid Machinery is 0.21 kWh·day⁻¹. 0.10 kWh·day⁻¹ of heat at around 100 °C needs to be extracted to facilitate condensation. The Methanol Synthesis needs to be heated each morning. An electric heater of 50 W was used and insulation was added to minimise heat loss. When the reactor temperature was reached the heater was turned down to around 6 W to compensate steady-state heat loss. This subsystem uses 0.16 kWh·day⁻¹. The Capillary Distillation turns on when the Methanol Synthesis is hot. It uses a 25 W heater to heat up the reaction products and separate them. The Capillary Distillation uses 0.17 kWh·day⁻¹. The remaining power after all other subsystems received theirs was given to the Alkaline Electrolysis. It was found that 1.19 kWh was received to produce 9.1 mole H₂. 0.44 kWh·day⁻¹ is converted into heat from which 0.20 kWh·day⁻¹ needs to be removed to guarantee the maximum operating temperature is not exceeded. This results in an average MeOH production of 3.0 mole·day⁻¹. The System efficiency (Solar Panel energy to methanol LHV) is 24.9 %.

5

System Discussion

This chapter ends the first phase of the thesis as shown in [Figure 5.1](#). It contains a discussion of the results of [chapter 4](#). The following research objectives are answered: 1) predicting the performance of the System for a full year and 2) identifying the most important System design parameters that influence this performance. A summary of the most important parameters can be found in [Appendix E](#).

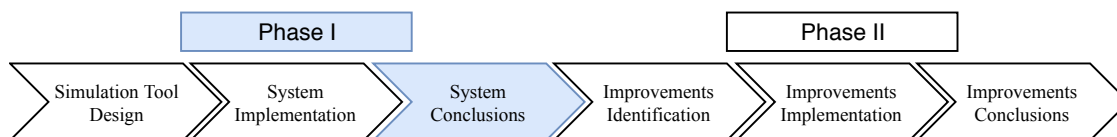


Figure 5.1: The third part of the thesis focuses on the conclusions of the first phase.

Solar Panel

The Solar Panel will not operate at its maximum power because of the mismatch between the IV-curves of the load, in this case the Alkaline Electrolysis, and Solar Panel. The results showed that by choosing the right amount of Alkaline Electrolysis cells, 16 in series, the Solar Panel energy is 98 % of the maximum energy it could produce. On average it produces $2.16 \text{ kWh}\cdot\text{day}^{-1}$.

The Solar Panel power increases if the irradiance of the location is higher. It is possible to have an average of $7.00 \text{ kWh}\cdot\text{day}^{-1}$ in some locations on earth. To have the highest Solar Panel irradiance the angles need to be optimised. In Tucson, Arizona these are 63° tilt and 165° azimuth. It has been derived from the datasheet that a lower Solar Panel temperature increases the maximum power. A colder location with the same irradiance is therefore favourable over a hotter one. On the other hand, it has to be taken into account that the other subsystems need more heating in a colder environment. Adding active cooling of only the Solar Panel might be an option as long as it uses less power than is additionally produced.

Direct Air Capture

The Direct Air Capture uses $0.38 \text{ kWh}\cdot\text{day}^{-1}$ (18 %) to capture 3.0 mole CO_2 and 9.1 mole H_2O while 6.67 mole CO_2 and 20.0 mole H_2O is needed. Improvements are thus needed e.g. by reusing the heat extracted during cooling. Another possibility lies in optimisation of the operating conditions and control. The maximum temperature for desorption could be decreased or the doors left open at night. It would also be beneficial if H_2O from the Capillary Distillation is recycled such that less H_2O needs to be adsorbed.

The cycle time of the Direct Air Capture is influenced by a complex interplay of different parameters: the amount of adsorbent, the fan, heater and cooling power and the geometry of the chambers. These parameters need to be optimised as a complete set not individually because a cycle can be limited by all of them. Insulation around the Direct Air Capture chambers makes sure that the maximum desorption temperature is reached quicker and with less energy. Afterwards it immediately needs to be cooled again to get ready for adsorption. This is however slowed down by the insulation. An optimum can be found between the costs of the insulation and the power needed for both adsorption and cooling.

Fluid Machinery

The impact of the Fluid Machinery on the energy use of the whole system is 9.7 % or 0.21 kWh·day⁻¹. The Fluid Machinery model neglects the geometry. Therefore, no conclusions can be drawn for physical design parameters. Since the Fluid Machinery model relates the energy use to the energy needed for isothermal compression it can be concluded that the amount of gases that are compressed influence its energy use. Options that decrease the need to compress all desorbed gases will thus influence the energy use. Another option is to improve the energetic efficiency. This can be improved by making a good design for the reciprocating pump such that internal losses are minimised.

In the pv-diagram of H₂O, Figure 4.19, it can be observed that during compression the two-phase region is passed. To prevent compression of a two-phase mixture an intermediate condensation step is needed. This means that heat needs to be extracted somewhere in this subsystem. This also means that after the condensation the mixture basically consists of liquid water and gaseous CO₂. This needs to be incorporated in the design since liquids and gases are compressed differently.

Alkaline Electrolysis

This subsystem uses the most energy of all subsystems. It produces 9.1 mole H₂ with 1.19 kWh·day⁻¹ (55 %). It operates at an efficiency of 63 %. A maximum efficiency of around 75 % can be expected by looking at Figure 2.7. To reach the business case target of 20.0 mole H₂ with the maximum efficiency it can be derived with Equation 4.6 that this subsystem needs 1.76 kWh·day⁻¹. The energy use of the other subsystems thus needs to be reduced or the Solar Panel energy production increased.

Efficiency improvements of the Alkaline Electrolysis have a large impact on System performance. It increases for increasing temperature. It is thus beneficial to operate at an as high as possible temperature. The heat generated during electrolysis can be used for that purpose. The heat that is generated is enough to increase the temperature to the desired one as observed in the results. However, this means that active cooling needs to be added for safety reasons due to increase in chemical corrosion caused by the KOH solution. There is thus an optimal solution to be found to find the best trade-off between insulation thickness, cooling and the efficiency increase related to a higher operating temperature. Another improvement in efficiency is achieved by decreasing the current density by using larger cell areas.

Methanol Synthesis

This subsystem uses 0.16 kWh·day⁻¹ (7.4 %). This is mainly used to heat-up the reactor at the beginning of the day after which it only needs to maintain its temperature. Although it does not have a lot of effect on the overall System performance the most important parameters of this subsystem are the mass of the reactor and the thermal conductivity and thickness of the insulation surrounding it.

Capillary Distillation

The total energy need of this subsystem is 0.17 kWh·day⁻¹ (7.9 %). This is a significant part of the total energy need of the System. The function of this subsystem is to separate MeOH and H₂O. It does this by evaporation of the mixture. The heat loss of this subsystem should thus be minimised in order to improve its efficiency. This has been done by adding insulation.

System

The System's energy use is 2.16 kWh·day⁻¹. It produces 3.0 mole MeOH. The overall efficiency for the System is 24.9 % (Solar Panel energy to methanol LHV). The business case states that 6.7 mole MeOH is needed. Therefore, improvements to the System design are needed. The most important to realise is that everything is interconnected. Design changes in one subsystem directly influence behaviour of another. Due to the fluctuating weather conditions it can never be predicted how such a design change influences System behaviour for every minute of the year. The Control model should thus be flexible enough to be able to react to such changes. Preferably, it also takes into account weather forecasts.

6

Improvements Identification

This chapter focuses on the first part of the second phase of the thesis: the identification of improvements to produce more MeOH. This is the fourth part of the main body of this thesis as is shown in [Figure 6.1](#). The chapters answers the fifth research objective by giving suggestions to improve the System design.

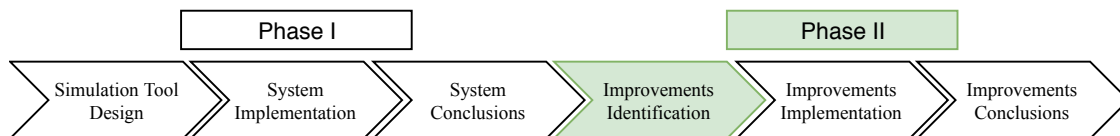


Figure 6.1: This section focuses on the first part of the second phase of the thesis. The investigation of improvements for the System to improve the performance.

The results presented in [chapter 4](#) gave insight into possibilities for improving the design. These have been subdivided into five directions as shown in [Figure 6.2](#). Four of them are related to improving the design of the System. These directions are 1) increasing System power, 2) improving Control, 3) increasing subsystem efficiency and 4) integrating heat. The last direction is 5) to improving the accuracy of the mathematical models that are used to describe the System. These five improvements will be discussed in the next five sections.

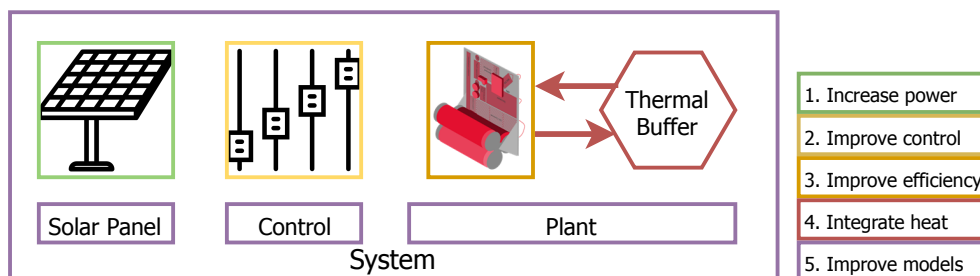


Figure 6.2: Schematic overview of possibilities for improvements: 1) increasing the System power, 2) improving the Control, 3) improving subsystem efficiency, 4) integrating heat and 5) improving the models.

6.1. Increasing System Power

The MeOH output increases if the System receives more energy while operating at the same efficiency. This subsection discusses how the energy can be increased by 1) changing the Solar Panel operating conditions and 2) by tracking the sun. An overview of the relative increases in energy for the five tested scenarios is shown in Figure 6.3.

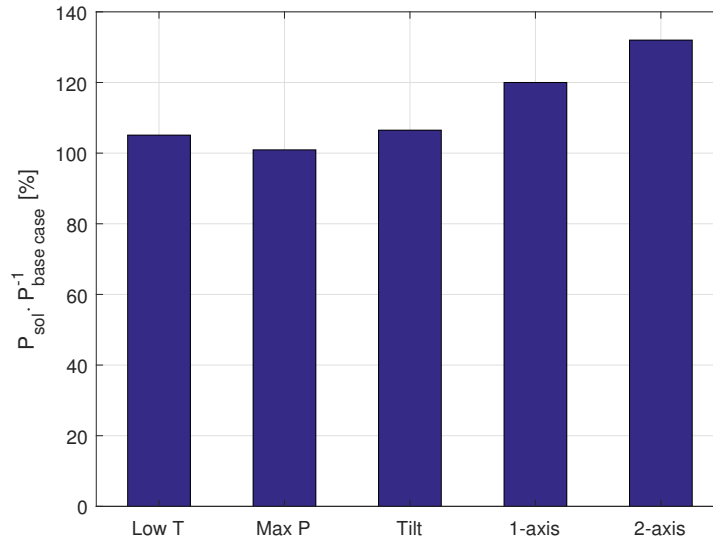


Figure 6.3: Differences of Solar Panel power, P_{sol} , for different situations compared to the base case: $P_{base\ case} = 2.16\ \text{kWh}\cdot\text{day}^{-1}$ (100 %). Small improvements can be made by decreasing the temperature (Low T, 105.1 %) or operating closer to the maximum power (Max P, 102.0 %). Larger improvements can be found in tilting the Solar Panel to a winter and summer angle (Tilt, 106.5 %), or using single (1-axis, 120.0 %) or double (2-axis 132.0 %) axis tracking of the sun.

Operating Conditions It has been derived from the Solar Panel datasheet, Figure 4.11, that the maximum Solar Panel power increases if the temperature is lower. It has been tested that $0.11\ \text{kWh}\cdot\text{day}^{-1}$ (+5.1 %) can additionally be produced if the Solar Panel were to operate at the ambient temperature throughout the year (Low T). The Solar Panel can also operate at a higher power by operating closer to the maximum power point. This maximum power corresponds to an average daily energy production of 2.18 kWh so the production can increase with 0.02 kWh (+0.93 %).

Tracking The Solar Panel could also be tilted twice a year (Tilt) to a winter (50°) and summer angle (80°) to produce an additional $0.14\ \text{kWh}\cdot\text{day}^{-1}$ (+6.5 %). Tracking the sun with one or two axes gives the largest improvements. Single axis tracking (1-axis) produces an additional $0.43\ \text{kWh}\cdot\text{day}^{-1}$ (+20 %) and double axis tracking (2-axis) $0.70\ \text{kWh}\cdot\text{day}^{-1}$ (+32 %).

6.2. Improving Control

The second option for improving the MeOH output is by using an improved Control model. The Control model can be improved upon within a single day and between multiple days. The main idea behind these improvements is that they optimise the moment of a certain process taking place.

Single Day Within a single day the amount of cycles of the Direct Air Capture can be optimised. In Figure 4.29 it was observed that desorption was started at the end of the day but could not finish because the sun went down. Due to cooling overnight this means that the next day desorption has to start again from ambient temperature. It would be better if the Control model made sure that the desorption would not be started and use the energy in another subsystem. Another option would be to finish the desorption and let the heat exchange with the environment do the cooling. The Alkaline Electrolysis could also be made to operate at a lower current density but longer. This can be done by giving priority to this subsystem at the beginning and ending of the day because the current is lower.

Multiple Days Over multiple days the Control model could also be improved upon. For example by taking into account the weather forecasts and coupling them to the states of the buffers and subsystems. Such an optimisation could be done by an Control Engineer in future research.

6.3. Increasing Subsystem Efficiency

The MeOH output furthermore increases if each subsystem operates at a higher efficiency, in other words if less energy is needed for the same mass conversion. This direction for improvements applies to the design of the subsystems as shown in Figure 6.4.

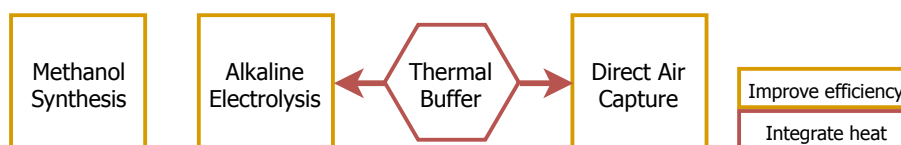


Figure 6.4: Schematic overview of two of the four directions for improving the System performance. The subsystem efficiency can be improved or heat integrated between them.

The Alkaline Electrolyser uses the most power of the System (55 %), increasing the efficiency at which power is converted to H_2 thus has a high impact on MeOH production. Parameters to do this are a larger electrode area or increasing the temperature. Another advantage of a higher temperature is that less heat has to be removed. The Fluid Machinery uses $0.21 \text{ kWh}\cdot\text{day}^{-1}$ (9.7 %) and operate at 20 % energetic efficiency (power to useful work). This efficiency could be improved upon by decreasing internal losses due to for example friction. Another option to increase subsystem efficiency is to decrease the thermal mass such that the same temperature can be reached with less energy. It has to be noted that safety of the subsystem should always be taken into account since decreasing the weight might cause earlier failing. The insulation thickness and material also influence the needed power to get a subsystem to the desired temperature and keep it there because of the heat loss to the environment.

6.4. Integrating Heat

This subsection discusses how the reuse of heat in other subsystems could contribute to a higher MeOH production. The heat sources that can potentially be used are discussed as well as how can can be coupled with Thermal Buffers as shown in Figure 6.4.

Heat Sources Heat from one Direct Air Capture chamber could be used to partially heat up the other chamber. The heat extracted by cooling is $0.09 \text{ kWh}\cdot\text{day}^{-1}$ at temperatures of 120 to 40 °C. The heat that is extracted for condensation in the Fluid Machinery is also a potential source for heat integration. This is equal to $0.10 \text{ kWh}\cdot\text{day}^{-1}$ and is available at around 100 °C. The largest amount of heat has to be extracted from the Alkaline Electrolysis. This is $0.20 \text{ kWh}\cdot\text{day}^{-1}$ and is available at 60 °C.

Coupling In searching for heat integration between different subsystems it is recommended to look at a separate well insulated Thermal Buffers not directly coupled heat integration for example with heat pipes. The reason for this is that heat is available at different temperatures at different moments in time because the power fluctuations cause continuously varying cycle times and heating and cooling rates for all subsystems.

6.5. Improved Models

The subsystem Energy and Mass Conversion functions can be improved upon by incorporating more details and verifying them with experimental results. The different teams within Zero Emission Fuels continuously work on prototypes and perform experiments on them. As soon as new information comes in the subsystem models can be updated. The design of the Simulation Tool makes sure that an old model can easily be swapped for a new one.

6.5.1. Improved Control Model

The largest improvement to make the model more physically realistic is to improve the Control model and more specific the Control function and the Power functions it contains. In the first phase these two functions determined the electrical operating point of the System by only taking into account the Solar Panel and Alkaline Electrolysis. In reality all electrical components of the System take part in the electrical circuit. By connecting them in parallel they can independently be switched on or off and thus controlled. The electrical circuit is shown in [Figure 6.5](#).

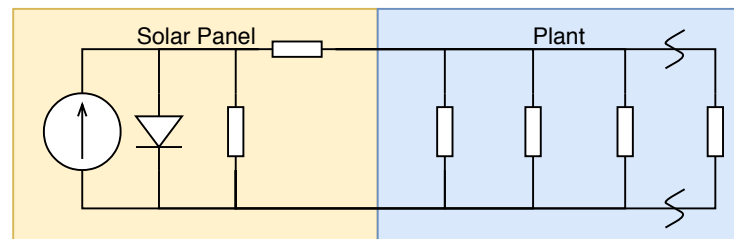


Figure 6.5: Schematic overview of an improved electrical circuit of the System. The different resistances of the Plant determine the operating point of the Solar Panel. The resistances in the Plant represent heaters, fans, Peltier elements and the equivalent resistance of the Alkaline Electrolysis. For comparison the old electrical circuit only contained one resistance. It has to be noted that a random amount of resistances is shown and that one has to be added for every electrical components in the System.

This electrical circuit does not only determine the electrical operating point of the System but also the amount of energy each subsystem receives. In other words, the energy cannot be distributed to a subsystem that does not take part in the electrical circuit and when it does take part its electrical parameters determine the amount of energy it receives. To identify the most important System design parameters, one of the research objectives, it is thus desired to incorporate all electrical components and their characteristics into the Control model.

7

Improvements Implementation

This chapter focuses on the implementation of a selection of the identified improvements of [chapter 6](#). The focus is on the last research objective: to verify the impact of the improvements on System performance. In [section 7.1](#) the improvements for the subsystem efficiency are implemented. Heat integration is discussed in [section 7.2](#) and the new Control model in [section 7.3](#).

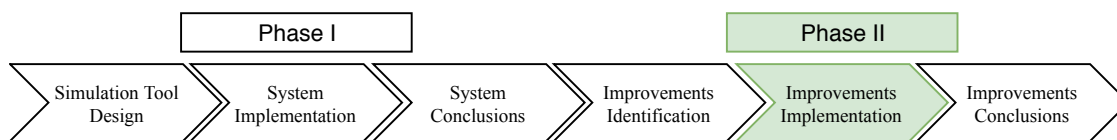


Figure 7.1: This section focuses on the second part of the second phase of the thesis. The implementation of the improvements in the Simulation Tool.

7.1. Increasing Subsystem Efficiency

The basic idea of this type of improvements is to alternate some design parameter such that less energy is needed for the same mass conversion. Four cases of improvements will be considered: 1) Alkaline Electrolysis 2) Methanol Synthesis 3) Fluid Machinery and 4) the previous three together. The Direct Air Capture and Capillary Distillation are not considered here but in [section 7.2](#).

Alkaline Electrolysis (AEC+) The Alkaline Electrolysis was improved by implementing 60 cm² electrodes instead of 30 cm². The simulation was run again and an increase in Electrolysis efficiency of 63.3 % to 66.6 % was observed. The maximum operating temperature was then also increased from 60 °C to 90 °C which resulted in an efficiency of 69.0 %. Finally, a Control threshold was implemented at 100 W Solar Panel power beneath which the Alkaline Electrolyser would have priority over the other subsystems. This resulted in a further increase in efficiency from 69.0 % to 70.3 % because the average current density decreased. If all these improvements are taken into account the System efficiency increases from 24.9 % to 29.8 %. Thereby producing 3.6 mole instead of 3.0 mole MeOH.

Methanol Synthesis (MS+) The Methanol Synthesis reactor mass has subsequently be decreased from 2 kg to 1 kg such that it needs less energy to reach the operating temperature of 210 °C. The insulation thickness and material have not been alternated. The energy demand of this subsystem decreased from 0.160 kWh·day⁻¹ to 0.135 kWh·day⁻¹. This change improves the System efficiency from 24.9 % to 25.3 %. The MeOH production increases from 3.0 to 3.05 mole.

Fluid Machinery (FM+) The energetic efficiency of the Fluid Machinery is increased from 20 % to 40 %. This means that half of the energy per compressed mole will be saved. The Fluid Machinery energy use decreases from 0.22 to 0.11 kWh·day⁻¹. This results in an increase of System efficiency from 24.9 % to 26.7 %. In terms of MeOH production this means an increase from 3.0 mole to 3.2 mole.

Together (System+) If all these improvements are implemented simultaneously the System efficiency improves from 24.9 % to 32.1 % thereby producing 3.9 instead of 3.0 mole MeOH. A summary of the improved System efficiency discussed in this section is shown in [Figure 7.2](#).

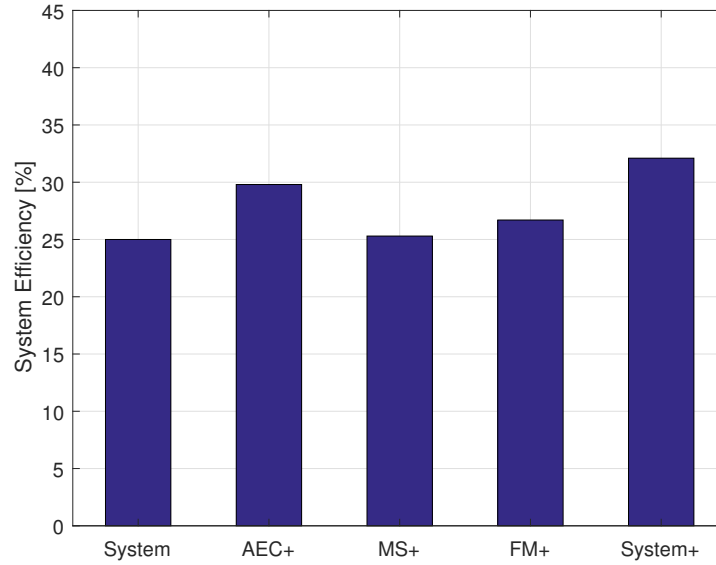


Figure 7.2: System efficiency improvements in different scenarios in which the subsystem efficiency is increased compared to the efficiency determined in phase one of the thesis (System). The scenarios are improved Alkaline Electrolysis (AEC+), improved Methanol Synthesis (MS+), improved Fluid Machinery (FM+) and all of them together (System+).

7.2. Integrating Heat

Zero Emission Fuels has chosen to use Peltier elements to facilitate heat integration. In [subsection 7.2.1](#) the mathematical model to describe them is discussed after which they are implemented in two case studies in [subsection 7.2.2](#).

7.2.1. Peltier Element Model

Peltier elements are thermoelectric devices. They have no moving components and can both cool and heat depending on the way current is sent through them. This makes them suitable to work with varying cycle times and variations in power. They are furthermore very compact and cheap. A Peltier element manufactured by LairdTech (PT4-12-F2-3030) was chosen [[36](#)]. This type has a maximum temperature difference of 70 °C and a cooling capacity of 30 Watts.

Model Peltier elements are described mathematically by Wijngaards [[37](#)]. The characteristic equations for the extracted heat, \dot{Q}_{peltier} and voltage, V_{peltier} are:

$$\dot{Q}_{\text{peltier}} = \Delta S T_c I - \kappa(T_h - T_c) - \frac{I^2 R}{2}, \quad V_{\text{peltier}} = IR + \Delta S(T_h - T_c) \quad (7.1)$$

In which ΔS describes the difference of the Seebeck coefficients, T_c is the temperature of the cold side where heat is extracted, I is the current, κ is the thermal conductivity, T_h is the hot side temperature and R is the electrical resistance. The characteristic equations are fitted on data from the datasheet with Matlab's least squares fitting function. The results are shown in [Figure 7.3](#). The best parameters to approximate the cooling capacity, \dot{Q}_{peltier} are $\Delta S = 0.052 \text{ J}\cdot\text{A}^{-1}\cdot\text{K}^{-1}$, $\kappa = 0.344 + 0.046I \text{ W}\cdot\text{K}^{-1}$, $R = 3.36 \text{ }\Omega$ and the best parameters to approximate the voltage, V_{peltier} are $R = 3.36 \text{ }\Omega$, $\Delta S = 0.049 - 0.008I \text{ W}\cdot\text{A}^{-1}\cdot\text{K}^{-1}$. These parameters only work if the temperature is implemented in Kelvin and the current in Ampere.

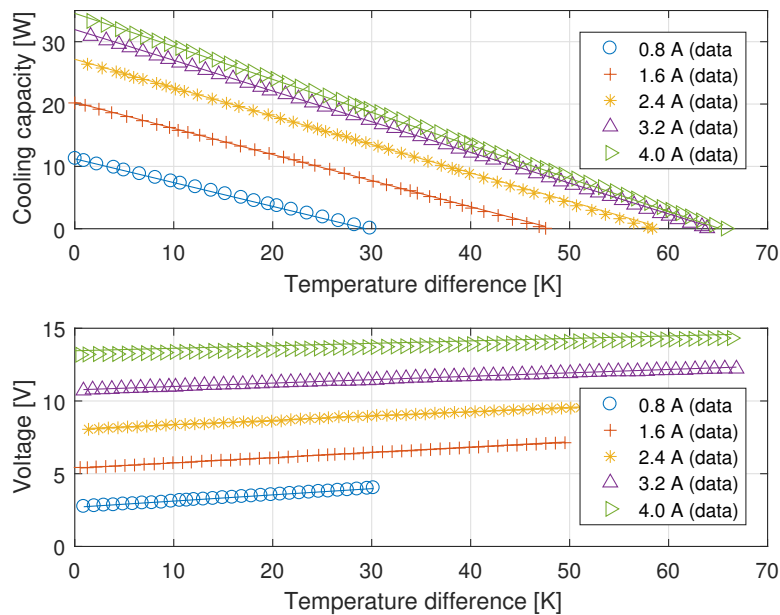


Figure 7.3: Peltier element cooling capacity (upper figure) and operating voltage (lower figure) as function of the temperature difference and applied current. The data is manually extracted from the datasheet of the manufacturer [36]. MatLab's least squares fitting function was applied to find the parameters of Equation 7.1 that best approximated these data points.

Verification The Peltier element is tested by connecting it to an infinite Thermal Buffer and a Direct Air Capture chamber. The results presented in Figure 7.4 show that this Peltier element is able to heat and cool the Direct Air Capture chamber. Since heat from the Thermal Buffer is used the Direct Air Capture has a lower energy input. The energy use for this specific day drops from 0.355 kWh to 0.208 kWh.

The Thermal Buffer was given a finite mass of 4 kg H₂O to make it more realistic. It was observed that all heat adsorbed during the day was lost over night. This was caused by the conduction to the Direct Air Capture chamber which is continuously open at night and thus cooled by outside air. To keep the energy in the Thermal Buffer it is desired to close the Direct Air Capture chambers at night. Increasing the Thermal Buffer from 4 kg to 64 kg H₂O decreased the daily temperature fluctuations from 10 °C to 1 °C.

Discussion This model assumes that all extracted heat, \dot{Q}_{peltier} is immediately removed from the subsystem. This means that effects of heat transportation through the different interfaces of the Direct Air Capture chamber and Thermal Buffer are not taken into account. The Peltier elements thus need to have a good thermal connection. There is a mismatch between the theory and the data as can be derived from the fitting procedure. The Seebeck coefficient, ΔS is approximated with two different values: one is depending on the current the other is not.

The model makes use of one specific Peltier element that was chosen to match the cooling capacity of the Direct Air Capture subsystem that was used in the first phase of the thesis. This Peltier element will be used in different case studies and might therefore not be perfectly suitable in all case studies.

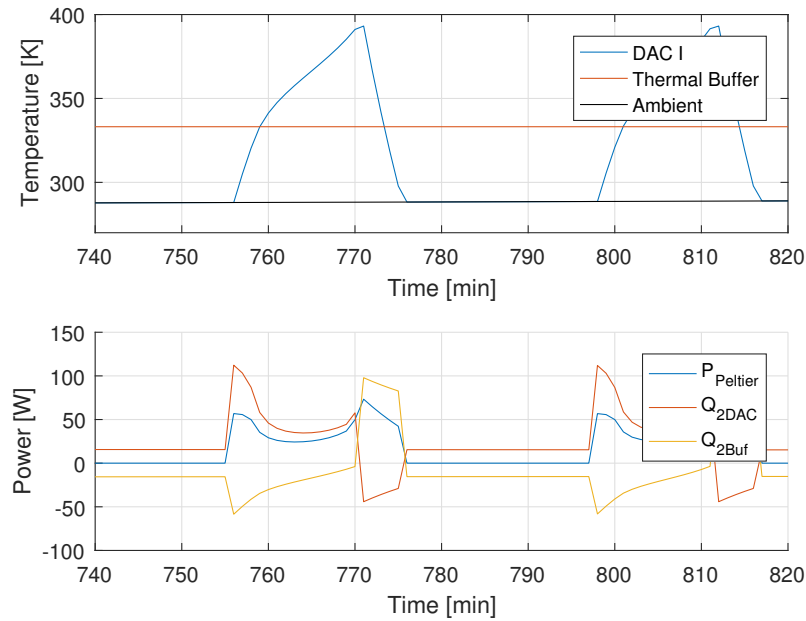


Figure 7.4: Temperature and power development over time of the Direct Air Capture chamber and a Thermal Buffer with infinite mass connected with a Peltier element. The Peltier element is able to heat and cool as expected. It uses less power to do the same amount of cycles because it partially uses heat from the Thermal Buffer.

7.2.2. Case Studies

The Peltier element model has been verified in the previous subsection and is now implemented in the Simulation Tool in two case studies. The first one, heat integration 1 (HI 1), connects the Direct Air Capture chambers through a Thermal Buffer with two Peltier elements. The second case study (HI 2) connects the Alkaline Electrolysis with the Capillary Distillation through a second Thermal Buffer also with two Peltier elements. These cases are shown in Figure 7.5.

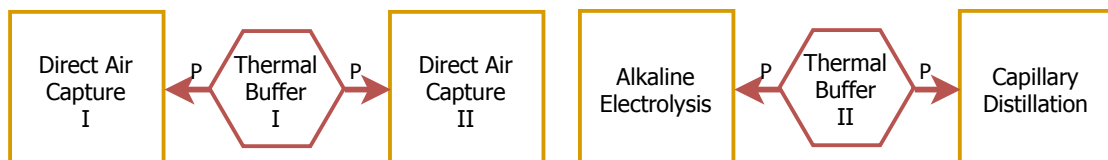


Figure 7.5: Schematic overview of the two case studies for heat integration. In the first case study the Direct Air Capture chambers are connected via Peltier elements (P) to Thermal Buffer I. In the second case study the Alkaline Electrolysis and Capillary Distillation are connected via Peltier elements to Thermal Buffer II.

In these cases a maximum of two subsystems is involved. This was preferred over a case in which all subsystems are connected to form a larger network with many different heat flows taking place simultaneously. Such a network would be more difficult to understand and verify.

Heat Integration Case 1 (HI 1)

This case was chosen because the Direct Air Capture chambers continuously alternate between heating up and cooling down in the same temperature range. The Thermal Buffer is introduced because the cycle times vary continuously, throughout the day and between days, which makes direct coupling e.g. with heat pipes unsuitable. A full year will be simulated and the Thermal Buffer will have an initial temperature equal to the ambient temperature. The Thermal Buffer loses heat to the environment. The total thermal resistance in the model is $10 \text{ K}\cdot\text{W}^{-1}$. The mass of the Thermal Buffer is $4 \text{ kg H}_2\text{O}$. The energy balance will be solved with Runge-Kutta4.

Results The result is an average buffer temperature of 324 K which is 29.6 K higher than the average ambient temperature. The energy use of the Direct Air Capture decreased with 26% from 0.45 kWh·day⁻¹ to 0.33 kWh·day⁻¹. The System efficiency increased from 24.9 % to 28.8 %. An overview of the parameters and results of this case study, HI 1, and the next one, HI 2, is shown in [Table 7.1](#).

Case Study	Subsystems	\bar{T}_{buffer} [°C]	m_{buffer} [kg]	R_{thermal} [K·W ⁻¹]	E_{saved} [kWh·day ⁻¹]	η_{System} [%]
HI 1	DAC	51	4	10	0.22	28.8
HI 2	AEC & DS	55	4	10	0.13	26.9

Table 7.1: Overview of the parameters used in the heat integration cases, HI 1 and HI 2, and their impact on system efficiency.

Heat Integration Case 2 (HI 2)

This case was chosen because the Alkaline Electrolysis was observed to need active cooling during most hours of the day. The Methanol Synthesis reactor continuously needs to be heated. It however operates at a temperature of 210 °C, which the chosen Peltier elements from LairdTech cannot reach [36]. The only subsystem that continuously needs heat and operates at a reachable temperature is the Capillary Distillation. Therefore, the connection between the Alkaline Electrolysis and Capillary Distillation was investigated in this second case study. The subsystems will most likely be asking for cooling and heating at separate moments in time. Therefore, it was decided to connect them just as with the first case study through a Thermal Buffer, instead of directly. The Thermal Buffer also loses heat to the environment. The total thermal resistance in the model is 10 K·W⁻¹. The mass of the Thermal Buffer is 4 kg H₂O.

Results The results show an average Thermal Buffer temperature of 328 K which is 34.4 K higher than the average ambient temperature. The energy use of the Capillary Distillation decreases with 68 % from 0.19 kWh·day⁻¹ to 0.060 kWh·day⁻¹. The System efficiency (Solar Panel power to MeOH) now becomes 26.9 %. With both case studies implemented it becomes 30.8 %. The subsystem efficiency improvements as well as both heat integration case studies showed an System efficiency of 36.0 %. A summary of all cases discussed in this subsection is shown in [Figure 7.6](#).

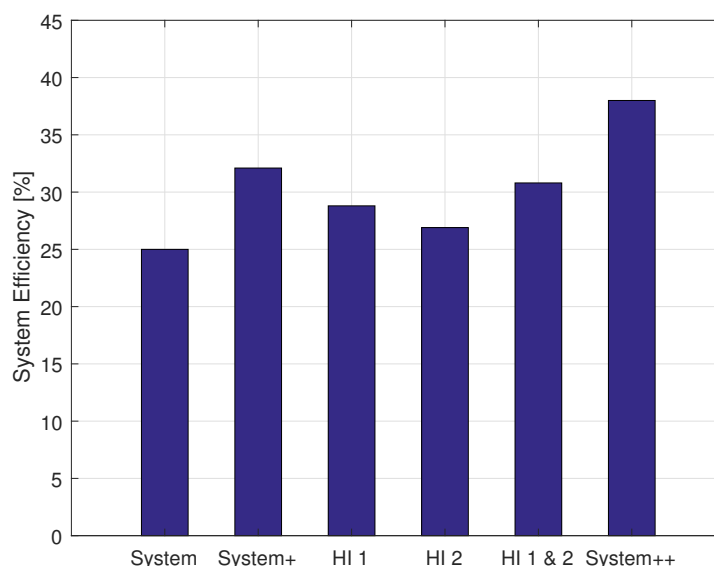


Figure 7.6: System efficiency in different scenarios in which heat integration (HI) is applied compared to the efficiency determined in phase one of the thesis (System) and the combined improvements of increasing the subsystem efficiencies (System+). The other scenarios are the Direct Air Capture case study (HI 1), the Alkaline Electrolysis and Capillary Distillation case study (HI 2), the two heat integration cases (HI 1 & 2) and HI 1, HI 2 and System+ combined (System++).

7.3. Improved Control Model

An overview of the new Control Model and its functions is given in Figure 7.7. First the new Control model is elaborated upon after which it is tested in three different cases.

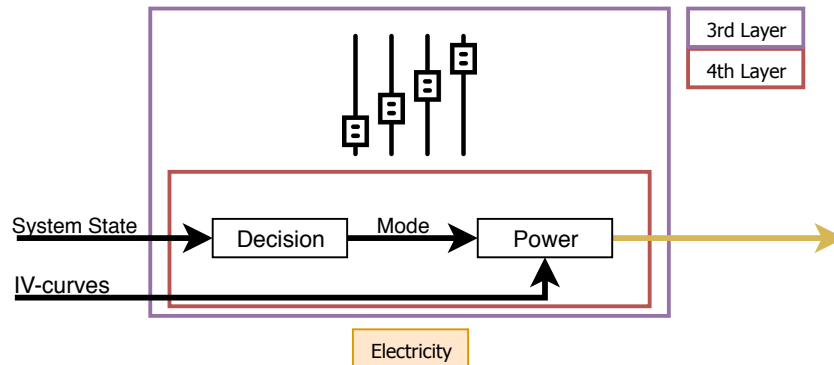


Figure 7.7: High level overview of the new Control Model. The decision function first decides the operation Mode of the subsystems based on the System state. The Power function subsequently determines the electrical operating point of the System and subsystems based on the operation Mode of each subsystem and the corresponding IV-curves. The main difference with the old Control model is that the Decision function takes place before the Power function instead of the other way around.

7.3.1. Decision function

The basic idea of the new Decision function is to switch on all subsystems simultaneously and switch to a different operation Mode if predetermined thresholds are exceeded. These thresholds should make sure that no dangerous System states are reached. The basis Mode of all subsystems is on as soon as sunlight falls on the Solar Panel.

Direct Air Capture & Fluid Machinery The Direct Air Capture chambers know four Modes. They switch from adsorbing to desorbing as soon as the loading becomes higher than the maximum sorbent loading. They switch from desorbing to cooling when the maximum temperature for desorption is reached and from cooling to adsorbing if the minimum temperature for adsorption is reached. As an additional prerequisite the Direct Air Capture chambers are not allowed to adsorb at the same time because only one fan is available. The Fluid Machinery is directly coupled to the desorption stage of the Direct Air Capture cycle and automatically switches on during this stage.

Alkaline Electrolysis The Alkaline Electrolysis knows three Modes. The first one is normal operation in which H_2 is produced. It will enter the second Mode as soon as the maximum operating temperature has been reached turning on a Peltier element for cooling. If the Peltier element cannot cool the subsystem anymore the Alkaline Electrolysis is switched off.

Methanol Synthesis & Capillary Distillation The Methanol Synthesis knows three different Modes. The first one is heating at maximum capacity until the operating temperature is reached. The second one is heating at a lower intensity such that the desired operating temperature is maintained. The last state is off when the operating temperature is exceeded. The Capillary Distillation turns on when the Methanol Synthesis is at its operating temperature after which it starts heating at maximum capacity. The Capillary Distillation is turned off as soon as the operating temperature is exceeded.

7.3.2. Power function

The new Power function has to find the cross-section of the IV-curves of the Solar Panel and Plant. The IV-curve of the Plant is now created from all electrical components instead of only the Alkaline Electrolysis. The new equivalent electrical circuit is shown in ???. The subsystems are connected in parallel such that each one can be switched on and off separately. An additional benefit of a parallel circuit is that the voltage over each subsystem is equal and that the currents can be added to find the System current.

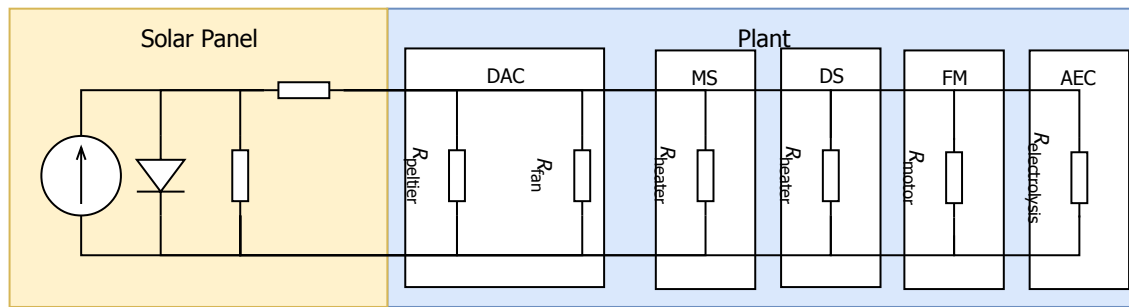


Figure 7.8: Equivalent electrical circuit of the improved System. The main difference with the electrical circuit of phase I is that all electrical devices are incorporated instead of only the Alkaline Electrolysis.

It is important that the calculation time of the Power function is minimised. The IV-curve of the Solar Panel varies continuously because of the varying irradiance and change in temperature. The IV-curve of the Plant also varies continuously due to different subsystems being switched on and off. The function thus has to find the operating point every time step and there are 525600 time steps in a year.

IV-curves The current can be determined for most electrical components by applying Ohm's law. To determine the current flowing through the Peltier elements, Equation 7.1 needs to be rewritten:

$$I = \frac{V_{\text{peltier}} + \Delta S(T_c - T_h)}{R} \quad (7.2)$$

To determine the current flowing through the Alkaline Electrolysis the inverse of Equation 2.7 is taken. To rewrite it the Lambert-W function needs to be introduced. The downside of this function is that MatLab calls the symbolic solver to find the solution. This takes around 0.1 second to solve per time step. For all 525600 time steps this means that the simulation of the full year would take around 14 hours. To work around this problem it was decided to implement a numerical root-finding method to find the Alkaline Electrolysis current. It was chosen to implement the Newton-Raphson method because of its fast convergence.

7.3.3. Case Studies

To verify the impact of the new Control model it is implemented in the Simulation Tool in three cases. These are compared to the results of the old Control model (CM). In the first case (CM+) the electrical System design parameters used in phase I are implemented together with the new Control Model. In the second case (CM+ Manual) the parameters are adjusted manually to improve the MeOH production. In the third case (CM+ GA) a genetic algorithm is applied to find the optimal set of parameters. An overview of the parameters and results of these cases can be found in Table 7.2.

Control Model (CM) This case uses the old Control model and takes into account all subsystem improvements (System+) discussed in section 7.1 as well as the first heat integration case (HI 1) discussed in subsection 7.2.2. Only the first heat integration case was chosen since the Peltier elements were specifically chosen for the Direct Air Capture not for the Alkaline Electrolysis or Capillary Distillation. This case result in a Solar Panel efficiency (Maximum power to power) of 98 % and a System efficiency of 36.0 %.

New Control Model (CM+) The new Control model needs to know the electrical resistance of each electrical device. In the old Control model each subsystem received a fixed amount of power. This is converted into a resistance with Ohm's law and by assuming a Solar Panel voltage of 33 V. The amount of Alkaline Electrolysis cells (16) and Peltier elements (1) was not changed. The results show a higher mismatch between the Solar Panel and Plant IV-curves. The Solar Panel only produced 81.0 % of its maximum power, $1.77 \text{ kWh} \cdot \text{day}^{-1}$. The System efficiency in this case is 6.9 %.

	Unit	CM	CM+	CM+ Manual	CM+ GA
n_{cells}	[-]	16	16	19	19
n_{peltiers}	[-]	1	1	3	3
P_{ms}	[W]	50			
R_{ms}	[Ω]		22	30	43.6
P_{fan}	[W]	27			
R_{fan}	[Ω]		44	40.0	38.8
P_{ds}	[W]	25			
R_{ds}	[Ω]		40	30	38.0
P_{fm}	[W]	50			
R_{fm}	[Ω]		22	10	10.1
η_{MPP}	[%]	98.0	81.0	93.0	93.4
η_{System}	[%]	36.0	6.9	38.9	39.8
n_{MeOH}	[mole·day ⁻¹]	4.3	0.7	4.7	4.8

Table 7.2: This table shows an overview of the parameters and their results. The old Control model (CM) is compared with the new Control model (CM+) after implementing manual improvements (CM+ Manual) and after optimisation with a genetic algorithm (CM+ GA).

Manual Improvements (CM+ Manual) The mismatch of the IV-curves was caused by the electrical characteristics of the Peltier elements and amount of cells in the Alkaline Electrolysis. The Plant IV-curve was improved by putting 3 Peltier elements in series and by adjusting the Alkaline Electrolysis cells from 16 to 19. This resulted in a Solar Panel power output of 93.0 % of the maximum power, 2.03 kWh·day⁻¹. Although this power output is lower than determined in the first phase of the thesis the System efficiency was found to be higher: 38.9 %.

Genetic Algorithm Improvements (CM+ GA) All electrical parameters directly and indirectly influence the MeOH production. It was therefore decided to implement a genetic algorithm. In the objective function MeOH production was maximised. The results showed a slight increase of production from 4.7 mole to 4.8 mole of MeOH. The System efficiency (Solar Panel power to MeOH) is 39.8 % and the Solar Panel power is 93.4 % of the maximum power. The impact on Solar Panel power of the different cases is shown for a random day of the year in [Figure 7.9](#).

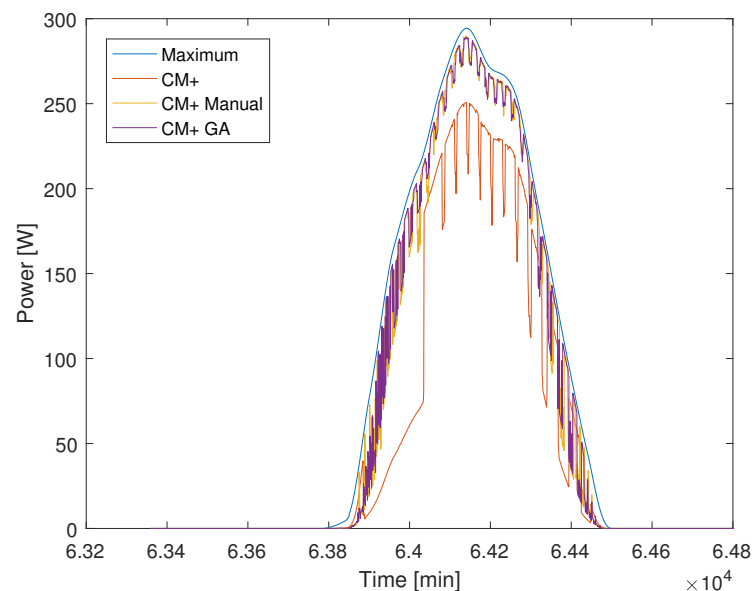


Figure 7.9: Effect of the new Control model on Solar Panel power compared to the maximum power for a random day. A wrongly designed System shows large deviations from the maximum power.

8

Improvements Discussion

In this chapter the results of the implementation of the improvements into the Simulation Tool are discussed. This chapter ends the second phase of the thesis as shown in Figure 8.1. This chapter focuses on three of the research objectives of this thesis: to identify the most important System design parameters, to give suggestions to improve the System and to verify the impact of these improvements. An overview of the results that are referred to in this chapter is shown in Figure 8.2.

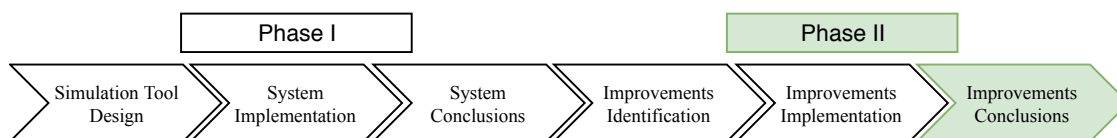


Figure 8.1: This section focuses on the last part of the thesis. The conclusions of the improvements.

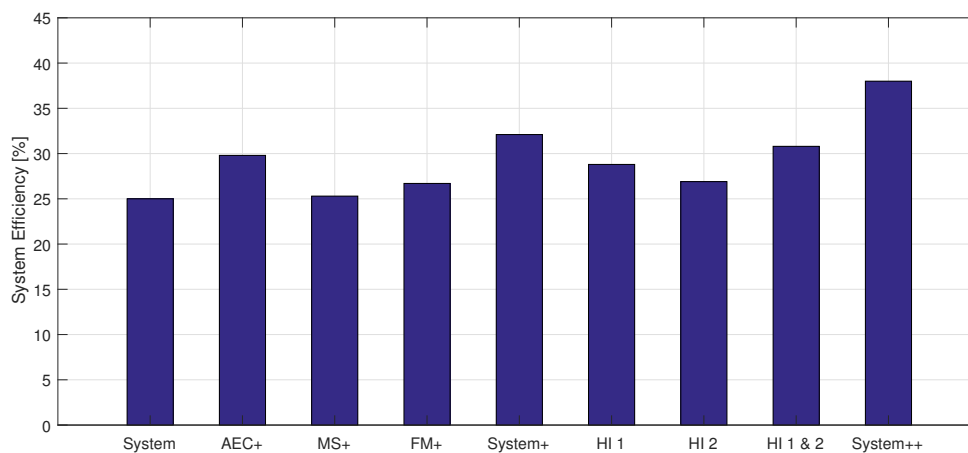


Figure 8.2: Overview of the System efficiency for different scenarios of subsystem efficiency improvements as well as heat integration. The scenarios are improved Alkaline Electrolysis (AEC+), improved Methanol Synthesis (MS+), improved Fluid Machinery (FM+), these previous three combined (System+), heat integration case study 1 (HI 1), heat integration case study 2 (HI 2), the previous two combined (HI 1 & 2) and all subsystem efficiency improvements and heat integration cases combined (System++).

8.1. Increasing Subsystem Efficiency

The improvements in the Alkaline Electrolysis (AEC+) have the largest effect on System efficiency because this subsystem uses the most energy of all subsystems. The most important parameters are the temperature and current density. The effect of doubling the Fluid Machinery efficiency (FM+) is a little less but still significant and thus worth pursuing. Improvements of reducing subsystem mass as has been investigated for the Methanol Synthesis reactor (MS+) have a positive effect on System efficiency. The effect is the smallest of the investigated improvements. If all these improvements are combined (System+) the System efficiency increases from 24.9 % to 32.1 %.

Discussion

The increase in Alkaline Electrolysis electrode area is an economic trade-off. The cost will increase for the electrodes as well as the casing surrounding it since more material is needed. The casing also needs to be thicker in order to withstand the same pressure. The increase in temperature of the Alkaline Electrolysis results in a more chemically aggressive electrolyte. The material of the casing should be able to withstand such an environment and temperature. The Fluid Machinery efficiency has never been verified experimentally. It remains uncertain whether the used efficiencies of 20 % and 40 % are achievable. If apart from the Methanol Synthesis the other subsystems are also made lighter the effect on System efficiency will be larger. It has to be noted that the mechanical stability should not be compromised as the mass is decreased.

This is not a complete investigation of improvements that can be made to the subsystems. An improvement that is not investigated but can be applied to all subsystems is related to the insulation. Increasing its thickness or using a material with a lower thermal conductivity also influences System efficiency. Another option is to create a casing in which all subsystems are protected from the environment which functions as a second layer of insulation. Directions to improve specific subsystems are found in the discussions of [chapter 4](#).

It was desired to investigate whether a significant impact on MeOH production could be made. These cases proved that it is possible but at the same time show that more improvements are needed to get closer to the business case target of 55 %.

8.2. Integrating Heat

The goal was to verify the effect of heat integration with Peltier elements and Thermal Buffers on System efficiency. Their influence was investigated in two case studies (HI 1 and HI 2). The System efficiency was observed to increase from 24.9 % to 30.8 %.

Peltier elements The characteristic equations from Wijngaards [37] provide insight in the behaviour of a Peltier element. The heat it transports from one side to the other is depending on three terms. These are conduction, joule heating and heat that is transported due to the thermoelectric (Peltier-Seebeck) effect. In the case studies the Peltier elements were successfully able to reduce subsystem energy use. At the same time the results showed that they are able to be used as a heater and a cooler by switching the current from positive to negative.

Thermal Buffer The availability of heat at different moments in time and at different temperatures makes heat integration via direct means impractical. In the case studies a Thermal Buffer proved to be a suitable option to temporarily store the heat. The insulation of the Thermal Buffer determines the steady-state heat loss to the environment. Increasing the total thermal resistance will result in a higher Thermal Buffer temperature. The Thermal Buffer temperature fluctuates over the year and day but remains relatively constant compared to the ambient temperature. During the day the temperature increases slightly because heat is stored due to operation of the subsystems. During the evening it drops slightly due to heat loss to the environment. Since H₂O has a large heat capacity it is able to stabilise the temperature fluctuation of the Thermal Buffer. The total buffer size determines the fluctuation. Increasing the buffer size from 1 kg to 64 kg reduces the daily temperature fluctuation from around 30 °C to 1 °C.

Discussion

No other options for heat integration are investigated. Only the effect of Peltier elements in combination with Thermal Buffers. These cases were also not optimised. More research is thus needed in this direction. For example more subsystems can be included like the Fluid Machinery from which heat needs to be extracted for the condensation step. The subsystems can also be connected in a more complex network involving not two but three or all of them. Optimisation of such a network can finally make sure that the heat integration network operates more optimal.

Peltier elements Only one type of Peltier element has been investigated. The Peltier elements was chosen for the Direct Air Capture case study since it matched the desired cooling capacity. In the Alkaline Electrolysis case study four Peltier elements had to be implemented to deliver the desired cooling capacity. It might be useful to fit a whole range of Peltier elements to identify the range for the parameters (Seebeck coefficient, thermal conduction and electrical resistance). A genetic algorithm can find the optimal values within this range for each case study. This will help in selecting the best Peltier element.

It has to be noted that the fitting function was applied on data that was obtained from manually extracting the data points. The accuracy of this process can not be verified other than by visual comparison. The Peltier elements were also operating at a fixed current. The Peltier element efficiency is however a function of the temperature difference and the current. If the Peltier elements are controlled to always work at their maximum efficiency the energy use is expected to drop further. The downside of this is that a different operating current also effects the added or removed heat and thus the cycle times and heating rates. The lag of switching the Peltier element from heating to cooling is not taken into account in this model and should be verified. The model assumed that it could immediately switch if the power was converted from positive to negative.

Thermal Buffer The optimal Thermal Buffer size and operating temperature have not been determined. For each case an optimal temperature can be found that minimises the energy use of a subsystem. The Thermal Buffer temperature can be influenced by adjusting the insulation thickness and material. The Thermal Buffer size influences the daily temperature fluctuations. Less fluctuations allow for more constant operations. This is again an economic trade-off since the cost is influenced by the insulation and Thermal Buffer size.

8.3. Improved Control Model

The importance of a more accurate Control model was observed in the cases that have been studied. An overview of the different cases with the old and new Control model is shown in [Figure 8.3](#). A decrease in Solar Panel efficiency (maximum power to power) was observed with all new Control models. However, the System efficiency increased from 36.0 % to 39.8 %. An important factor in this is that the Alkaline Electrolysis efficiency was improved from 70.3 % to 76.3 %. This can be explained by the fact that the Alkaline Electrolyser operates at a lower current density than expected.

Decision Function For the new Control model to work the Decision function needs to determine the operation Modes of all the subsystems at the beginning of the time step. In the results it was observed that the new Decision function is able to switch between the right Modes at the predetermined thresholds and that no dangerous System states are reached.

Power Function The calculation speed of the Power function should be maximised since more than half a million time steps need to be determined for each year of simulation. The Power function needs to find the current of each subsystem. To find the current both linear and nonlinear equations have to be solved. The Newton-Raphson algorithm proved quick enough to find the root of the nonlinear Alkaline Electrolysis equation.

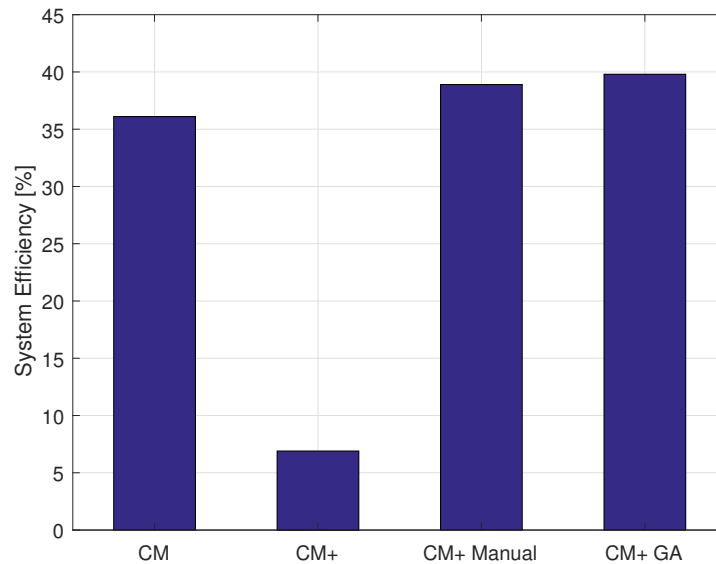


Figure 8.3: Overview of the results of the old Control model (CM) and the new one (CM+) with manual adjustments (CM+ Manual) and an optimised set of parameters using a genetic algorithm (CM+ GA)

Cases The manual design of the electrical parameters gives insight in the behaviour of the System. It was observed in the results that using this approach one can improve both Solar Panel and System efficiency. To find the global optimum by hand is either impossible or very time consuming because of the size of the solution space and the time it takes to simulate one year. The genetic algorithm proved to be a fruitful option to approximate it in around one day.

It was observed that the amount of Alkaline Electrolysis cells influence how close the Solar Panel operates near it's maximum power during the adsorption Mode of the Direct Air Capture. The Peltier elements that switch on during desorption or cooling cause a large mismatch between the IV-curves. Three Peltier elements in series proved to solve this issue because this positively influenced their IV-curve because the electrical resistance increased.

Discussion

Decision Function The Decision function is currently only based on the physical limits of the System and simply switches from one state to the other if a threshold is exceeded. It was already stated in [chapter 5](#) that a more flexible Control model can improve the System efficiency. This has not been investigated but is an interesting topic for further research.

Cases As more Peltier elements are added to facilitate heat integration, more components will contribute to the Plant IV-curve. Every additional electrical component will influence System efficiency and thus the need to also change other subsystem parameters. It is therefore recommended to always approach the design of the electrical circuit as a whole. Using the genetic algorithm some highly precise values can be obtained to achieve the best possible System efficiency. Components with those values might not be available on the market. Therefore, it is advised to only use these values as guidelines for choosing the electrical components of the System. It might however be an interesting exercise to see what values the genetic algorithm comes up with for them (Seebeck coefficient, thermal conductivity, electrical resistance) and verify those with Peltier elements on the market.

9

Conclusions & Recommendations

This chapter focuses on the conclusions and recommendations. In [section 9.1](#) an overview is given of the final improved System that was obtained in this thesis. The six research objectives are stated and answered one by one in [section 9.2](#). The recommendations are given in [section 9.3](#).

9.1. Improved System

An overview of the final design of the improved System is shown in [Figure 9.1](#). The Alkaline Electrolysis, Fluid Machinery and Methanol Synthesis are improved and heat integration is added to the Direct Air Capture.

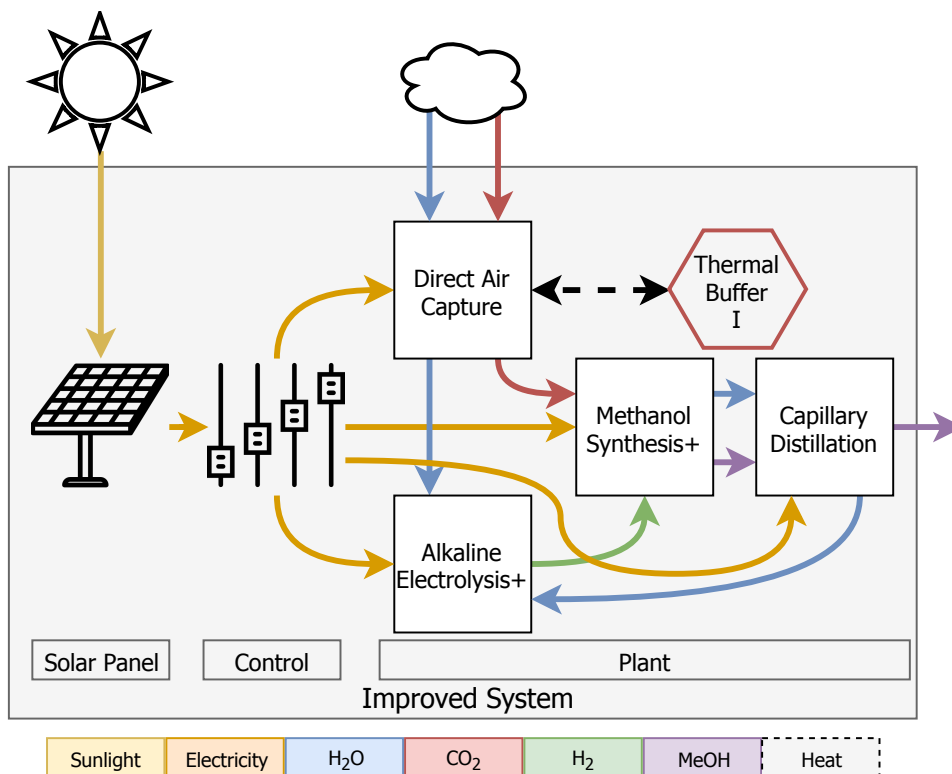


Figure 9.1: Overview of the improved System design. The subsystems are improved and heat integration is added to the Direct Air Capture.

9.2. Conclusions

The conclusions of the six research objectives are discussed in the next subsections.

Predict System Production

The main research objective is to predict Zero Emission Fuels' System production for every minute of the year at any location on earth a Simulation Tool is developed in this thesis in which different System designs can be implemented without having to change the Simulation Tool architecture. The Simulation Tool is verified in this thesis to work for data from Tucson, Arizona in 2005 and various different System designs. If data of the same format is used this finding suggests that the Simulation Tool is also able to predict the production for other locations. This means that this Simulation Tool can be used to quickly test minute by minute behaviour of a future System design for various locations. Something that was impossible prior to this study.

With the System design of January 1, 2018 an average daily production of 3.0 mole MeOH can be expected for Tucson, Arizona in 2005 if the average daily global horizontal irradiance is 7.00 kWh. The results showed that all System design parameters directly or indirectly influence the performance of the System. This suggests that the optimal System design is different for different locations. A major shortcoming is that the model contains assumptions that are not verified experimentally. The accuracy of the predictions can be improved upon by adjusting the models to the results of such experiments. It is also recommended to implement Mass Buffers that can temporarily store the components that are produced by the different subsystems.

Simulation Time

The second research objective states that the results should be determined within 15 minutes. In this thesis this has been achieved by minimising the calculation time of each function. Furthermore, the calculations of all none fluctuating variables and parameters are removed from the time loop that determines the System state for each minute. Iterations are also avoided or made to converge as quick as possible. MatLab's symbolic solver is not used since it too slow for the purpose of this thesis. The 1D models of the subsystems and the numerical techniques discussed in [section 2.3](#) proved suitable for this. No numerical instabilities are introduced and a simulation time of less than 6 minutes is achieved. This suggests that it is possible to test how any System behaves for ten locations on earth within an hour. This also means that if the target for one simulation remains at 15 minutes more detailed models can be implemented. New models also have limitations as it cannot be guaranteed that no numerical instabilities will occur since an explicit method was used for approximation of the time derivatives in this thesis. In such a situation it is advised to switch to an implicit time integration method.

Effect of Environmental Fluctuations

The third research objective states that it is desired to get insight into the variations in System behaviour due to varying environmental conditions. The main finding is that large fluctuations are to be expected between consecutive days and between seasons. The System was found to produce 1.0 mole methanol during a cloudy winter day and 4.2 during a sunny summer day. This has implications for the design of the System. All subsystems should be able to deal with these fluctuations without breaking down. This also influences the logistics of the company because in winter MeOH has to be collected less frequently than in summer. It has to be noted that the fluctuations in environmental conditions are investigated on smoothly interpolated data. In reality minute to minute variations will fluctuate more than anticipated in this thesis. The effect of this on System behaviour is interesting to investigate.

System Design

The fourth research objective was to get insight into the most important System design parameters.

Location If more sunlight is available the Solar Panel can produce more power. A location with high irradiance is therefore preferred. An average global horizontal irradiance of $7.00 \text{ kWh}\cdot\text{day}^{-1}$ is found for a few locations on earth. These locations are Northeastern Australia, the Red Sea area, Namibia and Chile. It has to be noted that in this thesis these locations have been tested by adjusting the irradiance data from Tucson, Arizona to an average of $7.00 \text{ kWh}\cdot\text{day}^{-1}$. The locations themselves could not be tested because of the absence of free data for them. No conclusions can be drawn for the ideal temperature because both the Solar Panel and Plant behaviour are influenced by it differently.

Solar Panel To maximise the irradiance that falls onto the Solar Panel the orientation angles always need to be optimised. In Tucson, Arizona the optimal angles are determined to be 63° tilt and 165° azimuth. To further increase the Solar Panel power output its temperature should be as low as possible. The electrical characteristics of the load determine how close the Solar Panel operates to the maximum power. The Solar Panel power output was found to be 93 % of the maximum power but decreases especially if adjustments are made to the amount of Alkaline Electrolysis cells in series. This finding endorses the importance of matching the electrical characteristics of the load and Solar Panel.

Control model The most important function of the Control model is to make sure that no dangerous System states are reached. This research has shown that the implemented Control model is able to do this. The most important parameters for the Control model are thus to set the right thresholds that represent physical damage in reality. The downside of this approach is that the switching between operation Modes is not optimal. Therefore, it is recommended to investigate possibilities to improve it.

Plant The most important subsystem of the Plant is the Alkaline Electrolysis because it uses the most energy. The operation of this subsystem is thus very important and its efficiency should be as high as possible. The design parameters that influence this are the current density and temperature. The current density should be minimised while the temperature should be maximised. An efficiency of around 65-75 % can be expected. To get closer to the business case target this means that this subsystem should receive even more energy than it currently does. Therefore, improvements to the other subsystems and the System as a whole are needed. A limitation of the subsystems models that make up the Plant model is that many of them have not been verified experimentally. To tackle this problem it has been tried to overestimate energy use but it cannot be guaranteed that they are correct.

Directions for Improvements

The fifth research objective was to identify directions to improve the technical design of the System.

Increase Energy It has been observed that a lower temperature increases the Solar Panel energy output and that the load needs to be matched to the Solar Panel IV-curve to operate as close as possible to the maximum power. In Tucson, Arizona 2-axis tracking can increase the energy output by up to 32 %. This means that 32 % more methanol can be produced if the System efficiency stays the same. The downside of tracking is that the complexity of the System and thus the cost increases. It has to be noted that the efficiency gains might be different at other locations.

Improve Subsystem Efficiency The second option to increase System efficiency is to improve the efficiency of each subsystem. The largest improvements are observed in the Alkaline Electrolysis. The effect of decreasing internal losses has been tested on the Fluid Machinery. Measures that can be taken to improve all subsystems are to be found in the insulation and thermal mass. If the insulation is improved or the thermal mass decreased less energy is needed to heat up the subsystem. This was tested on the Methanol Synthesis reactor. All improved subsystems together resulted in a System efficiency increase from 24.9 % to 32.1 %. These findings imply that to improve the System the largest focus should be on the Alkaline Electrolysis efficiency. A limitation of these findings is that only three improvements have been tested. It is also important to keep in mind that improving the efficiency is not just a technical but also an economical trade-off as all investigated improvements are thought to be associated one way or another with increased cost.

Improve Control The Control model can also influence the System efficiency. The effect of this has only been analysed qualitatively. It has been observed in the results that energy was wasted that could have been prevented with a different Control model. The Direct Air Capture started new desorption cycles at the end of the day which it could not complete because the sun went down. The power the Alkaline Electrolysis receives fluctuates strongly while it would benefit from a continuous and lower current. This implies that if the Control model makes better use of the information of the System state more methanol can be produced. This significance of this has to be quantified in future research. Another interesting direction is to incorporate weather forecasts.

Integrate Heat The last improvement that was investigated in this thesis was the integration of heat. The observation that different subsystems are heated and cooled throughout the day means that there is a potential for heat integration as has been demonstrated in two case studies. Peltier elements in combination with a Thermal Buffer proved suitable. The System efficiency was observed to increase from 24.9 % to 30.8 % if both case studies are implemented. The scope of this study is limited because it only verified the two cases with Peltier elements. It is expected that the System efficiency can be increased further if the heating and cooling of more subsystems is added. Other possibilities to integrate heat with heat pipes or heat exchangers have not been investigated. Therefore, it can only be concluded that a solution for heat integration but not an optimal one has been found.

Improved System Production

The last research objective was to verify the effect of the improvements on System efficiency. A selection of the identified improvements was implemented. The Alkaline Electrolysis, Fluid Machinery and Methanol Synthesis are improved and heat is integrated between the two Direct Air Capture chambers. Furthermore, a new Control model was implemented that matches the IV-curves of all subsystems with the Solar Panel instead of only the Alkaline Electrolysis. This System was observed to produce 4.8 mole methanol instead of 3.0 mole. This finding indicates that there still is a large challenge to reach the business case target of 6.7 mole and that more improvements are to be implemented to reach it. The most important limitation of this thesis is the uncertainty of the models. The uncertainty in every subsystem model influences the uncertainty of the System model. Therefore, the specific numbers predicted in this thesis should be interpreted carefully. However, both the relative improvements as well as the identified System parameters that mostly influence the methanol production are useful to keep in mind when designing future Systems.

9.3. Recommendations

It is interesting to make a comparison off different locations on earth to investigate the effect of different climates and different weather types. Such a comparison could provide insight into the effect on System efficiency of different ratios between direct normal irradiance, diffuse horizontal irradiance, temperature and seasonal and daily effects like rain or clouds. This is useful because it allows for identification of favourable and realistic conditions for the System to be placed in. Another interesting direction for future research is to compare hourly interpolated data and actual minute data to say something about how the fluctuations actually influence System performance. This is useful because it will provide insight into whether interpolation of hourly data is comparable to real minute behaviour.

This research mainly focused on the energy and mass balances of the subsystems. A next step would be to incorporate a momentum balance to be able to say something about the flows and pressures in the System. This can support the design of the tubes and Mass Buffers. A final option is to incorporate cost parameters for different locations on earth to improve the accuracy of the Business Case Model. This is useful because the technical System is only a small part of the considerations to choose a location.

9.4. Final Remark

The Simulation Tool developed in this thesis should only be used to improve the technical design. There are however many more considerations that influence this. The company activities and their interaction have been shown in the introduction in [Figure 1.3](#). In this figure it can be seen that the output of the System Model, the methanol production and System behaviour, is only one of many inputs for the Business Case Model. This model is more important because in the end it is desired to have a profitable business not just a working System. This means that a technically optimal design is not necessarily an economically optimal design. It should thus be realised that the real design decisions will most likely be based on technical, economical and maybe even political arguments.

Bibliography

- [1] European Environment Agency, *Global Total Primary Energy Consumption by Fuel*, <https://www.eea.europa.eu/data-and-maps/figures/global-total-primary-energy-consumption-by-fuel> (2009), accessed: 2018-08-12.
- [2] S. Sutanto, J. W. Dijkstra, J. A. Z. Pieterse, J. Boon, P. Hauwert, and D. W. F. Brillman, *CO₂ removal from biogas with supported amine sorbents: First technical evaluation based on experimental data*, *Separation and Purification Technology* **184**, 12 (2017).
- [3] P. Basarkar, *Experimental Characterization of a Novel Small-Scale Natural Circulation Loop Methanol Synthesis Reactor*, *Ph.D. thesis*, Technical University Delft (2018).
- [4] R. Smith, *Chemical Process Design and Integration* (John Wiley & Sons, Inc., 2005) p. 687, [arXiv:arXiv:1011.1669v3](https://arxiv.org/abs/1011.1669v3).
- [5] J. M. Douglas, *Conceptual design of chemical processes* (McGraw-Hill Book Company, New-York, 1988) p. 601.
- [6] Bergman and Incropera, *Fundamentals of Heat and Mass Transfer*, seventh ed. (John Wiley & Sons, Inc., 2011).
- [7] A. F. Mills and Carlos F M Coimbra, *Basic Heat and Mass Transfer* (Pearson Education Limited, 2013) p. 1032.
- [8] A. H. M. Smets, K. Jäger, O. Isabella, R. A. C. M. M. Swaaij van, and M. Zeman, *Solar Energy; The Physics and Engineering of Photovoltaic Conversion Technologies and Systems* (UIT Cambridge Ltd, 2015).
- [9] E. I. Ortiz-Rivera and F. Z. Peng, *Analytical Model for a Photovoltaic Module using the Electrical Characteristics provided by the Manufacturer Data Sheet*, *36th Power Electronics Specialist Conference (PESC)*, 2087 (2005).
- [10] A. H. Rahim, A. S. Tijani, M. Fadhullah, S. Hanapi, and K. I. Sainan, *Energy Procedia*, Vol. 79 (Elsevier B.V., 2015) pp. 204–211.
- [11] C. Qi and Z. Ming, *Photovoltaic Module Simulink Model for a Stand-alone PV System*, *Physics Procedia* **24**, 94 (2012).
- [12] M. G. Villalva, J. R. Gazoli, and E. R. Filho, *Comprehensive Approach to Modeling and Simulation of Photovoltaic Arrays*, *IEEE Transactions on Power Electronics* **24**, 1198 (2009).
- [13] M. Mattei, G. Notton, C. Cristofari, M. Muselli, and P. Poggi, *Calculation of the polycrystalline PV module temperature using a simple method of energy balance*, *Renewable Energy* **31**, 553 (2006).
- [14] S. Armstrong and W. G. Hurley, *A thermal model for photovoltaic panels under varying atmospheric conditions*, *Applied Thermal Engineering* **30**, 1488 (2010).
- [15] I. R. Caluianu and F. Bălărețu, *Thermal modelling of a photovoltaic module under variable free convection conditions*, *Applied Thermal Engineering* **33-34**, 86 (2012).
- [16] J. Seader, E. J. Henley, and D. K. Roper, *Separation Process Principles, Chemical and Biochemical Operations*, 3rd ed. (John Wiley & Sons, Inc., 2011).
- [17] S. Brunauer, L. S. Deming, W. E. Deming, and E. Teller, *On a Theory of the van der Waals Adsorption of Gases*, *Journal of the American Chemical Society* **62**, 1723 (1940).

- [18] A. D. Ebner, M. L. Gray, N. G. Chisholm, Q. T. Black, D. D. Mumford, M. A. Nicholson, and J. A. Ritter, *Suitability of a solid amine sorbent for CO₂ capture by pressure swing adsorption*, *Industrial and Engineering Chemistry Research* **50**, 5634 (2011).
- [19] A. Godula-Jopek, *Hydrogen Production by Electrolysis* (Wiley-VCH GmbH, 2015).
- [20] J. Evangelista, B. Philips, and L. Gordon, *Electrolytic hydrogen production: an analysis and review*, Tech. Rep. (Lewis Research Center, Cleveland, Ohio, 1975).
- [21] K. M. V. Bussche and G. F. Froment, *A Steady-State Kinetic Model for Methanol Synthesis and the Water Gas Shift Reaction on a Commercial Cu / ZnO / Al₂O₃ Catalyst*, *Journal of Catalysis* **10**, 1 (1996).
- [22] G. E. Gutiérrez Neri, *Simulation of Small Scale Convective Flow Reactor for Methanol Synthesis Production*, *Ph.D. thesis*, Technical University Delft (2018).
- [23] M. J. Bos and D. W. F. Brillman, *A novel condensation reactor for efficient CO₂ to methanol conversion for storage of renewable electric energy*, *Chemical Engineering Journal* **278**, 527 (2015).
- [24] D. R. Seok and S. Hwang, *Zero gravity distillation utilizing the heat pipe principle*, *AIChE Journal* **31**, 2059 (1985).
- [25] E. A. Ramirez-González, C. Martínez, and J. Alvarez, *Modeling Zero-Gravity Distillation*, *Industrial and Engineering Chemistry Research* **31**, 901 (1992).
- [26] C. Vuik, F. Vermolen, M. Gijzen van, and M. Vuik, *Numerical Methods for Ordinary Differential Equations*, 2nd ed. (Delft Academic Press, Delft, 2015).
- [27] R. P. Canale and S. C. Chapra, *Mathematics and Computers in Simulation*, sixth ed. (The McGraw-Hill Companies, Inc., 2010) [arXiv:arXiv:1011.1669v3](https://arxiv.org/abs/1011.1669v3).
- [28] Meteotest Genossenschaft, *Meteonorm Desktop App*, (2018), accessed: 2018-03-14.
- [29] SolarGIS s.r.o., *SolarGIS iMaps application*, <https://solargis.info/imaps/> (2018), accessed: 2018-02-15.
- [30] J. Remund, *Neue Modelle für die realistische Generierung von Minutenwerten*, PV-Symposium Bad Staffelstein **49** (2017).
- [31] M. Hofmann, S. Riechelmann, C. Crisosto, R. Mubarak, and G. Seckmeyer, *Improved synthesis of global irradiance with one-minute resolution for PV system simulations*, *International Journal of Photoenergy* **2014** (2014), 10.1155/2014/808509.
- [32] W. C. Swinbank, *Long-wave radiation from clear skies*, *Quarterly Journal of the Royal Meteorological Society* **89**, 339 (1963).
- [33] Engineering Toolbox, *Convective Heat Transfer*, https://www.engineeringtoolbox.com/convective-heat-transfer-d_430.html (2003), accessed: 2018-03-27.
- [34] M. J. Moran, H. N. Shapiro, D. D. Boettner, and M. B. Bailey, *Thermodynamics, Fundamentals of Engineering*, seventh ed. (John Wiley & Sons, Inc., 2011).
- [35] M. Farzaneh-Gord, A. Niazmand, M. Deymi-Dashtebayaz, and H. R. Rahbari, *Thermodynamic analysis of natural gas reciprocating compressors based on real and ideal gas models*, *International Journal of Refrigeration* **56**, 186 (2015).
- [36] Laird Technologies, *Lairdtech handbook for thermoelectric modules*, (2018).
- [37] D. D. L. Wijngaards, E. Cretu, S. H. Kong, and R. F. Wolffenbuttel, *Modelling of integrated Peltier elements*, Proceedings of the 3rd International Technical Conference on Modelling and Simulation of Microsystems, 27 (2000).



Material Properties

Table A.1: This table contains a list of all material properties used throughout this thesis

Symbol	Description	Value	Units
$c_{p,alu(S)}$	Specific heat of solid aluminium	0.91	[kJ·kg ⁻¹ K ⁻¹]
$c_{p,CO_2(V)}$	Specific heat of carbon dioxide gas	39.61	[J·mole ⁻¹ K ⁻¹]
$c_{p,H_2O(L)}$	Specific heat of liquid water	4.187	[kJ·kg ⁻¹ K ⁻¹]
$c_{p,H_2O(V)}$	Specific heat of water vapour	1.995	[kJ·kg ⁻¹ K ⁻¹]
$c_{p,mono(S)}$	Specific heat of solid monolith	0.86	[kJ·kg ⁻¹ K ⁻¹]
$\Delta H_{evap,H_2O}$	Heat of evaporation of water	2030	[kJ·kg ⁻¹]
$\Delta H_{melt,H_2O}$	Heat of melt of water	334	[kJ·kg ⁻¹]
LHV_{MeOH}	Lower heating value of methanol	19.51	[kJ·g ⁻¹]
M_{CO_2}	Molar mass of carbon dioxide	44	[g·mole ⁻¹]
M_{H_2}	Molar mass of hydrogen	2	[g·mole ⁻¹]
M_{H_2O}	Molar mass of water	18	[g·mole ⁻¹]
M_{MeOH}	Molar mass of methanol	32	[g·mole ⁻¹]
κ_{alu}	Thermal Conductivity of aluminium	205	[W·m ⁻¹ K ⁻¹]
κ_{mono}	Thermal Conductivity of monolith	168	[W·m ⁻¹ K ⁻¹]
κ_{PVC}	Thermal Conductivity of PVC	0.19	[W·m ⁻¹ K ⁻¹]
κ_{steel}	Thermal Conductivity of steel	43	[W·m ⁻¹ K ⁻¹]
ρ_{alu}	Density of aluminium	2720	[kg·m ⁻³]
ρ_{H_2O}	Density of water	1000	[kg·m ⁻³]
ρ_{mono}	Density of monolith	400	[kg·m ⁻³]
ρ_{steel}	Density of steel	7850	[kg·m ⁻³]

B

Model Assumptions

This appendix contains all model assumptions of [chapter 4](#) and [chapter 7](#).

Location

	Steady-State	System	Improved System
City	Tucson	Tucson	Tucson
State	Arizona	Arizona	Arizona
Latitude	32.23	32.23	32.23
Longitude	-110.91	-110.91	-110.91

Data

	Steady-State	System	Improved System
Year	-	2005	2005
Sample Rate	Year	Hour	Hour
Interpolation	-	Cubic Hermite	Cubic Hermite
Accuracy	Year	Minute	Minute
CO ₂ concentration	-	400 ppm	400 ppm

Solar Panel

	Steady-State	System	Improved System
Brand	JA Solar	JA Solar	JA Solar
Power	300 W	300 W	300 W
Geometry	-	Flat plate	Flat plate
Length	-	1.65 m	1.65 m
Width	-	0.992 m	0.992 m
Material	-	Glass	Glass
Mass	-	18.2 kg	18.2 kg
Reflectivity	-	0.1	0.1
Efficiency	16.51 %	16.51 %	16.51 %
Tilt	-	63 °	63 °
Azimuth	-	165 °	165 °
Albedo	-	0.1	0.1

Control

	Steady-State	System	Improved System
Algorithm	-	Hierarchical	All on
Power	-	5 W	-
Resistance	-	-	1500 Ω

Direct Air Capture

	Steady-State	System	Improved System
Geometry	-	Cylinder	Cylinder
Length	-	0.1 m	0.1 m
Radius	-	0.056 m	0.056 m
Monolith Material	SiO ₂	Activated Carbon	Activated Carbon
Monolith mass	0.73 kg	0.4 kg	0.4 kg
Insulation	-	Yes	Yes
Thermal resistance	-	10 K·W ⁻¹	K·W ⁻¹
Adsorbent	-	Polyethylenimine	Polyethylenimine
Adsorbent mass	0.44 kg	0.12 kg	0.12 kg
Fan power	-	27 W	-
Fan resistance	-	-	- Ω
Airflow	-	0.0125 m ³ ·s ⁻¹	0.0125 m ³ ·s ⁻¹
Heater power	-	100 W	-
Heater resistance	-	-	Ω
Cooler power	-	30 W	-
Cooler resistance	-	-	Ω

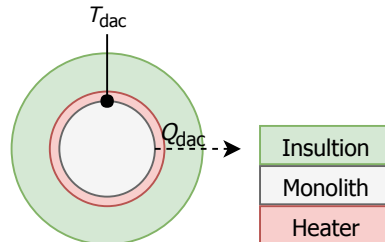


Figure B.1: Schematic overview of the simplified Direct Air Capture chamber

Fluid Machinery

	Steady-State	System	Improved System
Efficiency	-	20 %	40 %
CO ₂ compression	-	477 kJ·mole ⁻¹	477 kJ·mole ⁻¹
H ₂ O compression	-	524 kJ·mole ⁻¹	524 kJ·mole ⁻¹

Alkaline Electrolysis

	Steady-State	System	Improved System
Geometry	-	Cylinder	Cylinder
Length	-	0.16 m	0.16 m
Radius KOH	-	0.035 m	0.035 m
Radius PVC	-	0.0375 m	0.0375 m
Radius Steel	-	0.0425 m	0.0425 m
Materials	-	PVC, Steel	PVC, Steel
Electrolyte	-	KOH 30 wt%	KOH 30 wt%
Electrode area	14 cm ²	30 cm ²	60 cm ²
Cells in series	16	16	19
Operating temperature	60 °C	60 °C	90 °C
Thermal resistance	-	5 K·W ⁻¹	5 K·W ⁻¹

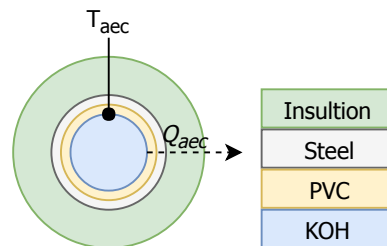


Figure B.2: Schematic overview of the simplified Alkaline Electrolysis

Methanol Synthesis

	Steady-State	System	Improved System
Geometry	-	Cylinder	Cylinder
Length	-	0.8 m	0.8 m
Radius reactor	-	0.01 m	0.01 m
Radius Steel	-	0.02 m	0.0155 m
Materials	-	Steel	Steel
Mass	-	2 kg	1 kg
Operating temperature	-	140 °C	140 °C
Thermal resistance	-	10 K·W ⁻¹	10 K·W ⁻¹
Heater power	-	50 W	-
Heater resistance	-	-	Ω

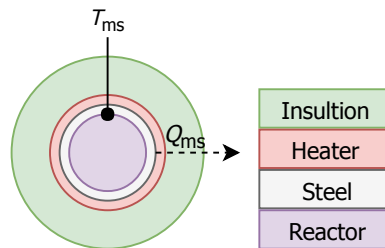
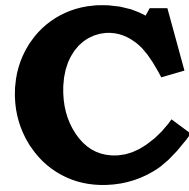


Figure B.3: Schematic overview of the simplified Methanol Synthesis reactor

Capillary Distillation

	Steady-State	System	Improved System
Geometry	-	Cylinder	Cylinder
Mass	-	1 kg	1 kg
Heater type	-	Heater	Heater
Heater power	-	25 W	-
Heater resistance	-	-	Ω
Separation energy	-	47.5 kJ·mole ⁻¹	kJ·mole ⁻¹
Operating temperature	-	60 - 100 °C	60 - 100 °C
Thermal resistance	-	10 K·W ⁻¹	10 K·W ⁻¹



Key Performance Indicators

The Key Performance Indicators (KPIs) are:

- Average amount of methanol produced per day. This is the most important metric since it is directly related to the amount of money that can be made with a single System.
- Average Plant efficiency. This metric determines how efficiently the Plant converts the available power from the Solar Panel into methanol (lower heating value).
- Average Solar Panel irradiance. This metric helps to choose the Solar Panel angle which corresponds to the maximum irradiance.
- Average Solar Panel efficiency. This metric determines how much of the irradiance that falls onto the Solar Panel module is converted into electric power.
- Solar Panel maximum power efficiency. This metric is related to the quality of the electrical design since it measures how much power is actually produced in relation to how much could be produced if the Solar Panel were to operate at it's maximum power point continuously.
- Average global horizontal irradiance per day. This metric is useful to compare different locations on earth
- Average energy use per subsystem. This metric helps to determine whether the subsystem is actually behaving as expected.
- Average relative energy use per subsystem. This metric determines how the power is distributed over the different subsystems and thus helps to identify which subsystems use the most energy.
- Average heat production compared to the total energy input. This metric helps to determine which subsystem wastes the most amount of energy in the form of heat and helps to identify which subsystems can be improved upon most.

D

Alkaline Electrolysis Experiments

This appendix shows an overview of the experimental work conducted on the Alkaline Electrolysis to obtain the data points used in this thesis to obtain the IV-curves. Next a summary of the unpublished internship report of Sebastian Diaz Rodriguez about the experimental setup is given.

D.1. Experimental Setup

Figure D.1 shows the latest model of a complete single-cell testing stack. It was designed with the purpose of determining the IV-curve of one cell, while also allowing to observe the behavior of the bubbles inside the AEC. For this latter purpose, a transparent sheet of PMMA was installed on each face of the device. Additionally, the hydrogen side was made with twice the volume of the oxygen side to make sure that the bubbling regimes we observed would be representative to the regime expected in the high-pressure setup, considering that twice the amount of hydrogen is produced than oxygen. The testing stack of Figure D.1 was also designed to be able to separate the hydrogen and oxygen produced from the electrolysis. This was done mostly as a safety issue than to capture and measure the volume of gases. An attempt to capture these was made but failed, however this measurement was not critical for this phase.

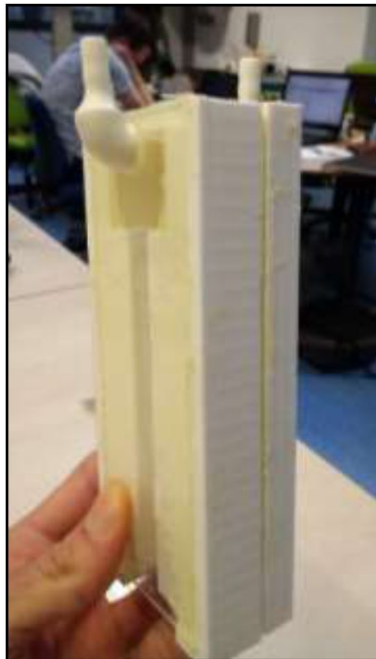


Figure D.1: Single-cell testing stack.

Probably the most important functionality of the single-cell testing stack was that it allowed to test the temperature dependency of the IV-characteristic. For this purpose, the bottom of the stack was left open so that the electrolyte would enter the stack from underneath at the temperature we wanted to test, controlling it with a hotplate and a thermocouple. [Figure D.2](#) shows the lab setup of the experiment carried out to determine the IV-curves for the cells made with the different electrodes available.

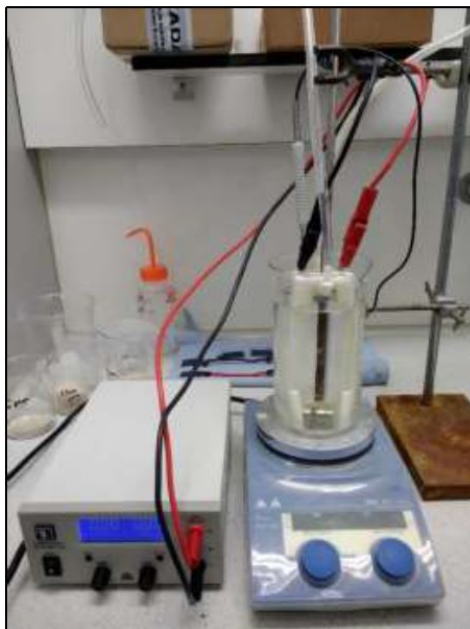
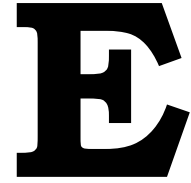


Figure D.2: Experimental setup for a single-cell testing stack.

The temperature dependence of the Permascand cells was determined by running the setup of [Figure D.2](#) at temperatures higher than room temperature. The objective was to obtain a set of IV-characteristics that could be used to fit the parameters of [Equation 2.7](#).



Important System Parameters

This appendix contains an overview of the important parameters of the subsystems as derived in [chapter 5](#).

- Location depending variables like temperature and irradiance determine the maximum power
- The electrical characteristics of the load and the Solar Panel orientation angles (tilt and azimuth) influence the actual power.
- Adsorption rate is mainly influenced by fan power
- Desorption rate is mainly influenced by heating power, insulation thickness and the vacuum pressure the Fluid Machinery can create.
- Direct Air Capture cooling rate is mainly influenced by cooling power and insulation thickness
- Cycle time and energy use are a complex interaction of all Direct Air Capture design parameters.
- The amount of gases that need to be compressed and internal losses e.g. due to friction mainly influence the energy use of the Fluid Machinery
- An intermediate condensation step is needed to prevent crossing the two-phase region inside a reciprocating pump
- All subsystems determine the energy that is available for the Alkaline Electrolysis.
- Temperature and current density mainly influence the efficiency of the Alkaline Electrolysis. Parameters that can influence this are insulation thickness and electrode cell area.
- Cooling is needed to make sure that the maximum operating temperature is not exceeded. It is desired to minimise cooling since this decreases the power that can be used to produce H₂.
- The mass of the Methanol Synthesis and the insulation material and thickness mainly influence the energy use of this subsystem
- The most important parameters influencing the Capillary Distillation are the insulation material and thickness.
- The System power is mainly influenced by the characteristics of the Solar Panel and the load it is connected to. The electrical parameters of the load need to be adjusted to match the Solar Panel IV-curve.
- The System efficiency is influenced by a complex interplay of all subsystem design parameters as well as how it is controlled. The Alkaline Electrolysis uses the most energy of all subsystems but it is desired to give it even more because H₂ production is an energy intensive process.



Guidelines for System Design

To support the process of optimising the System design to maximise MeOH production for any location the following general guidelines can be used:

1. Identify a location on earth with promising irradiance using SolarGIS.
2. Download hourly or minute data from a weather station close by using Meteonorm or another database. If necessary interpolate to obtain minute data.
3. Scale the irradiance data such that the average global horizontal irradiance matches the exact location's average global horizontal irradiance.
4. Calculate the optimal Solar Panel angle using an optimisation algorithm or by calculating the full solution space.
5. Adjust subsystem models to local conditions preferably with locally obtained experimental data.
6. Optimise the System design manually or use optimisation algorithms to find an optimal set of electrical and geometrical parameters, Peltier Elements and Thermal Buffers and thresholds for the Control model.